Universidade de São Paulo
Instituto de Física

Oscilador Paramétrico Ótico para uma interface átomos-luz.

Rayssa Bruzaca de Andrade

Orientador: Prof. Dr. Paulo Alberto Nussenzveig

Tese de doutorado apresentada ao Instituto de Física da Universidade de São Paulo, como requisito parcial para a obtenção do título de Doutora em Ciências.

Banca Examinadora:
Prof. Dr. Paulo Alberto Nussenzveig (IFUSP)
Prof. Dr. Sebastião Pádua (UFMG)
Prof. Dr. Antonio Zelaquett Khoury (UFF)
Prof. Dr. Luciano Soares Cruz (UFABC)
Prof. Dr. Gabriel Teixeira Landi (IFUSP)

São Paulo
2018

University of São Paulo
Physics Institute

An optical parametric oscillator for a light-atomic media interface

Rayssa Bruzaca de Andrade

Supervisor: Prof. Dr. Paulo Alberto Nussenzveig

Thesis submitted to the Physics Institute of the University of São Paulo in partial fulfillment of the requirements for the degree of Doctor of Science.

Examining Committee:
Prof. Dr. Paulo Alberto Nussenzveig (IFUSP)
Prof. Dr. Sebastião Pádua (UFMG)
Prof. Dr. Antonio Zelaquett Khoury (UFF)
Prof. Dr. Luciano Soares Cruz (UFABC)
Prof. Dr. Gabriel Teixeira Landi (IFUSP)

São Paulo
2018

FICHA CATALOGRÁFICA
Preparada pelo Serviço de Biblioteca e Informação
do Instituto de Física da Universidade de São Paulo

Andrade, Rayssa Bruzaca de

Oscilador paramétrico ótico para a interface átomos-luz.
São Paulo, 2018.

Tese (Doutorado) – Universidade de São Paulo. Instituto de Física. Depto. de Física Experimental.

Orientador: Prof. Dr. Paulo Alberto Nussenzveig
Área de Concentração: Ótica Quântica, Informação Quântica.

Unitermos: 1. Física; 2. Física teórica; 3. Física experimental; 4. Mecânica quântica.

USP/IF/SBI-051/2018

"Nobody ever figures out what life is all about, and it doesn't matter. Explore the world. Nearly everything is really interesting if you go into it deeply enough."

Richard Feynman

Resumo

Nesse trabalho apresentamos uma descrição das propriedades quânticas dos feixes de luz produzidos por um Oscilador Paramétrico Ótico (OPO) acima do limiar, bombeado por um laser de Titânio Safira com comprimento de onda de 780 nm, linha $D2$ do Rb, com espectro de ruído de um feixe coerente. Os feixes gêmeos possuem comprimentos de onda na região de 1560 nm que compreende a janela de transmissão de fibras óticas.

Os estados emitidos pelo OPO em estudo são aproximadamente gaussianos[1], o que nos permite descrevê-los em termos de momentos de primeira e segunda ordem. Como analisamos o espectro de ruído das flutuações de cada feixe, os momentos de primeira ordem são nulos, o que nos permite descrever o estado do sistema em termos de uma matriz de covariância.

Apresentamos então o comportamento do espectro de ruído e das correlações entre os feixes de bombeio refletido, sinal e complementar. Ademais, aplicamos diferentes critérios de emaranhamento para estudar o sistema. Apresentamos uma previsão do emaranhamento bipartido utilizando o critério de Duan [2]. Para as correlações tripartidas, utilizamos o critério de Furusawa[3]. Realizamos um estudo da bipartição bombeio e quadratura soma. E, aplicamos o critério PPT para variáveis contínuas[4], transpondo independente cada feixe em estudo. O critério PPT é necessário e suficiente para demonstrar emaranhamento entre bipartições para estados gaussianos.

Com o objetivo de explorar qual o comportamento do sistema frente ao critério de "steering"no modelo desenvolvido por Reid[5], estudamos teoricamente o critério de inferência para quadraturas bipartidas: entre os feixes gêmeos ou entre um dos feixes gêmeos e o feixe de bombeio. Finalizamos essa análise caracterizando a inferência entre os três modos, através da bipartição modo do bombeio e combinação das quadraturas soma dos feixes gêmeos.

Apresentamos a formulação de um protocolo de teletransporte quântico de um estado coerente de entrada formado pelo feixe do Titânio Safira, cuja medida de Bell é realizada utilizando o bombeio refletido pelo OPO como estado emaranhado para os feixes sinal e complementar, como uma primeira possibilidade de implementar o protocolo. Também propomos um protocolo em que o feixe sinal auxilia no processo de teleportação. Dessa forma, a fidelidade do sistema aumenta e supera o limite da não clonagem.

Descreveremos as primeiras medidas de correlações entre os feixes emitidos pelo OPO para esse sistema. A caracterização de emaranhamento tripartido nessa nova configuração é o primeiro passo para a implementação de protocolos de ótica quântica utilizando uma fonte de estados emaranhados que é compatível tanto com sistemas atômicos de Rubídio quanto com a região de telecomunicações, formando assim uma rede quântica de transferência e aprisionamento de informação.

Abstract

In this work, we discuss a description of quantum properties of light beams produced by an Optical Parametric Oscillator (OPO) above threshold, pumped by a 780 nm Titanium Sapphire laser, resonant with the D2 line of Rb, with a noise spectrum of a coherent beam. The twin beams have wavelengths around 1560nm, in the telecommunication band.

The states emitted by the OPO under study are approximately Gaussian[1], which allows us to describe them in terms of first and second order moments. As we analyze the noise spectrum of the fluctuations of each beam, the first order moments are null, which allows us to describe the state of the system in terms of a covariance matrix.

We present the behavior of the noise spectrum and the correlations between the reflected pump, signal and idler beams. In addition, we applied different entanglement criteria to study the system. We present a prediction of the bipartite entanglement using Duan criterion[2]. For tripartite correlations, we use the Furusawa criterion[3]. We performed a study of bipartition pump and sum quadrature. As well, we applied the PPT criterion[4] for continuous variables, independently transposing each beam under study. The PPT criterion is necessary and sufficient to demonstrate entanglement between bipartitions for Gaussian states.

In order to explore the behavior of the system using the steering criterion in the model developed by Reid[5], we theoretically study the criterion of inference for bipartite quadratures: between the twin beams or between one of the twin beams and the pump beam. In addition, we analyzed the inference between the three modes, through the bipartition pump mode and combination of sum quadrature of the twin beams.

We develop a quantum teleportation protocol of a coherent input state, composed by the Titanium Sapphire beam whose Bell measurement is performed using the pump reflected by the OPO as an entangled state for the signal and idler beams as a first possibility to implement the protocol. Furthermore, we propose a protocol in which the signal beam assists in the process of teleportation. Thus, the fidelity of the system increases and exceeds the limit of non-cloning.

We will describe the first measurements of correlations between the beams emitted by the OPO for this system. The tripartite entanglement characterization is the first step in the implementation of quantum optical protocols using a source of entangled states that is compatible with both Rubidium atomic systems and the telecommunications region, thus forming a quantum network.

Agradecimentos

Nenhum caminho se constrói sozinho. E, sendo assim:

Iniciarei agradecendo ao meu orientador Paulo Nussenzveig por seu incentivo para a realização da pesquisa e na busca de novos caminhos, pelas conversas sobre física que sempre foram esclarecedoras. Gostaria de agradecer o professor Marcelo Martinelli por todas as discussões sobre teoria e sobre a arte do experimento, por entrarmos nas entranhas do laser, dos sistemas de travamento e de qualquer caixa que precisasse ser aberta (de forma consciente, é claro!), sua presença foi fundamental para o desenvolvimento desse projeto.

Agradeço aos professores membros da banca por todas as sugestões e críticas referentes a esse trabalho.

Aos colegas de laboratório sou imensamente grata por todo o conhecimento que adquiri com vocês. Início agradecendo ao pos-doc Breno, sua colaboração foi essencial. Foram longas horas de discussão, de trabalho em equipe, de alinhamentos e travamentos e, como não poderia deixar de ser, de noites não dormidas para realizar as medidas. Não há pão de queijo suficiente que eu deixe em sua mesa como forma de agradecimento, muito obrigada. Agradeço ao Luiz, que entrou de mansinho no experimento como "nosso"aluno de iniciação e agora continuará o experimento no seu mestrado. Obrigada por confiar em nós no seu processo de aprendizagem e, por limpar os titânio safira todas as vezes que foi necessário (hehehe). Tulio, que por um tempo fez parte do nosso time e que agora alça voos em um outro sistema, muito obrigada pelo compartilhamento de conhecimento e pela amizade.

Agora, que o time que fez parte da equipe do OPO TISAF foi citado, vamos a galera do lab. Igor, acho que sobreviveremos a essa etapa!!! Obrigada por estar sempre presente, mesmo quando ausente!! Bárbara, que mais do que um laboratório, dividimos uma casa... muito obrigada por ser minha amiga!!! Aos demais colegas do lab, que somos muitos, vocês fizeram os meus dias, a maior parte das vezes, mais divertido. Com vocês aprendi mais do que física, aprendi a tomar cachaça (primeira vez foi depois da qualificação!!), beber vinho e só não conseguiram me fazer tomar café, mas um passo de cada vez!

Sou muito grata aos funcionários do IF por terem me auxiliado em tudo o que puderam e que foi necessário. Edi, Luiz e Bianca, por terem auxiliado nas questões burocráticas. Eduardo (eletrônica) e Marcos (mecânica), obrigada por terem feito possíveis todos os pedidos solicitados, mesmo quando nem nós sabíamos direito como eles poderiam ser feitos. Edu, especialmente obrigada por me ensinar mais sobre a arte da eletrônica. Marcos, que muito insistiu que conseguiu que eu aprendesse um pouco de desenho técnico, obrigada por sempre entregar as peças com um padrão de qualidade superior ao esperado. Sem a contribuição de vocês o trabalho teria sido mais difícil.

Aos amigos que são amigos desde um tempo em que já não contamos mais. Não citarei todos os nomes, porém não posso deixar de escrever alguns, que me aguentaram e me amaram em situações que nem eu mesma sabia que conseguiria continuar. Camila Letti, Isabela, Natália e Bárbara, obrigada por estarem por perto sempre. Klara, obrigada por ser meu ombro amigo até hoje.

Agradeço ao Grupo Passos para o Futuro, que faz um trabalho de voluntariado maravilhoso, obrigada por me receberem de braços abertos. Foi um aprendizado ao longo de todos esses anos e serei sempre grata. Que a semente plantada por nós continue se perpetuando e, que mais e mais crianças sejam favorecidas por atitudes lindas como a do grupo.

Hermano, obrigada pelo companheirismo, por me amar e por estar comigo mesmo quando eu fico distante. Obrigada pelo acolhimento que a sua família me propicia, com vocês me sinto em casa.

Aos meus familiares, especialmente a minha mãe Elinesia e meus tios Renilson e Maria, fonte de inspiração e motivação. Renilson e Ednólia, obrigada por me acolherem e me oferecerem um lar, muito do que sou hoje provem do incentivo e dos conselhos que recebi, sempre estive em casa ao lado de vocês. Aos meus irmãos, por todos os momentos felizes e dificuldades que enfrentamos juntos, ser irmão é uma arte! Vocês maninhos me deram sobrinhos lindos e gostaria que meus sobrinhos soubessem que é difícil não os acompanhar crescer, porém não os deixo de amar, isso a distância não nos impede de sentir. Minha irmã Claudia, que cedo também saiu de casa em busca de seus sonhos, tenho muito orgulho e amor por você.

Estudar física sempre exigiu uma dedicação que não posso mensurar em termos do tempo que tive que me privar da companhia da minha família e amigos, espero que compreendam o porquê de tanta distância e que saibam que sempre foram lembrados e amados.

Agradeço ao CNPq pelo fomento.

Contents

Introduction

Every day we transmit and process a large amount of information, such as when we use a computer to send an electronic mail. These processes occur through physical systems which have intrinsic characteristics and limitations, and it is natural to seek new principles to improve them. In this sense, the information coded by quantum states allows new protocols for security, transport and storage, as in the studies on quantum cryptography [6], teleportation [7] and quantum memories [8], using quantum properties such as entanglement.

Entanglement was a central element of discussions on the completeness of the description of quantum mechanics in the century XX, starting with the famous article written by Einstein, Podolsky and Rosen [9] and then systematically studied by several scientists, of whom we can cite: Bohr [10], Schrödinger [11] and Bell [12]. However, only in the last 30 years has entanglement been seen as an important tool in the development of new theoretical and experimental proposals in the field of quantum computing [13, 14] and quantum cryptography [15] since entangled systems present properties such as the impossibility of treating its subsystems independently, so that the scientific community is constantly seeking to improve the methods for generation and control of these systems.

The Optical Parametric Oscillator (OPO) is a source of light that can generate entangled beams and consists of an optical cavity and a crystal that has nonlinear susceptibility of second order. Its operation is based on the parametric down conversion in which a photon of the pump beam is annihilated while interacts with the crystal generating two other photons, called signal and idler photons. The beams that are resonant with the optical cavity are amplified at each interaction with the nonlinear medium. For a given pump power, the gains outweigh the intracavity losses, and the system oscillates. Passing this threshold the system oscillates and there is light emission with high level coherence.

Our intent is to study the quantum correlations in a triply resonant OPO and the main applications within a quantum information network of entangled states generated by our source. The main feature of the OPO under study is the region of wavelengths we work with. The pump beam is a tunable Titanium Sapphire laser in a range of $730 - 800nm$ ([16]). This region is compatible with D1 ($794.98nm$) and D2 ($780.24nm$) lines of Rb. The beams emitted by the OPO have wavelengths around $1560nm$, that's in the telecommunications region (*C-band*) [17], that makes transmission through the already established infrastructure possible.

As it has already been demonstrated experimentally by our group [18], the reflected pump, signal and idler beams can be entangled. Entanglement between different frequencies of the spectrum allows the exchange of quantum information to subsystems that are compatible with the entangled frequencies. In this context, we can construct a network of quantum information, in which there is an interface of atoms and light to perform storage and transmission of information. The pump reflected by the OPO could interact with an atomic system and the twin beams could interact with other subsystems, and the transmission could be performed by optical fibers.

The pump beam used in the OPO for analysis frequencies above 9MHz behaves as a coherent state, its noise level is equal to the standard quantum noise. We can use part of this beam as an input state in a quantum teleportation process, in which the Bell measurement could be performed by mixing a coherent state with the reflected pump generated by the OPO (necessary entangled state for the teleportation process). The initial state information would be teleported to the twin beams generated by the OPO. In this way, we would be performing teleportation of a beam whose initial state was prepared at a completely different frequency from the station where the teleportation will be carried out. The teleportation of a coherent state in the regime of continuous variables was first described by Braunstein [19] and the experimental demonstration performed by Furusawa in 1998 [7].

The possibilities mentioned are the applications that we envision accomplishing in this project. However, for it to be possible, it is necessary to have a thorough knowledge of the entangled source states that we use. We need to characterize the quantum correlations of the OPO and the entanglement between the generated beams. Doing this, we will be able to predict if it is possible to implement the protocols above suggested.

In this thesis we present a theoretical discussion of the main concepts necessary for understanding the processes that occur in the OPO and the first experimental results using this source to produce entangled states of light. During the last 10 years our group has specialized in building and generating entangled state using an OPO as a resource. The first measurement of tripartite correlations above threshold was performed in the group [18]. With the purpose to build a tripartite entangled source that made us able to communicate with atoms and transfer the information with minimal losses, we start with this source.

We will also present the first experimental results of the correlations between the beams emitted by the OPO pumped by a Titanium Sapphire laser. The first measurement of entanglement between the bipartition sum of the phases and subtraction of the amplitudes quadratures between the twin beams was performed, characterized by Duan criterion. In the chapter 1 we will study the principal concepts necessary to understand this work, as the field quadratures and its quantum description, the self-homodyne technique used to acquire the information of each beam and a brief description of gaussian states and its representation in a covariance matrix. In this chapter we also present the entanglement criteria studied in this thesis. In

chapter 2 we will give a broader description of the quantum treatment performed for OPO as well as theoretical predictions about the behavior of the system. We performed a theoretical simulation of steering criterion for our system in chapter 3, using the parameters of the system to analyze which are the better regions to measure steering in the bipartition in study. We will also present a theoretical proposal of teleportation and its feasibility to be carried out with the system that we have in chapter 4. And, at the end, we will describe the tests performed in the experimental apparatus so far in chapter 5.

Chapter 1

Quantum nature of light

The curiosity about the nature of light has instigated us since the antiquity until this day. In Greece, more than 2500 years ago, light was described as corpuscles, since then a lot of theories and experiments were performed and different concepts changed during this time. In the end of the 19th century we had the publication of the electromagnetic theory of Maxwell where he shows that the velocity of propagation of the electromagnetic waves in vacuum is the same observed by astronomers for light. Shortly thereafter Henrich Herzt from an experiment with transmitters and radio wave detectors shows experimentally that the propagation velocity of electromagnetic radiation is the light velocity, confirming Maxwell's predictions. Another remarkable fact in the end of 19th century was the "UV catastrophe" where the predictions of Rayleigth theory regarding the density of energy in function of the temperature of a black body it was not confirmed experimentally. Planck, early in 20th century, proposed that black bodies are resonators that emit electromagnetic energy in packets of $h\nu$ which allowed the correct expression of the energy density of a black body as a function of temperature. At this point, new description of the light nature emerged by the photoelectric description, firstly studied by Leonard then described by Einstein in 1905. In 1928 Bohr announces "The complementary principle" which regards the wave particle duality. Among 1925 and 1930 we have a lot of developments in the theoretic description of quantum radiation of light and the interaction between photons and electrons in works performed by Dirac, Schroedinger, Pauli, Jordan and Heisenberg. After this we have the invention of the LASER and MASER which allows advancement in experiments on the nature of light.

In this chapter we will study the principal concepts related to the quantum nature of light, we will start with a brief review of the properties of the quantized electromagnetic field, the representation in sets of basis states and in the phase space, we indicate the follow references for more details about this subject [20, 21]. We will introduce the continuous variable space and Gaussian states that represent the states studied in this work. We will talk about the photodetection theory and the methods used to perform the quantum tomography of our system.

1.1 Quantized electromagnetic field

To study quantum features of light we need first to quantize the electromagnetic field (QEM). In this section we will review the quantized electromagnetic field and its representation in terms of the field quadratures. In terms of the annihilation and creation operators, the quantized electromagnetic field is written as [21]:

$$\hat{\mathbf{E}}(\mathbf{r},t) = \sum_{\mathbf{k}} \xi_{\mathbf{k}} \epsilon_{\mathbf{k},\lambda} \left[\hat{a}_{\mathbf{k},\lambda} e^{i(\mathbf{k}.\mathbf{r}-\omega_k t)} + \hat{a}^{\dagger}_{\mathbf{k},\lambda} e^{-i(\mathbf{k}.\mathbf{r}-\omega_k t)} \right], \tag{1.1}$$

where $\xi_{\mathbf{k}}$ is the normalization factor, $\mathbf{k}$ is the propagation wave vector that is perpendicular to the unit polarization vector $\epsilon_{\mathbf{k},\lambda}$, λ is the polarization index and ω_k is the angular frequency associated with the magnitude of $|\mathbf{k}| = \frac{\omega_k}{c}$. We will simplify the notation using $\kappa = \{\mathbf{k}, \lambda\}$ to represent one mode of the field. The bosonic operators $\hat{a}_\kappa$ and $\hat{a}_\kappa$ satisfy:

$$[\hat{a}_\kappa, \hat{a}^{\dagger}_{\kappa'}] = \delta_{\kappa\kappa'} \qquad [\hat{a}_\kappa, \hat{a}_{\kappa'}] = [\hat{a}^{\dagger}_\kappa, \hat{a}^{\dagger}_{\kappa'}] = 0. \tag{1.2}$$

The Hilbert space that describes the quantized field is the Fock space. For a multimode field, the Fock state is denoted by:

$$|\{n_\kappa\}\rangle \equiv |n_1\rangle \otimes |n_2\rangle \otimes ..... \otimes |n_\kappa\rangle ... \otimes .., \tag{1.3}$$

where the quantity n_i is the number of quanta of light in the i-th mode κ. For a single mode field, the number operator acts in a Fock states as:

$$\hat{n} |n\rangle = n |n\rangle , \tag{1.4}$$

being $\hat{n} = \hat{a}^{\dagger}\hat{a}$, and n the eigenvalue of the operation. The Hamiltonian associated with the quantized electromagnetic field describes a system with an arbitrary number of harmonic oscillators:

$$\begin{aligned} \hat{H} &= \sum_{\kappa} \hbar\omega_\kappa (\hat{a}^{\dagger}_\kappa \hat{a}_\kappa + \frac{1}{2}) \\ &= \sum_{\kappa} \hbar\omega_\kappa (\hat{n}_\kappa + \frac{1}{2}), \end{aligned} \tag{1.5}$$

where each mode is multiplied by the energy of a photon in that mode plus the energy of the vacuum fluctuations in each mode. The Fock states are eigenvectors of the Hamiltonian of the QEM, for a single mode field:

$$\hat{H} |n\rangle = E_n |n\rangle \tag{1.6}$$

with energy eigenvalues $E_n = \hbar\omega(n + \frac{1}{2})$.

1.1.1 Quadratures of the field

Suppressing the quantities that define the dimension of the field, the temporal part of a single-mode quantized electromagnetic field in the interaction picture is written in terms of the quadratures field operators $\hat{X}$ and $\hat{Y}$ as:

$$\hat{E}(t) = \hat{X}_\theta(t)\cos\omega t + \hat{Y}_\theta(t)\sin\omega t, \tag{1.7}$$

where the quadrature operators $\hat{X}_\theta(t)$ e $\hat{Y}_\theta(t)$ are related with the bosonic operators $\hat{a}(t)$ and $\hat{a}^\dagger(t)$ written in the Heisenberg picutre as:

$$\begin{aligned} \hat{X}_\theta(t) &= e^{-i\theta}\hat{a}(t) + e^{i\theta}\hat{a}^\dagger(t), \\ \hat{Y}_\theta(t) &= -i(e^{-i\theta}\hat{a}(t) - e^{i\theta}\hat{a}^\dagger(t)), \end{aligned} \tag{1.8}$$

and θ is an arbitrary phase relative to incident field [22].

For an arbitrary state $|\psi\rangle$, two operators $\hat{A}$ and $\hat{B}$ satisfy the inequality:

$$\sqrt{\langle(\Delta\hat{A})^2\rangle\,\langle(\Delta\hat{B})^2\rangle} \geq \frac{1}{2}|\,\langle[\hat{A},\hat{B}]\rangle\,|, \tag{1.9}$$

where the variance $(\Delta\hat{A})^2$ is:

$$(\Delta\hat{A})^2 \equiv \langle\Psi|\,\hat{A}^2\,|\Psi\rangle - (\langle\Psi|\,\hat{A}\,|\Psi\rangle)^2. \tag{1.10}$$

The Hermitian operators $\hat{X}_\theta(t)$ and $\hat{Y}_\theta(t)$ are dimensionless and they satisfy the canonical commutation relation:

$$[\hat{X}_\theta(t), \hat{Y}_\theta(t')] = 2i\delta(t-t'), \tag{1.11}$$

and Equation 1.9 gives the Heisenberg uncertainty relation between them:

$$\Delta\hat{X}_\theta(t)\Delta\hat{Y}_\theta(t) \geq 1. \tag{1.12}$$

1.2 Coherent States

Coherent states are minimum uncertainty states and they are the closest quantum mechanical state to a classical description of the field. Laser are a very common source of light that generates this kind of state. In the standard form, the coherent states was introduced by Roy J. Glauber [23] and they are eigenstates of the annihilation operator $\hat{a}$:

$$\hat{a}\,|\alpha\rangle = \alpha\,|\alpha\rangle\,, \tag{1.13}$$

where $\alpha = |\alpha| e^{i\theta}$ are the complex eigenvalues, $|\alpha|$ is the amplitude and θ is the phase of the state $|\alpha\rangle$. The coherent states can be expanded in terms of the Fock states $|n\rangle$ [24]:

$$|\alpha\rangle = e^{-\frac{|\alpha|^2}{2}} \sum_{n=0}^{\infty} \frac{\alpha^n}{\sqrt{n!}} |n\rangle . \tag{1.14}$$

The mean number of photons in a coherent states is:

$$\langle \hat{n} \rangle = \langle \alpha | \hat{n} | \alpha \rangle = |\alpha|^2 = \overline{n}, \tag{1.15}$$

and the probability to detecting n photons in the state $|\alpha\rangle$ is $P_n = |\langle n|\alpha\rangle|^2$:

$$P_n = e^{-\overline{n}^2} \frac{\overline{n}^n}{n!}, \tag{1.16}$$

that is a Poisson statistics with a mean value of $\overline{n}$, and it has the property that its variance is equal to the mean:

$$(\Delta \hat{n})^2_\alpha = \langle \hat{n}^2 \rangle_\alpha - (\langle \hat{n} \rangle)^2_\alpha = |\alpha|^2 = \overline{n}. \tag{1.17}$$

The scalar product of two coherent states $|\alpha\rangle$ and $|\beta\rangle$ is:

$$|\langle \alpha | \beta \rangle| = e^{-|\alpha - \beta|^2}, \tag{1.18}$$

what shows us that two coherent sates are not orthogonal. However, the coherent states form an overcomplete basis:

$$\frac{1}{\pi} \int |\alpha\rangle \langle \alpha| \, d^2\alpha = 1. \tag{1.19}$$

It is possible to show that all coherent state have an minimum uncertainty:

$$\begin{aligned} (\Delta \hat{X})^2 = (\Delta \hat{Y})^2 &= 1, \\ \langle (\Delta \hat{X})^2 \rangle \langle (\Delta \hat{Y})^2 \rangle &= 1, \end{aligned} \tag{1.20}$$

where we can see that in a coherent states we have equal uncertainties in the quadratures and the minimum value of the uncertainty product. This behavior is the same when the fluctuations are computed in the vacuum state, because of this these noise is called shot-noise or standard quantum limit.

We can represent the fluctuations of the field quadratures in the phase space using a phasor diagram for a quantized light field. In the figure 1.1 we have the representation of a coherent and a squeezed state. We will discuss about the squeezed states in the next section. The vacuum coherent state is represented by the dashed circle in the part *a*) of the figure 1.1. We

can see that the mean value of the field is zero and the uncertainty has equal values in both quadratures. In part *b*) we have a coherent state represented by a circle displaced for the origin, the mean value of the field is $|\alpha|$ and the angle between the axis and the mean value of the field is ϕ.

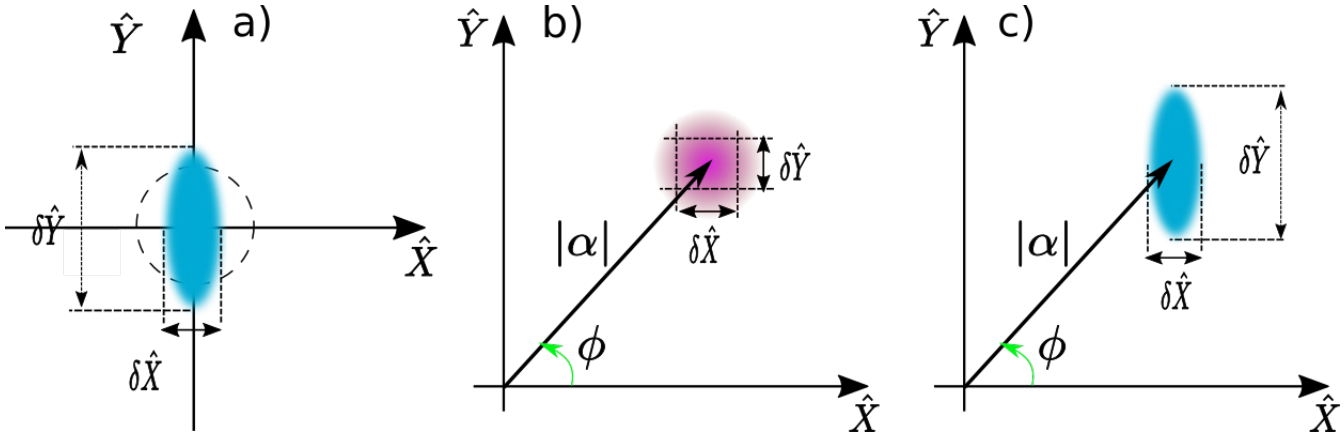

Figure 1.1: In the figure is represented the phase space diagram for a) a squeezed (in blue) and a coherent (dashed line) vacuum state, b) a coherent state and in c) a squeezing state where the fluctuations in $\delta\hat{X}$ are squeezed.

1.3 Squeezed States

Another class of minimum uncertainty states are the squeezed states that presents less quantum fluctuations in one quadrature than a coherent state what implies that the conjugated quadrature will present excess of noise. We can produce squeezed states with non linear optics and this class of states was first experimentally demonstrated in a Four Wave Mixing experiment by R.E Slusher in 1985 [25]. A squeezed state $|\varepsilon\rangle$ is defined as the unitary operator $\hat{S}(\varepsilon)$ applied in the vacuum state as [26]:

$$|\varepsilon\rangle = \hat{S}(\varepsilon)\,|0\rangle\,, \tag{1.21}$$

where $\hat{S}(\varepsilon) = e^{\frac{1}{2}\varepsilon\hat{a}^{2\dagger} - \frac{1}{2}\varepsilon^*\hat{a}^2}$ is the unitary operator of squeezing with a factor $\varepsilon = re^{i\theta}$. Where $\hat{S}(\varepsilon)$ obeys the relations $\hat{S}^\dagger(\varepsilon) = \hat{S}^{-1}(\varepsilon) = \hat{S}(-\varepsilon)$, and has the properties:

$$\begin{aligned} \hat{S}^\dagger(\varepsilon)\hat{a}\hat{S}(\varepsilon) &= \hat{a}\cosh r - \hat{a}^\dagger e^{i\theta}\sinh r, \\ \hat{S}^\dagger(\varepsilon)\hat{a}^\dagger\hat{S}(\varepsilon) &= \hat{a}^\dagger\cosh r - \hat{a}e^{-i\theta}\sinh r. \end{aligned} \tag{1.22}$$

These properties are useful to demonstrate that squeezed states are minimum uncertainty states whose quadratures fluctuations for $\theta = 0$ is given by:

$$(\Delta\hat{X})^2 = e^r, \qquad (\Delta\hat{Y})^2 = e^{-r},$$
$$\langle(\Delta\hat{X})^2\rangle \langle(\Delta\hat{Y})^2\rangle = 1. \tag{1.23}$$

In Equation 1.23 we can see that both quadratures present different amount of fluctuations, each quadrature presenting fluctuation in term of the factor r that is called the *squeeze factor* [26]. Squeezed states presents sub-Poissonian statistics meaning that it's noise level is less than the shot noise limit. In the phase space diagrams in figure 1.1 we have two representation for a squeezed state. In the part a) we have a vacuum squeezed state (in blue) where the fluctuations in the quadrature $\delta\hat{X}$ is less than in conjugated quadrature. The displaced squeezed stated is shown in part c) of the figure where we have an amplitude-squeezed stated with a mean value of the field equal to $|\alpha|$.

1.4 Continuous Variable Systems

Describing the observables of a quantum system in a continuous variable domain enables to encode quantum correlations and information in a continuum spectrum associated to position and momentum of a particle. In this sense, we can perform different protocols as: quantum communication, teleportation and quantum key distribution.

Formally, a continuous variable system has an infinite Hilbert space and its observables have a continuous spectrum. The N bosonic modes of the quantized harmonic oscillator can be described by a Hilbert space that is associated with the tensor product:

$$\mathcal{H} = \otimes_{k=1}^{N} \mathcal{H}_k, \tag{1.24}$$

of infinite-dimensional Fock spaces $\mathcal{H}_k$'s each of them associated with a single mode and its N pairs of bosonic field operators $\{\hat{a}_k, \hat{a}_k^\dagger\}_{k=1}^N$[27]. We can write the annihilation and creation operators in terms of the quadratures operators $\{\hat{p}_\kappa, \hat{q}_\kappa\}_{k=1}^N$ and to group this operators together in a vector $\hat{\mathbf{x}}$ as:

$$\hat{\mathbf{x}} = (\hat{p}_1, \hat{q}_1, \hat{p}_2, \hat{q}_2, ...\hat{p}_n, \hat{q}_n)^T, \tag{1.25}$$

that obeys the canonical commutation relation written in a compact form:

$$[\hat{x}_i, \hat{x}_j] = 2i\Omega_{ij}, \tag{1.26}$$

where Ω is the symplectic form:

$$\Omega = \bigoplus_{k=1}^{N} \omega \qquad \omega = \begin{pmatrix} 0 & 1 \\ -1 & 0 \end{pmatrix}. \tag{1.27}$$

The density operator $\hat{\rho}$ represents the quantum state that contains all the physical information about the N-bosonic system. The density operator is a positive-trace class operator acting on the Hilbert space $\hat{\rho} : \mathcal{H} = \otimes_{k=1}^{N} \mathcal{H}_k$ [27]. In an infinite dimensional system one way to describe the quantum state of the system is in terms of the quasi-probability distributions, that are associated with a specific ordination of the bosonic operators, i.e, those function can be written in normal order(Glauber and Sudarsahn P-representation), symmetric order (Wigner function) and anti-normal order(Husimi Q-function). These class of function are called quasi probability function because they don't have all the properties of a probability function. One of the most remarkable is that some of them can assume negative values for a certain class of states. The mean value of this function is represented by the s-ordered characteristic function defined as:

$$\chi_{\rho}^{s}(\varepsilon) = Tr[f(\hat{a}_{\kappa}, \hat{a}_{\kappa}^{\dagger})\hat{\rho}], \tag{1.28}$$

where $s = \{-1, 0, 1\}$ represents, respectively, the Q-function, Wigner function and P-representation, $f(\hat{a}_{\kappa}, \hat{a}_{\kappa}^{\dagger})$ is a function of $\hat{a}$ and $\hat{a}^{\dagger}$ in some ordination, ε belongs to real 2N - dimensional space. For our goal the usual treatment is using the Wigner function representation, that are in a symmetric ordination. Because of the Heisenberg uncertainty principle, it is not possible to define a point in the phase space for the canonical variables. But, we can use the Wigner function to compute the statistical properties of the quantum state in study. In terms of the canonical variables the Wigner function[28] is written as:

$$W(p, q) = \frac{1}{2\pi\hbar} \int_{-\infty}^{\infty} e^{-\frac{i}{\hbar}px} \langle q - \frac{x}{2} | \hat{\rho} | q + \frac{x}{2} \rangle \tag{1.29}$$

The Equation 1.29 appeared for the first time on the Wigner's paper about Thermodynamics [29] in 1932. The marginal distributions of the Wigner function give us the correct probability distribution associated to the measurement of the remaining quadrature. For example, the $\int_{-\infty}^{\infty} W(q, p)dp = \langle q | \hat{\rho} | q \rangle$ and to the other quadrature $\int_{-\infty}^{\infty} W(q, p)dq = \langle p | \hat{\rho} | p \rangle$[30].

The class of states that will represent the states studied in this work are Gaussian states that include coherent states, squeezed states, thermal states, among others. Gaussian states are fully characterized by its first and second moments and exhibit a Wigner function with Gaussian marginal distributions. The first moment are the mean value of the quadratures operators $\hat{\mathbf{x}}$:

$$\langle \hat{\mathbf{x}} \rangle = Tr(\hat{\mathbf{x}}\hat{\rho}). \tag{1.30}$$

The second moment can be organized in a covariance matrix $\mathbf{V}$, defined as:

$$\mathbf{V} = \frac{1}{2}(\langle \hat{\mathbf{x}} \cdot \hat{\mathbf{x}}^T \rangle + \langle \hat{\mathbf{x}} \cdot \hat{\mathbf{x}}^T \rangle^T), \tag{1.31}$$

the diagonal elements of $\mathbf{V}$ are the variances of the quadratures $\vec{\mathbf{x}}$ and the off-diagonal elements the correlation between quadratures of different modes. The covariance matrix is real and symmetric, $\mathbf{V} = \mathbf{V}^T$. For a system composed of two different modes, let us say $\hat{\mathbf{x}} = (\hat{p}_1, \hat{q}_1, \hat{p}_2, \hat{q}_2)$, the covariance matrix is given by:

$$\mathbf{V} = \begin{pmatrix} \Delta^2\hat{p}_1 & C(\hat{p}_1\hat{q}_2) & C(\hat{p}_1\hat{p}_2) & C(\hat{p}_1\hat{q}_2) \\ & \Delta^2\hat{q}_1 & C(\hat{q}_1\hat{p}_2) & C(\hat{q}_1\hat{q}_2) \\ & & \Delta^2\hat{p}_2 & C(\hat{p}_2\hat{q}_1) \\ & & & \Delta^2\hat{q}_2 \end{pmatrix} \tag{1.32}$$

where an example of a diagonal element is $\Delta^2\hat{p}_1 \equiv \langle \hat{p}_1^2 \rangle - \langle \hat{p}_1 \rangle^2$ and an off-diagonal is the correlation $C(\hat{p}_1\hat{p}_2) \equiv \langle \hat{p}_1\hat{p}_2 \rangle - \langle \hat{p}_1 \rangle \langle \hat{p}_2 \rangle$.

In terms of the covariance matrix, the Wigner representation of Gaussian states are defined as:

$$W(\mathbf{x}) = \frac{1}{\pi\sqrt{\det \mathbf{V}}} e^{-\frac{1}{2}\mathbf{x}^T\mathbf{V}^{-1}\mathbf{x}}, \tag{1.33}$$

where $\mathbf{x}$ are the eigenvalues of quadratures operators $\hat{\mathbf{x}}$.

The covariance matrix represents a physical Gaussian state if the matrix obeys some rules. In a classical point of view the covariance matrix needs to be real, symmetric and positive definite[27]. But, a quantum system has to obey an extra rule:

$$\mathbf{V} + i\mathbf{\Omega} \geq 0. \tag{1.34}$$

This condition is a generalization of the uncertainty principle and it is necessary and sufficient to describe a physical density matrix $\hat{\rho}$ for a Gaussian state.

1.5 Photodetection Theory

Our interest is to measure the quantum correlations between the three beams emitted by the OPO, the reflected pump, signal and idler beams. To carry out the measurements of that correlations, we need to know the quantum fluctuations associated with the fields of interest. The standard way to study these fluctuations is to analyze the operators that compose the electromagnetic field as an average value that is associated with a central frequency, called carrier frequency, plus a fluctuation term, related to the sidebands. In the region of the sidebands these are the states that we have interest in to study. In the figure 1.2 we have a representation

of the spectrum of the field.

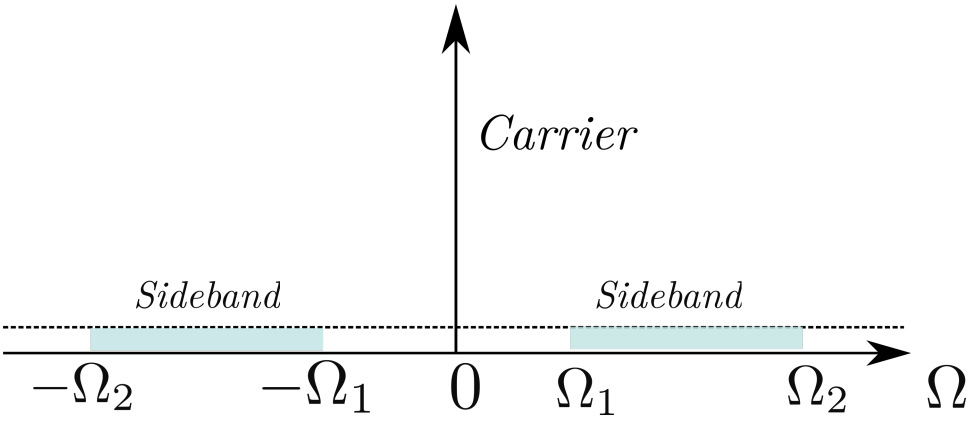

Figure 1.2: Representation of the electromagnetic spectrum. The central region represents the carrier of the field that is densely populated. The regions around the carrier are called sidebands and have a small photon concentration.

The regions of the spectrum that we are interested in measuring are directly related to the conditions of our experimental apparatus. Entanglement measurements occur in a region bounded by the bandwidth of the OPO, which sets the upper limit, and by the bandwidth of the analysis cavities, which sets the lower limit. The frequency at which we analyze our experiment should be such that it is larger than the bandwidth of the analysis cavities and shorter than the bandwidth of the OPO.

In the laboratory, we have direct access to the intensity of the beam. This measure gives us access to the fluctuations of the amplitude quadrature of the electromagnetic field, in order to have access to the fluctuations of the phase quadrature (quadrature conjugated to the amplitude quadrature), we must use interferometric techniques. In the present case, we used the self-homodyne technique [31] where occurs the conversion of information present in phase quadrature into amplitude quadrature.

From the quantization of the electric field (discussed in the section 1.1), we have that the electric field operator is described in terms of the creation and annihilation operators that have a well defined commutation relation. The field quadratures, therefore, are written in terms of a combination of these two operators and are subject to the Heisenberg uncertainty principle. In this way, we cannot measure both with absolute precision. We say that if one quadrature has noise compression, the other quadrature will present excessive noise. The standard unit we use as a reference to know whether we have excess or noise compression is the standard quantum noise or shot-noise limit that allows us to identify intrinsically quantum system characteristics. Thus, all measurements are normalized by shot-noise.

In the following subsections we will discuss about the photocurrent operator and the electronic photocurrent operator 1.5.1. Following by the noise spectrum of the electromagnetic field 1.5.2. And the last section 1.5.3 is about the method used to measure the fluctuations in

amplitude and phase quadratures, called self-homodyne detection.

1.5.1 Photocurrent Operator

In the laboratory we measure the intensity of the light using photodiodes that work based in the photoelectric effect: in the emission of electron (photoelectrons) when light interact with the material. The mean intensity measured by the photodiode is proportional to the autocorrelation Glauber function [23]:

$$\langle \hat{I}(\mathbf{r},t)\rangle = \langle \hat{E}^{-}(\mathbf{r},t)\hat{E}^{\dagger}(\mathbf{r},t)\rangle\,, \tag{1.35}$$

where $\hat{I}$ is the photocurrent operator, $\langle\hat{O}\rangle$ is the expectation value computed in the initial state of the field $\hat{\rho}$, the non-hermitian operators $\hat{E}^{-}(t) = (\hat{E}^{+}(t))^{\dagger}$ are related with the process of creation(emission) and annihilation(absorption) of photons and $\mathbf{r}$ is the position of the detector (we will consider for the next calculations that we are in the detector's reference frame, so $|\mathbf{r}| = 0$). The positive frequency operator is described by:

$$\hat{E}^{+}(\mathbf{r},t) = \sum_{\kappa} \varepsilon_{\kappa}\hat{a}_{\kappa}e^{i(\mathbf{k}.\mathbf{r}-\omega_k t)}. \tag{1.36}$$

The kind of states that we have access in laboratory represent a bright beam with a well defined carrier frequency ω_0 and a continuous of quantum modes with an unknown state that we would like to measure. The carrier mode is represented by a coherent state $|\alpha_{\omega_0}\rangle$ with an amplitude given by $\alpha = |\alpha|e^{i\theta}$ in Hilbert space of the carrier $\mathcal{H}_p$. The unknown states are $|\psi\rangle$ and the Hilbert space of the sidebands $\mathcal{H}_{sb}$, in such a way that the global state and the global Hilbert space $\mathcal{H}$ are given by:

$$|\Psi\rangle = |\alpha_{\omega_0}\rangle \otimes |\psi\rangle \qquad\qquad \mathcal{H} = \mathcal{H}_c \otimes \mathcal{H}_{sb}. \tag{1.37}$$

The measurement that we performed is insensitive to any correlation between the carrier and the sidebands, and because of that we can separate the field operator in the following parts:

$$\hat{E}^{+}(t) \;=\; \hat{E}^{+}_{c}(t) + \hat{E}^{+}_{sb}(t). \tag{1.38}$$

Our goal now is to compute the mean average of the photocurrent given in Equation 1.35 in the state of Equation 1.37:

$$\begin{aligned}\langle \hat{I}(t)\rangle &= \langle\psi|\langle\alpha_{\omega_0}|\,\hat{E}^{-}\hat{E}^{+}(t)\,|\alpha_{\omega_0}\rangle\,|\psi\rangle \\ &= \langle \hat{E}^{-}_{c}(t)\hat{E}^{+}_{c}(t)\rangle + \langle \hat{E}^{-}_{c}(t)\hat{E}^{+}_{sb}(t)\rangle + \langle \hat{E}^{-}_{sb}(t)\hat{E}^{+}_{c}(t)\rangle + \langle \hat{E}^{-}_{sb}(t)\hat{E}^{+}_{sb}(t)\rangle\,.\end{aligned} \tag{1.39}$$

In the Equation 1.39 we will expand the first two terms in order to show how we compute them, remembering that $\hat{a}_{\omega'}\,|\alpha_{\omega_0}\rangle = \delta(\omega_0 - \omega')\alpha\,|\alpha_{\omega_0}\rangle$ and that $\omega(\omega')$ contain all frequencies to be

analyzed, including the carrier. The first term that we will analyze contain only the operators of the carrier:

1.

$$\begin{aligned}
\langle \hat{E}_c^-(t)\hat{E}_c^+(t)\rangle &= \langle\psi|\langle\alpha_{\omega_0}| \int d\omega e^{i\omega t}\hat{a}_\omega^\dagger \int d\omega' e^{-i\omega' t}\hat{a}_{\omega'} |\alpha_{\omega_0}\rangle |\psi\rangle \\
&= \langle\psi|\langle\alpha_{\omega_0}| \int d\omega e^{i\omega t}\delta(\omega_0-\omega)\alpha \int d\omega' e^{-i\omega' t}\delta(\omega_0-\omega')\alpha |\alpha_{\omega_0}\rangle |\psi\rangle \\
&= e^{i\omega_0 t}\alpha^* e^{-i\omega_0 t}\alpha \\
\langle \hat{E}_c^-(t)\hat{E}_c^+(t)\rangle &= |\alpha|^2. \qquad (1.40)
\end{aligned}$$

And in the second one it contains one operator related with the carrier and another with the sidebands:

2.

$$\begin{aligned}
\langle \hat{E}_c^-(t)\hat{E}_{sb}^+(t)\rangle &= \langle\psi|\langle\alpha_{\omega_0}| \int_c d\omega e^{i\omega t}\hat{a}_\omega^\dagger \int_{sb} d\omega' e^{-i\omega' t}\hat{a}_{\omega'} |\alpha_{\omega_0}\rangle |\psi\rangle \\
&= e^{i\omega_0 t}\alpha^* \langle\psi| \int_{sb} d\omega' e^{-i\omega' t}\hat{a}_{\omega'} |\psi\rangle \\
&= |\alpha| e^{-i\theta} \langle\psi| \int_{sb} d\omega' e^{-i(\omega'-\omega_0)t}\hat{a}_{\omega'} |\psi\rangle . \qquad (1.41)
\end{aligned}$$

Only the terms in first order in the sideband operators will be relevant, due the fact that $\langle\alpha_{\omega_0}|\hat{a}_{\omega_0}^\dagger\hat{a}_{\omega_0}|\alpha_{\omega_0}\rangle \gg \langle\psi_\omega|\hat{a}_\omega^\dagger\hat{a}_\omega|\psi_\omega\rangle$. Using the terms above (Equation 1.40 and Equation 1.41) and remembering that the carrier frequency is not considered in the measurement, so the photocurrent operation is explicitly given by:

$$\langle\hat{I}(t)\rangle \approx |\alpha|^2 + |\alpha| \langle\psi| (e^{-i\theta}\int^{\omega\neq\omega_0} d\omega' e^{-i(\omega'-\omega_0)t}\hat{a}_{\omega'} + e^{i\theta}\int^{\omega\neq\omega_0} d\omega' e^{i(\omega'-\omega_0)t}\hat{a}_{\omega'}^\dagger) |\psi\rangle . \qquad (1.42)$$

The first term in the Equation 1.42 represents the mean value of the field and in the photodetection process we call this the DC (signal related with low frequencies) part. The second term is related with the sidebands that are amplified by the carrier amplitude, these are the terms that we would like to measure in the laboratory and is called the HF (signal related with high frequencies) part. Let us write the Equation 1.42 in a more compact way. First, we will replace the integral in the above equation for the bosonic operators:

$$\hat{a}(t) = \int' d\omega e^{-i(\omega-\omega_0)t}\hat{a}_\omega \qquad \hat{a}^\dagger(t) = \int' d\omega e^{i(\omega-\omega_0)t}\hat{a}_\omega^\dagger, \qquad (1.43)$$

where the integral is performed in all frequencies with the exception of the carrier frequency,

represented by the symbol $'$ in Equation 1.43. We obtain a compact form to write the photocurrent:

$$\begin{aligned}\langle\hat{I}(t)\rangle &= |\alpha|^2 + |\alpha|\langle\psi|e^{-i\theta}\hat{a}(t) + e^{i\theta}\hat{a}^\dagger(t)|\psi\rangle, \\ \langle\hat{I}(t)\rangle &= |\alpha|^2 + |\alpha|\langle\delta\hat{I}_\theta(t)\rangle, \quad where \quad \delta\hat{I}_\theta(t) = e^{-i\theta}\hat{a}(t) + e^{i\theta}\hat{a}^\dagger(t).\end{aligned} \tag{1.44}$$

We will rewrite the operators in the equation Equation 1.43 in terms of frequency $\Omega = \omega - \omega_0$ with the goal to explicitate the dependence in terms of the sideband frequency $\hat{a}(t) = \int_{-\infty}^{\infty} d\omega e^{-i\Omega t}\hat{a}_{\omega_0+\Omega}$ and $\hat{a}^\dagger(t) = \int_{-\infty}^{\infty} d\Omega e^{i\Omega t}\hat{a}^\dagger_{\omega_0+\Omega}$. Replacing these operators in the Equation 1.44 we have:

$$\delta\hat{I}_\theta(t) = e^{-i\theta}\int_{-\infty}^{\infty} d\Omega e^{-i\Omega t}\hat{a}_{\omega_0+\Omega} + e^{i\theta}\int_{-\infty}^{\infty} d\Omega e^{i\Omega t}\hat{a}^\dagger_{\omega_0+\Omega}. \tag{1.45}$$

In order to reduce the notation we will replace $\omega_0 + \Omega \to \Omega$ and we will change the integration limits in order to write the integral in terms of $\pm\Omega$:

$$\delta\hat{I}_\theta(t) = \int_0^{\infty} d\Omega\left[e^{-i\Omega t}\left(e^{-i\theta}\hat{a}_\Omega + e^{i\theta}\hat{a}^\dagger_{-\Omega}\right) + e^{i\Omega t}\left(e^{-i\theta}\hat{a}_{-\Omega} + e^{i\theta}\hat{a}^\dagger_\Omega\right)\right] \tag{1.46}$$

The approach used in this section was based in the reference [31] and more details can be seen in the thesis [1, 32].

Spectral photocurrent fluctuations

Now, we have explicitly in terms of the sidebands the photocurrent acquired by the photodector. The spectral resolution is achieved doing the Fourier transform of $\delta\hat{I}(t)$. To perform this experimentally, the output of the phodetector is sent to a demodulation circuit where the photocurrent Equation 1.45 will be mixed to an electronic oscillator (eLO) with a frequency Ω_{af}, known as analysis frequency. The resulting signal will pass through a low pass filter that will have a bandwidth. Therefore, the output current will change in a time scale with the inverse of this bandwidth. The electronic oscillator will be represented by a photocurrent as:

$$\delta I_{af}(t) = I_{af}e^{i\Omega_{af}t} + I^*_{af}e^{-i\Omega_{af}t} \tag{1.47}$$

After passing through the mixer, the resulting signal is given by:

$$\begin{aligned}\hat{I}_{mix} &= \delta\hat{I}_\theta(t)\delta I_{af}(t) \\ &= e^{-i\theta}\int_{-\infty}^{\infty} d\Omega' e^{-i(\Omega'-\Omega_{af})t}\hat{a}_{\Omega'}I_{af} + e^{i\theta}\int_{-\infty}^{\infty} d\Omega' e^{i(\Omega'-\Omega_{af})t}\hat{a}^\dagger_{\Omega'}I^*_{af} \\ &+ e^{-i\theta}\int_{-\infty}^{\infty} d\Omega' e^{-i(\Omega'+\Omega_{af})t}\hat{a}_{\Omega'}I^*_{af} + e^{i\theta}\int_{-\infty}^{\infty} d\Omega' e^{i(\Omega'+\Omega_{af})t}\hat{a}^\dagger_{\Omega'}I_{af}.\end{aligned} \tag{1.48}$$

Here we will integrate in the time domain that will represent the resulting signal after passing the low pass filter:

$$\begin{aligned}\hat{I}_{out} &= \int_{-\infty}^{\infty} dt \hat{I}_{mix} \\ &= e^{-i\theta}\int_{-\infty}^{\infty} d\Omega^{'}\hat{a}_{\Omega^{'}} I_{af}\delta(\Omega^{'}-\Omega_{af}) + e^{i\theta}\int_{-\infty}^{\infty} d\Omega^{'}\hat{a}^{\dagger}_{\Omega^{'}} I^{*}_{af}\delta(\Omega^{'}-\Omega_{af}) \\ &+ e^{-i\theta}\int_{-\infty}^{\infty} d\Omega^{'}\hat{a}_{\Omega^{'}} I^{*}_{af}\delta(\Omega^{'}+\Omega_{af}) + e^{i\theta}\int_{-\infty}^{\infty} d\Omega^{'}\hat{a}^{\dagger}_{\Omega^{'}} I_{af}\delta(\Omega^{'}+\Omega_{af}) \end{aligned} \tag{1.49}$$

The output current after the demodulation process is given by:

$$\hat{I}_{out} = (e^{-i\theta}\hat{a}_{\Omega_{af}} + e^{i\theta}\hat{a}^{\dagger}_{-\Omega_{af}})I_{af} + (e^{i\theta}\hat{a}^{\dagger}_{\Omega_{af}} + e^{i\theta}\hat{a}_{-\Omega_{af}})I^{*}_{af}, \tag{1.50}$$

where we can identify the spectral component of the photocurrent :

$$\hat{I}_{\Omega} = e^{-i\theta}\hat{a}_{\Omega} + e^{i\theta}\hat{a}^{\dagger}_{-\Omega}. \tag{1.51}$$

We see that the photocurrent ($\hat{I}^{\dagger}_{\Omega} = \hat{I}_{-\Omega}$) is a non-hermitian operator with frequency Ω defined by the electronic local oscillator. Another way to express Equation 1.50 is expliciting the complex amplitude $I_{af} = |\mathcal{A}|e^{i\phi}$ and separating the equation in real and imaginary parts:

$$\begin{aligned}\hat{I}_{out} &= |\mathcal{A}|\left[\cos\phi(e^{-i\theta}\hat{a}_{\Omega} + e^{i\theta}\hat{a}^{\dagger}_{-\Omega} + e^{i\theta}\hat{a}^{\dagger}_{\Omega} + e^{-i\theta}\hat{a}_{-\Omega})\right] \\ &+ |\mathcal{A}|\left[i\sin\phi(e^{-i\theta}\hat{a}_{\Omega} + e^{i\theta}\hat{a}^{\dagger}_{-\Omega} - e^{i\theta}\hat{a}^{\dagger}_{\Omega} - e^{-i\theta}\hat{a}_{-\Omega})\right]. \end{aligned} \tag{1.52}$$

Let us write this operator in term of two observables $\hat{I}_{\sin}$ and $\hat{I}_{\cos}$ and in terms of the hermitian quadratures $\hat{p}_{\Omega} = \hat{a}_{\Omega} + \hat{a}^{\dagger}_{\Omega}$ and $\hat{q}_{\Omega} = -i(\hat{a}_{\Omega} - \hat{a}^{\dagger}_{\Omega})$ operators described in terms of the upper (Ω) and lower ($-\Omega$) sidebands:

$$\begin{aligned}\hat{I}_{cos} &= \cos\theta(\hat{p}_{\Omega} + \hat{p}_{-\Omega}) + \sin\theta(\hat{q}_{\Omega} + \hat{q}_{-\Omega}) \\ \hat{I}_{sin} &= \cos\theta(\hat{q}_{\Omega} - \hat{q}_{-\Omega}) - \sin\theta(\hat{p}_{\Omega} - \hat{p}_{-\Omega}), \end{aligned} \tag{1.53}$$

where $\hat{I}_{\Omega} = \hat{I}_{cos} + i\hat{I}_{sin}$ and $[\hat{I}_{cos}, \hat{I}_{sin}] = 0$.

We can see in Equation 1.53 that the hermitian field operators are written in a symmetric and antisymmetric combination of the sidebands quadratures operators. We can rewrite this equation in the symmetric and antisymmetric basis, where we recognize:

$$\begin{aligned}\hat{I}_{cos} &= \cos\theta\hat{p}_s + \sin\theta\hat{q}_s = \hat{X}^{\theta}_{s} \\ \hat{I}_{sin} &= \cos\theta\hat{q}_a - \sin\theta\hat{p}_a = \hat{X}^{\theta+\frac{\pi}{2}}_{a}, \end{aligned} \tag{1.54}$$

that are combination associated with homodyne detection[31]. The component $\hat{I}_{cos}$ refers to the symmetric mode and the component $\hat{I}_{sin}$ to the antisymmetric mode, where the quadratures operators in the sidebands are related with them in symmetric (s) and antisymmetric (a) combination as:

$$\hat{p}_{s/a} = \frac{\hat{p}_{\Omega} \pm \hat{p}_{-\Omega}}{\sqrt{2}} \qquad \hat{q}_{s/a} = \frac{\hat{q}_{\Omega} \pm \hat{q}_{-\Omega}}{\sqrt{2}}. \tag{1.55}$$

To measure the signals in Equation 1.54 we can perform a experimental situation like in the figure 1.3 where we mix the photocurrent with two electronic signal that are in quadratures:

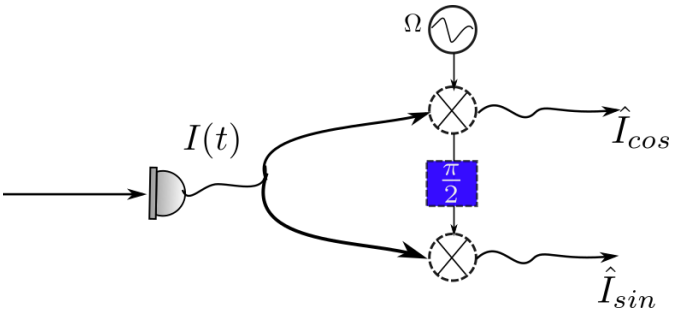

Figure 1.3: Schematic representation of how to acquire the photocurrents $\hat{I}_{cos}$ and $\hat{I}_{sin}$. We combine the output signal from the photodetection with two electronic local oscillator with frequency Ω and phase difference of $\pi/2$.

1.5.2 Noise spectrum

To characterize the fluctuations of the light we will use the photocurrent autocorrelation function $C_i(t, t')$ between times t and t':

$$C_i(t, t') = \langle i(t) i(t') \rangle - \langle i(t) \rangle \langle i(t') \rangle . \tag{1.56}$$

In the frequency domain, we will compute the noise spectral density of the photocurrent. For a stationary process:

$$S_i(\Omega) = \int_{-\infty}^{\infty} C_i(\tau) e^{i\Omega\tau} d\tau. \tag{1.57}$$

In the stationary process the autocorrelation function depends only of the difference $\tau = t - t'$. Let us define the photocurrent as $i(t) = \langle i(t) \rangle + \delta i(t)$, a mean value plus a fluctuation term. The noise power for the photocurrent fluctuations can be defined as the Fourier transformation of the photocurrent:

$$\delta i(\Omega) = \int_{-\infty}^{\infty} \delta i(t) e^{i\Omega t} dt \qquad \delta i(t) = \int_{-\infty}^{\infty} \delta i(\Omega) e^{-i\Omega t} \frac{d\Omega}{2\pi}. \tag{1.58}$$

According to the Wiener-Khintchine [33] theorem, we can write the noise spectrum in the frequency domain as:

$$\begin{aligned}\langle \delta i(\Omega)\delta i(\Omega')^* \rangle &= \langle \int_{-\infty}^{\infty} dt e^{i\Omega t}\delta i(t) \int_{-\infty}^{\infty} dt' e^{-i\Omega t'}\delta i(t') \rangle \\ &= \int_{-\infty}^{\infty} d\tau C(\tau) e^{i\Omega'\tau} \int_{-\infty}^{\infty} dt e^{it(\Omega-\Omega')} \\ &= S(\Omega) 2\pi\delta(\Omega-\Omega'). \end{aligned} \tag{1.59}$$

If we would like to compute the noise spectrum of a quantum operator $\hat{O}$, we will replace the random variable $i(t)$ by an Hermitian operator and the classical mean value by a quantum mean value. In this context, we can write the Wiener-Khintchine theorem as:

$$2\pi\delta(\Omega-\Omega')S_{\hat{X}_\theta}(\Omega) = \langle \delta\hat{X}_\theta(\Omega)\delta\hat{X}_\theta(\Omega')\rangle, \tag{1.60}$$

where $\delta\hat{X}_\theta(\Omega)$ represents a general quadrature of the field. The noise spectrum is proportional to the variance of the generalized quadrature and is represented by a noise ellipse in the complex plane. If $\theta = \phi$, we have the noise spectrum of the amplitude quadrature and if $\theta = \phi + \frac{\pi}{2}$, the noise spectrum of phase quadrature. In the Fresnel plane the representation of phase and amplitude quadratures is given in the figure 1.4, where we can see that aligned with the mean field we have the amplitude quadrature represented by $\delta\hat{p}$ and in quadrature, the phase quadrature represented by $\delta\hat{q}$.

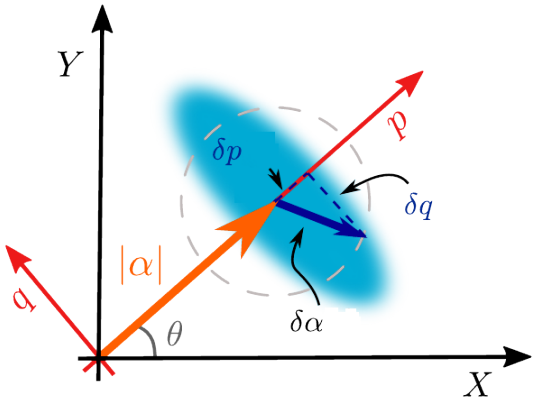

Figure 1.4: Schematic representation of the noise ellipse. When the quadrature $\delta\hat{X}_\theta(\Omega)$ is aligned with the mean field, it is called amplitude quadrature and it is represented by $\delta\hat{p}$, and in quadrature the phase quadrature represented by $\delta\hat{q}$.

Stationarity aspects

The stationarity condition implies that Equation 1.60 becomes:

$$\begin{aligned} S(\Omega) &= \langle \hat{I}_\Omega \hat{I}_{-\Omega} \rangle , \\ \langle \hat{I}_\Omega \hat{I}_{\Omega'} \rangle &= 0 \qquad \forall \qquad \Omega' \neq -\Omega. \end{aligned} \tag{1.61}$$

Computing this for the photocurrent operator $\hat{I}_\Omega = \frac{i\hat{I}_{\text{sin}} + \hat{I}_{\text{cos}}}{2}$, we have:

$$\langle \hat{I}_\Omega \hat{I}_{-\Omega} \rangle = \frac{1}{2} \langle \hat{I}^2_{cos} \rangle + \frac{1}{2} \langle \hat{I}^2_{sin} \rangle \tag{1.62}$$

and,

$$\langle \hat{I}_\Omega \hat{I}_\Omega \rangle = 0 \rightarrow \begin{cases} \Delta^2 \hat{I}_{cos} - \Delta^2 \hat{I}_{sin} = 0 \\ \langle \hat{I}_{\text{cos}} \hat{I}_{\text{sin}} \rangle = 0. \end{cases} \tag{1.63}$$

In the next section we will see how we measure both quadratures, phase and amplitude and, how we write the covariance matrix of a set of data.

1.5.3 Noise ellipse rotation - measuring the quadratures of the field

In order to have an overall knowledge of the system under study, we must have access to the fluctuations of the amplitude and phase quadratures. We have seen that the fluctuation in amplitude quadrature is in the direction of the mean value of the field in the Fresnel representation (see figure 1.4), that we can acquire using photodetectors. However, in order to have access to the fluctuations in phase quadrature, we need interferometric methods. In our case, we will use the self-homodyne technique, which consists in using an empty optical cavity that causes the rotation of the noise ellipse, that is, it allows the conversion of phase fluctuations to amplitude fluctuations. Our interest is to know how the cavity affects the field fluctuations and what is the noise spectrum of the beam reflected by this cavity. This work was first analyzed by [34] and is well detailed in references of the group [22, 35, 31].

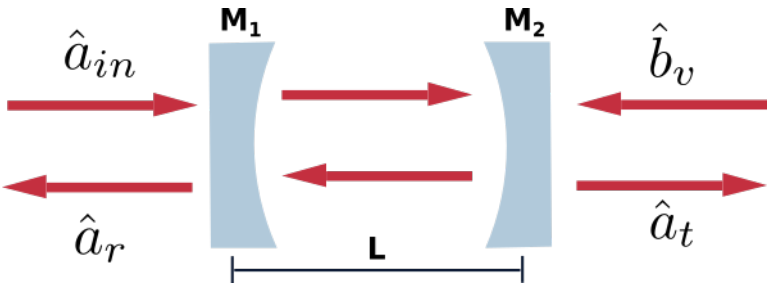

Figure 1.5: Representation of the fields in the empty cavity.

An empty cavity acts in the annihilation operator as:

$$\hat{a}_\omega \rightarrow r(\Delta_\omega)\hat{a}_\omega + t(\Delta_\omega)\hat{b}_\omega, \tag{1.64}$$

where $\hat{a}_\omega$ is the field operator, $\hat{b}_\omega$ is the vacuum operator, $\Delta_\omega = \frac{\omega-\omega_c}{BW}$ is the detuning normalized by the bandwidth (BW) of the cavity, $t(\Delta_\omega) = \sqrt{1-r^2(\Delta_\omega)}$ and ω_c is the resonance frequency of the cavity. For a high finesse cavity close to resonance, we can write the reflection coefficient as:

$$r(\Delta_\omega) = -\frac{\sqrt{R_{min}} + 2i\Delta_\omega}{1-2i\Delta_\omega} \qquad \text{where} \quad \sqrt{R_{min}} = \frac{\sqrt{R_1}-\sqrt{R_2}}{1-\sqrt{R_1R_2}}, \tag{1.65}$$

where R_{min} is the minimum reflexion of the cavity and R_i are the reflection coefficients of each mirror that composes the cavity. We saw in the subsection 1.5.1 that the photocurrent operator is defined as $\hat{I}_\Omega = e^{-i\theta}\hat{a}_\Omega + e^{i\theta}\hat{a}^\dagger_{-\Omega}$ where $\hat{a}_\Omega = \hat{a}_{\omega_0+\Omega}$ and $\hat{a}_{-\Omega} = \hat{a}_{\omega_0-\Omega}$, replacing Equation 1.64 in the photocurrent operator $\hat{I}_\Omega$ we have:

$$\hat{I}_\Omega = e^{-i\theta}(r(\Delta_\Omega)\hat{a}_\Omega + t(\Delta_\Omega)\hat{b}_\Omega) + e^{i\theta}(r^*(\Delta_{-\Omega})\hat{a}^\dagger_{-\Omega} + t^*(\Delta_{-\Omega})\hat{b}^\dagger_{-\Omega}), \tag{1.66}$$

the phase $e^{-i\theta}$ is related with carrier mode and defined as $e^{-i\theta} = \frac{r^*(\Delta)}{|r(\Delta)|}$ and $r(\Delta_{\pm\Omega}) = r(\Delta \pm \Omega)$. Let us define the quantities:

$$R_\Omega(\Delta) = \frac{r^*(\Delta)}{|r(\Delta)|}r(\Delta+\Omega) \qquad T_\Omega(\Delta) = \frac{r^*(\Delta)}{|r(\Delta)|}t(\Delta+\Omega). \tag{1.67}$$

Our point here is to write the photocurrent operator of the self-homodyne detection as a function of the observables photocurrent $\hat{I}_{\sin}$ and $\hat{I}_{\cos}$. In order to do this we will write the photocurrent operator in terms of the symmetric (s) and antisymmetric (a) basis as defined in Equation 1.55 and in function of the quantities:

$$\begin{aligned} g_+ &= x_+ + iy_+ = \frac{R_\Omega(\Delta) + R^*_{-\Omega}(\Delta)}{2}, \\ g_- &= x_- + iy_- = \frac{i(R_\Omega(\Delta) - R^*_{-\Omega}(\Delta))}{2}. \end{aligned} \tag{1.68}$$

Replacing equations 1.68 and 1.67 in 1.66, we are able to write the photocurrent operator as:

$$\begin{aligned} \hat{I}_\Omega &= \frac{1}{\sqrt{2}}\left[(x_+\hat{p}_s + x_-\hat{q}_s + y_-\hat{p}_a - y_+\hat{q}_a) + i(y_+\hat{p}_s + y_-\hat{q}_s - x_-\hat{p}_a + x_+\hat{q}_a)\right], \\ &+ \frac{1}{\sqrt{2}}\left[(x^v_+\hat{p}^v_s + x^v_-\hat{q}^v_s + y^v_-\hat{p}^v_a - y^v_+\hat{q}^v_a) + i(y^v_+\hat{p}^v_s + y^v_-\hat{q}^v_s - x^v_-\hat{p}^v_a + x^v_+\hat{q}^v_a)\right], \end{aligned} \tag{1.69}$$

where we identify the general experession $\hat{I}_\Omega = \frac{(\hat{I}_{cos}+i\hat{I}_{sin})}{\sqrt{2}} + \hat{I}_v$:

$$\begin{aligned}\hat{I}_{cos} &= x_+\hat{p}_s + x_-\hat{q}_s + y_-\hat{p}_a - y_+\hat{q}_a, \\ \hat{I}_{sin} &= y_+\hat{p}_s + y_-\hat{q}_s - x_-\hat{p}_a + x_+\hat{q}_a,\end{aligned} \tag{1.70}$$

and the same for the noise contribution from the vacuum $\hat{I}_v$ with the vacuum operators. We can see that each hermitian component depends on both symmetric and antisymmetric basis what made us able to reconstruct the complete quantum tomography of the system.

1.5.4 Covariance Matrix

The knowledge of the covariance matrix of our system is sufficient for us have the quantum tomography of our states due the fact that we are working with fluctuations of the field and our states are Gaussian. In this section we will show the covariance matrix for one single beam and for two beams in the symmetric and antisymmetric basis, as well as in the sideband basis.

Covariance matrix of a single beam

The measurement that we performed are direct related to the symmetric (s) and antisymmetric (a) basis, the vector that represent the quadratures in this basis for one mode is $\hat{\mathbf{x}} = (\hat{p}_s, \hat{q}_s, \hat{p}_a, \hat{q}_a)$, using Equation 1.31 we can write the covariance matrix in $\mathcal{S}/\mathcal{A}$ basis as:

$$\mathbf{V}_{s/a} = \begin{pmatrix} \Delta^2\hat{p}_s & C(\hat{p}_s\hat{q}_s) & C(\hat{p}_s\hat{p}_a) & C(\hat{p}_s\hat{q}_a) \\ & \Delta^2\hat{q}_s & C(\hat{q}_s\hat{p}_a) & C(\hat{q}_s\hat{q}_a) \\ & & \Delta^2\hat{p}_a & C(\hat{p}_a\hat{q}_a) \\ & & & \Delta^2\hat{q}_a \end{pmatrix}. \tag{1.71}$$

Where the terms can be derived from the condition given by Equation 1.54:

$$\mathbf{V}_{s/a} = \begin{pmatrix} \alpha & \gamma & \delta & 0 \\ \gamma & \beta & 0 & \delta \\ \delta & 0 & \beta & -\gamma \\ 0 & \delta & -\gamma & \alpha \end{pmatrix}. \tag{1.72}$$

It is interesting to note that the difference between the symmetric and antisymmetric matrix is a rotation of $\frac{\pi}{2}$ in one of the modes. To write the covariance matrix in the upper and lower

sidebands it is necessary to perform the following transformation:

$$\mathbf{\Lambda} = \begin{pmatrix} \frac{1}{\sqrt{2}} & 0 & \frac{1}{\sqrt{2}} & 0 \\ 0 & \frac{1}{\sqrt{2}} & 0 & \frac{1}{\sqrt{2}} \\ \frac{1}{\sqrt{2}} & 0 & -\frac{1}{\sqrt{2}} & 0 \\ 0 & \frac{1}{\sqrt{2}} & 0 & -\frac{1}{\sqrt{2}} \end{pmatrix}. \tag{1.73}$$

The covariance matrix in the sideband are given by:

$$\mathbf{V}_{\pm\Omega} = \mathbf{\Lambda}^T.\mathbf{V}_{s/a}.\mathbf{\Lambda}. \tag{1.74}$$

Two beams covariance matrix

Where we are evaluating the noise spectrum of two beams, the vector that will define the covariance matrix is composed of two modes $\hat{\mathbf{x}} = (\hat{p}_{1s}, \hat{q}_{1s}, \hat{p}_{2s}, \hat{q}_{2s}, \hat{p}_{1a}, \hat{q}_{1a}, \hat{p}_{2a}, \hat{q}_{2a})$, given by:

$$\mathbf{V}_{s/a} = \begin{pmatrix} \mathbf{V}_s^{(12)} & \mathbf{C}_{s/a}^{(12)} \\ \mathbf{C}_{s/a}^{(12)T} & \mathbf{V}_a^{(12)} \end{pmatrix}. \tag{1.75}$$

Due the stationarity conditions given in Equation 1.61 the symmetric part and the correlations between the symmetric and antisymmetric operators are given by:

$$\mathbf{V}_s^{(12)} = \begin{pmatrix} \alpha^{(1)} & \gamma^{(1)} & \mu & \epsilon \\ \gamma^{(1)} & \beta^{(1)} & \zeta & \nu \\ \mu & \zeta & \alpha^{(2)} & \gamma^{(2)} \\ \epsilon & \nu & \gamma^{(2)} & \beta^{(2)} \end{pmatrix}, \qquad \mathbf{C}_{s/a}^{(12)} = \begin{pmatrix} \delta^{(1)} & 0 & \kappa & -\eta \\ 0 & \delta^{(1)} & \tau & -\lambda \\ -\lambda & \eta & \delta^{(2)} & 0 \\ -\tau & \kappa & 0 & \delta^{(2)} \end{pmatrix}, \tag{1.76}$$

the antisymmetric basis is equal to the symmetric basis up to a local basis rotation.

1.5.5 Noise spectrum - reconstruction of the quantum state of one beam

Now, we would like to compute the noise spectrum of one beam reconstructed by the analysis cavity. In that case, the Equation 1.60 becomes:

$$\begin{aligned} S_{RD}(\Omega) &= \langle \hat{I}_\Omega \hat{I}_{-\Omega} \rangle \\ &= \frac{1}{2}\Delta^2 \hat{I}_{cos} + \frac{1}{2}\Delta^2 \hat{I}_{sin} + \frac{1}{2}\Delta^2 \hat{I}_v. \end{aligned} \tag{1.77}$$

To compute this terms we will need to write the variances of the photocurrent operator given in Equation 1.70 using the coefficients of the Equation 1.68. After this calculation, one will

find:

$$S_{RD} = \alpha c_\alpha + \beta c_\beta + \gamma c_\gamma + \delta c_\delta + c_v, \tag{1.78}$$

where the coefficients $|g_+|^2 = c_\alpha$, $|g_-|^2 = c_\beta$, $2g_+^* g_- = c_\gamma + ic_\delta$ and $c_v = 1 - c_\alpha - c_\beta$.

In the figure 1.6 we can see how is the behavior of each coefficient of the Equation 1.78.

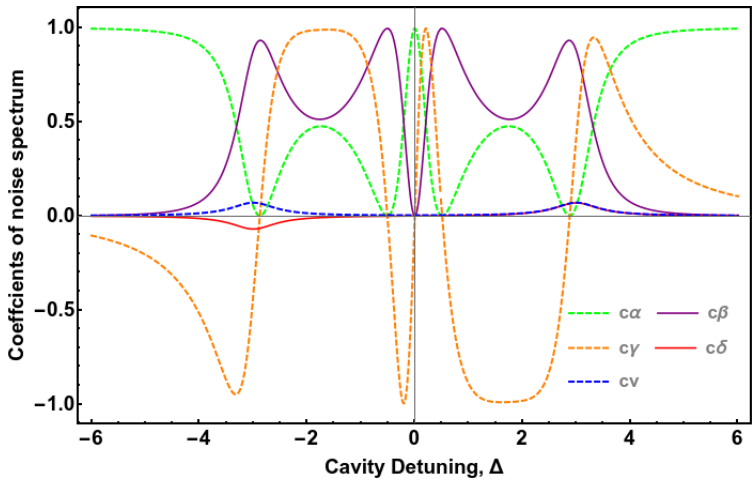

Figure 1.6: Coefficients of the noise spectrum in function of Δ. Parameters $R_{min} = 0.86$ and $\Omega' = 3$.

The coefficient c_α is related with the amplitude quadrature and c_β with the phase quadrature. Our main purpose is convert phase noise in amplitude noise in the output of the cavity and that can be seen in the figure 1.6. For $\Delta \approx -3$ we have the maximum of the coefficient c_β while c_α is zero. The term c_γ is related with the part real of the cross correlation between these coefficients g_+ and g_- and close to the detuning related with the conversion of phase in amplitude, where this coefficient change to the minimum value to the maximum value crossing the zero in the point of the conversion. It is also perceptible that this term is related with a small detuning in relation with the resonance of the carrier. The term c_δ is related with the imaginary part of the coefficient $g_+^* g_-$ that is responsible to access the term δ in the covariance matrix, we can see that this term is null close to the resonance with the carrier, but it has a small value when the cavity is in resonance with each sideband. In this case, when the cavity is in resonance with each sideband, part of the light is transmitted by the cavity. The coefficient c_v is the vacuum contribution due the losses in the system.

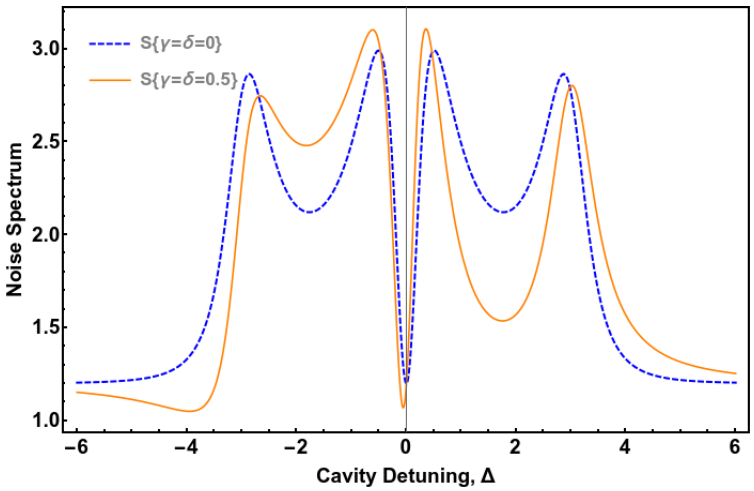

Figure 1.7: a) Noise spectrum of one beam in function of Δ. Parameters $R_{min} = 0.86$ and $\Omega^{'} = 3$.

In the figure 1.7 we have the noise ellipse rotation of one beam. In blue we are considering that the terms γ and δ are nulls. In this case, we can see that far from zero detuning we have the information about the amplitude quadrature related with the term α in the Equation 1.78 where we used in this simulation $\alpha = 1.2$, close to the resonance with each sideband, there are the conversion of the quadrature amplitude in phase, the value of the variance of the phase quadrature is given by the term β and we used here $\beta = 3$. The noise spectrum considering the effect of the terms γ e δ are shown in the orange curve. The term γ represents a correlation between the phase and amplitude quadrature of the analyzed field and the presence of this correlation can be identified by a small detuning displacement of the resonance of the carrier. The parameter δ represents a energy imbalance between the sidebands, that we can see in the orange curve of the figure 1.7 a difference in the high of each sideband peak (close to $\Delta \approx \pm 3$).

1.5.6 Noise spectrum - reconstruction of the quantum state - generalization for two beams

To reconstruct the quantum state of our system, we need to characterize the correlations between the three beams in the symmetric and antisymmetric combination. To perform this characterization we need to know the noise spectrum of each bipartition. The correlations between two different beams is given by:

$$\begin{aligned} \langle \hat{I}_{\Omega}^{(1)} \hat{I}_{-\Omega}^{(2)} \rangle &= \frac{1}{2} \langle (\hat{I}_{cos}^{(1)} + i\hat{I}_{sin}^{(1)})(\hat{I}_{cos}^{(2)} - i\hat{I}_{sin}^{(2)}) \rangle \\ &= \frac{1}{2} \left[\langle \hat{I}_{cos}^{(1)} \hat{I}_{cos}^{(2)} \rangle + \langle \hat{I}_{sin}^{(1)} \hat{I}_{sin}^{(2)} \rangle + i(\langle \hat{I}_{sin}^{(1)} \hat{I}_{cos}^{(2)} \rangle - \langle \hat{I}_{cos}^{(1)} \hat{I}_{sin}^{(2)} \rangle) \right], \end{aligned} \tag{1.79}$$

where we can see that is possible to separate in the real and imaginary parts:

$$\begin{aligned} Re\{\langle \hat{I}_{\Omega}^{(1)} \hat{I}_{-\Omega}^{(2)} \rangle\} &= \frac{1}{2}\left[\langle \hat{I}_{cos}^{(1)} \hat{I}_{cos}^{(2)} \rangle + \langle \hat{I}_{sin}^{(1)} \hat{J}_{sin}^{(2)} \rangle\right], \\ Im\{\langle \hat{I}_{\Omega}^{(1)} \hat{I}_{-\Omega}^{(2)} \rangle\} &= \frac{1}{2}\left[\langle \hat{I}_{sin}^{(1)} \hat{I}_{cos}^{(2)} \rangle - \langle \hat{I}_{cos}^{(1)} \hat{I}_{sin}^{(2)} \rangle\right]. \end{aligned} \tag{1.80}$$

Applying the stationarity conditions:

$$\begin{aligned} \langle \hat{I}_{cos}^{(1)} \hat{I}_{cos}^{(2)} \rangle &= \langle \hat{I}_{sin}^{(1)} \hat{I}_{sin}^{(2)} \rangle, \\ \langle \hat{I}_{sin}^{(1)} \hat{I}_{cos}^{(2)} \rangle &= -\langle \hat{I}_{cos}^{(1)} \hat{I}_{sin}^{(2)} \rangle. \end{aligned} \tag{1.81}$$

We obtain for the real and imaginary part of the correlation between two beams:

$$\begin{aligned} Re\{\langle \hat{I}_{\Omega}^{(1)} \hat{I}_{\Omega}^{(2)} \rangle\} &= \mu c_{\mu} + \epsilon c_{\epsilon} - \kappa c_{\kappa} - \eta c_{\eta} + \zeta c_{\zeta} + \nu c_{\nu} - \tau c_{\tau} - \lambda c_{\lambda}, \\ Im\{\langle \hat{I}_{\Omega}^{(1)} \hat{I}_{\Omega}^{(2)} \rangle\} &= \mu c_{\eta} + \epsilon c_{\kappa} + \kappa c_{\epsilon} - \eta c_{\mu} + \zeta c_{\lambda} + \nu c_{\tau} + \tau c_{\nu} + \lambda c_{\zeta}, \end{aligned} \tag{1.82}$$

where the coefficients $g_{pi} = g_{+,i}$ and $g_{mi} = g_{-,i}$ are the same that in Equation 1.68 for each beam ($i = \{1, 2\}$) $g_{p1}^{*} g_{p2} = c_{\mu} - i c_{\eta}$, $g_{m1}^{*} g_{m2} = c_{\nu} - i c_{\tau}$, $g_{p1}^{*} g_{m2} = c_{\epsilon} - i c_{\kappa}$ and $g_{m1}^{*} g_{p2} = c_{\zeta} - i c_{\lambda}$.

To measure the correlation between the sideband of two beams we perform two kind of measurements, first we need to measure the correlations between the twin beams in a synchronous configuration. When we do this, both cavities have the same detuning and this allow us to have access to the correlations between the phase and amplitude quadratures of both beams. To have access to the cross correlation between the two beams,in other words, to have access for example to the correlation C_{ps1qa2} we need to measure the two cavities in an asynchronous way. One cavity will be detuned and the other cavity will be out of resonance. Performing this measurement we are able to reconstruct the complete covariance matrix of the two beams accessing all the terms of the matrix 1.76.

1.6 Entanglement

Entanglement was a central element in the "completeness" discussion of the quantum mechanical description in the century XX, initiated in the famous paper by Einstein, Podolsky and Rosen[9], and subsequently studied systematically by several scientists, from which we cite Bohr[10], Schrödinger [11] and Bell[12]. However, only in the last 30 years entanglement has been seen as an important tool in the development of new theoretical and experimental formulations, such as, the development of quantum computation[13, 14] and cryptography[15], entangled systems have properties such as the impossibility of treating its subsystems in an independent manner. Due to all these properties, the scientific community is constantly seeking to improve the methods for generating and controlling these systems.

As an intrinsically quantum property, entanglement is a type of correlation that occurs when the global state is non-separable. A separable state may be written(suppose a system of two subsystems):

$$\hat{\rho} = \Sigma w_A \hat{\rho}_A^1 \otimes \hat{\rho}_A^2, \tag{1.83}$$

where $\hat{\rho}_A^1$ e $\hat{\rho}_A^2$ are the subsystems density matrices. A state is said to be entangled if it cannot be written as a tensor product of its parts.

Various separability criteria in the discret and continuous variable domain were studied with the goal of finding relations that implies if a state is entangled or not. In the paper by Peres[36], it is shown a necessary and sufficient criterion of separability valid for 2⊗2 and 2⊗3 systems. This criterion was generalized for continuous variables, where it was found a criterion of separability for bipartite systems that is necessary and sufficient for all gaussian bipartite states[4]. Simultaneously to Simon's work, the criterion known as the DGCZ criterion was published by Duan et al[2], where they demonstrated a separability criterion for systems in the domain of continuous variables that based on variances calculation for a pair of EPR operators, a necessary and sufficient criterion for Gaussian states. For multipartite systems, the criterion developed by van Loock and Furusawa[3] is a necessary condition to check the separability conditions between the subsystems.

We will shall briefly describe each one of this criteria in the following subsections.

1.6.1 Bipartite Entanglement

We will describe the entanglement between bipartite combinations first using the criterion developed by Duan et al for continuous variable systems (known as DCGZ criterion), based on the sum of variances of EPR operators.

An EPR pair is composed by conjugated linear operators of two systems. In the OPO case, we are interested in the relation of the conjugated quadratures phase and amplitude, therefore we are interested in the pair:

$$\hat{p}_- = \frac{\hat{p}_1 - \hat{p}_2}{\sqrt{2}} \qquad \hat{q}_+ = \frac{\hat{q}_1 + \hat{q}_2}{\sqrt{2}}, \tag{1.84}$$

where $[\hat{p}_-, \hat{q}_+] = 0$, which implies that these can be determined with an arbitrary precision simultaneously.

The bipartite inseparability is verified computing the sum of the variances of the operators in Equation 1.84 where the average is computed in the separable density matrix $\hat{\rho}$ given in Equation 1.83:

$$\Delta^2 \hat{p}_- = \langle \hat{p}_-^2 \rangle - \langle \hat{p}_- \rangle^2, \qquad \Delta^2 \hat{q}_+ = \langle \hat{q}_+^2 \rangle - \langle \hat{q}_+ \rangle^2, \tag{1.85}$$

where we find that the sum of these two variances are given by:

$$\Delta^2\hat{p}_- + \Delta^2\hat{q}_+ = \frac{1}{2}(\Delta^2\hat{p}_1 + \Delta^2\hat{p}_2 + \Delta^2\hat{q}_1 + \Delta^2\hat{q}_2) - Corr(\hat{p}_1, \hat{p}_2) + Corr(\hat{q}_1, \hat{q}_2), \tag{1.86}$$

if $\hat{\rho}$ is separable, $Tr(\hat{p}_1\hat{p}_2\hat{\rho}) = \sum_a p_a Tr(\hat{p}_1\hat{\rho}^{(1)})Tr(\hat{p}_2\hat{\rho}^{(2)})$, which implies that $\langle\hat{p}_1\hat{p}_2\rangle = \langle\hat{p}_1\rangle\langle\hat{p}_2\rangle$, where we used that $\langle\hat{O}\rangle = Tr(\hat{O}\hat{\rho})$. With this conditions, the Equation 1.86 is:

$$\Delta^2\hat{p}_- + \Delta^2\hat{q}_+ = \frac{1}{2}(\Delta^2\hat{p}_1 + \Delta^2\hat{p}_2 + \Delta^2\hat{q}_1 + \Delta^2\hat{q}_2), \tag{1.87}$$

due the uncertainty principle, where $\Delta^2\hat{p}_j\Delta^2\hat{q}_j \geq |[\hat{p}_j, \hat{q}_j]|^2$, we can rewrite the equation above as:

$$\Delta^2\hat{p}_- + \Delta^2\hat{q}_+ \geq \frac{1}{2}(\Delta^2\hat{q}_1 + \frac{|[\hat{p}_1, \hat{q}_1]|^2}{\Delta^2\hat{q}_1} + \Delta^2\hat{q}_2 + \frac{|[\hat{p}_2, \hat{q}_2]|^2}{\Delta^2\hat{q}_2}), \tag{1.88}$$

the minimum value of $f(y) = y\gamma_1 + \frac{\gamma_2}{y}$ is equal to $y = \sqrt{\gamma_1\gamma_2}$, replacing $y = \Delta^2\hat{q}_j$, $\gamma_1 = 1$ and $\gamma_2 = |[\hat{p}_j, \hat{q}_j]|^2$, we obtain that the inequality 1.88 has the limit:

$$\Delta^2\hat{p}_- + \Delta^2\hat{q}_+ \geq 2, \tag{1.89}$$

that means if $\hat{\rho}$ is separable, the inequality above needs to be obeyed. The violation of this inequality is a sufficient condition for considering the state entangled [2].

1.6.2 Tripartite Entanglement

An extension of the DGCZ [2] criterion for continuous variables is the criterion used by Van Loock [3] for a multipartite system. In this paper they discuss the separability conditions for a system formed by an arbitrary number of parts and modes. As in the previous criteria, we are interested in knowing which states can not be written as a tensorial product of its subsystems, that is,

$$\hat{\rho}_{sep} = \Sigma_a p_a \hat{\rho}_a^{(1)} \otimes \hat{\rho}_a^{(2)} \otimes \hat{\rho}_a^{(3)} \otimes ..... \otimes \hat{\rho}_a^{(N)}, \tag{1.90}$$

condition that needs to be improved due to the possibility of describe the state using bis-separable forms [22]. For example, for the tripartite case, we have the following bisseparable forms:

$$\begin{aligned} \hat{\rho}_{bisep1} &= \Sigma\eta_n\hat{\rho}_n^{(1)} \otimes \hat{\rho}_n^{(2,3)}, \\ \hat{\rho}_{bisep2} &= \Sigma\eta_n\hat{\rho}_n^{(2)} \otimes \hat{\rho}_n^{(1,3)}, \\ \hat{\rho}_{bisep3} &= \Sigma\eta_n\hat{\rho}_n^{(3)} \otimes \hat{\rho}_n^{(1,2)}, \end{aligned} \tag{1.91}$$

where $[\hat{\rho}^{(k)} \otimes \hat{\rho}^{(i,j)}]$ means that the subsystem $\{i, j\}$ cannot be separable, but is separable from the part k. From calculations analogous to the one performed for the DGCZ criterion, we

obtain a set of inequalities that must be satisfied by the biseparable states in Equation 1.91 that correspond to P. van Look and A. Furusawa separability criterion [3].

$$\begin{aligned} V_0 &= \Delta^2\left(\frac{\hat{p}_1-\hat{p}_2}{\sqrt{2}}\right)+\Delta^2\left(\frac{\hat{q}_1+\hat{q}_2}{\sqrt{2}}-\alpha_0\hat{q}_0\right)\geq 2, \\ V_1 &= \Delta^2\left(\frac{\hat{p}_0+\hat{p}_1}{\sqrt{2}}\right)+\Delta^2\left(\frac{\hat{q}_1-\hat{q}_0}{\sqrt{2}}+\alpha_2\hat{q}_2\right)\geq 2, \\ V_2 &= \Delta^2\left(\frac{\hat{p}_0+\hat{p}_2}{\sqrt{2}}\right)+\Delta^2\left(\frac{\hat{q}_2-\hat{q}_0}{\sqrt{2}}+\alpha_1\hat{q}_1\right)\geq 2, \end{aligned} \tag{1.92}$$

where α_j are numbers that minimize V_j. Computing the parameters α_j we can rewritten the Equation 1.93 as:

$$\begin{aligned} V_0 &= \Delta^2\left(\frac{\hat{p}_1-\hat{p}_2}{\sqrt{2}}\right)+\Delta^2\left(\frac{\hat{q}_1+\hat{q}_2}{\sqrt{2}}\right)-\beta_0\geq 2, \\ V_1 &= \Delta^2\left(\frac{\hat{p}_0+\hat{p}_1}{\sqrt{2}}\right)+\Delta^2\left(\frac{\hat{q}_1-\hat{q}_0}{\sqrt{2}}\right)-\beta_1\geq 2, \\ V_2 &= \Delta^2\left(\frac{\hat{p}_0+\hat{p}_2}{\sqrt{2}}\right)+\Delta^2\left(\frac{\hat{q}_2-\hat{q}_0}{\sqrt{2}}\right)-\beta_2\geq 2,, \end{aligned} \tag{1.93}$$

where the terms β_j are given by:

$$\beta_0=\frac{(C_{\hat{q}_0\hat{q}_1}+C_{\hat{q}_0\hat{q}_2})^2}{2\Delta^2\hat{q}_0}, \qquad \beta_1=\frac{(C_{\hat{q}_0\hat{q}_1}-C_{\hat{q}_1\hat{q}_2})^2}{2\Delta^2\hat{q}_1}, \qquad \beta_2=\frac{(C_{\hat{q}_0\hat{q}_2}+C_{\hat{q}_1\hat{q}_2})^2}{2\Delta^2\hat{q}_2}. \tag{1.94}$$

We can see in Equation 1.94 that each inequality enable us to see the entanglement between two beams in a combination in quadrature subtracting the term β_i. For example, in the first inequality we have the subtraction of the amplitude quadrature and the sum of the phase quadratures between the twin beams subtracting the term β_0. This term is related with the correlations between the third beam and the beams being analyzed and through it, it is added the quantum information of the global system. It is enough to violate the first two inequalities to demonstrate tripartite entanglement [18].

1.6.3 Positive Partial Transposition - PPT criterion

In this section we will present the PPT criterion for discrete variables as in the Peres article [36] and its extension for continuous variable systems proposed by Simon [4]. The essence of the PPT criterion is to demonstrate the separability using the partial transposition. As we discussed before, the density matrix of the global system $\hat{\rho}$ composed by the subsystems $\hat{\rho}_1$ and $\hat{\rho}_2$ can be written as in Equation 1.83. In Peres paper it was shown that a necessary separability condition is that a density matrix $\hat{\sigma}$ obtained by the partial transposition of $\hat{\rho}$ has non-negative

eigenvalues:

$$\hat{\sigma} = \sum_A w_A (\hat{\rho}_A^1)^T \otimes \hat{\rho}_A^2. \tag{1.95}$$

If $(\hat{\rho}_A^1)^T$ is really a density matrix it obeys the follows properties:

- $\hat{\rho}$ is positive semi-definite (eigenvalues ≥ 0);
- $\hat{\rho} = (\hat{\rho}^T)^* \rightarrow \hat{\rho}$ is Hermitian;
- $Tr(\hat{\rho}) = 1$,

so $\hat{\sigma}$ is a legitimate density matrix and $\hat{\rho}$ in Equation 1.95 can be write in a separable form. If not, the system is inseparable, what is a sufficient condition for entanglement [27]. We will apply this criterion in pair of spin $\frac{1}{2}$ in a Werner state, as in Peres paper. The density matrix of this system is:

$$\hat{\rho} = \lambda \begin{pmatrix} 0 & 0 & 0 & 0 \\ 0 & \frac{1}{2} & -\frac{1}{2} & 0 \\ 0 & -\frac{1}{2} & \frac{1}{2} & 0 \\ 0 & 0 & 0 & 0 \end{pmatrix} + \frac{1-\lambda}{4} \begin{pmatrix} 1 & 0 & 0 & 0 \\ 0 & 1 & 0 & 0 \\ 0 & 0 & 1 & 0 \\ 0 & 0 & 0 & 1 \end{pmatrix}, \tag{1.96}$$

where we used the ordination $\{|0_A 0_B\rangle, |0_A 1_B\rangle, |1_A 0_B\rangle, |1_A 1_B\rangle\}$. Transposing the first subsystem we have:

$$\hat{\rho}^{T_A} = \lambda \begin{pmatrix} \frac{1-\lambda}{4} & 0 & 0 & -\frac{1}{2}\lambda \\ 0 & \frac{1+\lambda}{4} & 0 & 0 \\ 0 & 0 & \frac{1+\lambda}{4} & 0 \\ -\frac{1}{2}\lambda & 0 & 0 & \frac{1-\lambda}{4} \end{pmatrix}, \tag{1.97}$$

where we obtain the eigenvalues $\{\frac{1+\lambda}{4}, \frac{1+\lambda}{4}, \frac{1+\lambda}{4}, \frac{1-3\lambda}{4}\}$. That will be always positive if $\lambda < \frac{1}{3}$, and in this case the density matrix 1.96 is separable, if not, the state is entangled. In the Horodecki paper[37], it was demonstrated that Peres criterion is necessary and sufficient for systems with dimensions 2x2 and 2x3, where the first number means the number of system and the second one the number of levels.

PPT in continuous variable systems

In a continuous variable system, the dynamic is studied in the phase space through the quasi probability Wigner function representation. According to Simon [4], the partial transposition operation in a CV system is like a mirror reflexion in the phase space. The Wigner function is related with the density operator as in Equation 1.29, and the transposition operation transform

the Wigner function as follow:

$$W(p_1, q_1, p_2, q_2) \rightarrow^{PT} W(p_1, q_1, p_2, -q_2), \tag{1.98}$$

which implies that if a transposition operator applied in the Wigner function generated a new density operator $\hat{\sigma}$ whose Wigner function is given by

$$W(\Gamma\hat{\mathbf{x}}) \qquad \rightarrow \qquad \Gamma = diag(1, 1, 1, -1), \tag{1.99}$$

we can write separability criterion for a bipartite system in continuous variable domain. We will use to describe the criterion the vector $\hat{\mathbf{x}}$ used in the subsection 1.4 to describe a system composed of two parts.

$$\hat{\mathbf{x}} = (\hat{p}_1, \hat{q}_1, \hat{p}_2, \hat{q}_2), \qquad x = (p_1, q_1, p_2, q_2). \tag{1.100}$$

This set of operators obeys the follow commutation rules:

$$\begin{aligned} [\hat{x}_i, \hat{x}_j] &= i\Omega_{i,j} \\ \Omega &= \bigoplus_{k=1}^{N} \omega \qquad \omega = \begin{pmatrix} 0 & 1 \\ -1 & 0 \end{pmatrix}. \end{aligned} \tag{1.101}$$

This transposition in Wigner function implies that the covariance matrix will undergo the $V \rightarrow^{PT} \tilde{V} = \Gamma V \Gamma$, what made us able to rewrite the uncertainty principle in Equation 1.34 as:

$$\tilde{V} + i\Omega \geq 0, \tag{1.102}$$

if this condition is obeyed, necessarily the state being analyzed is separable. If not, the state described by $\tilde{V}$ is unphysical.

We can simplify the Equation 1.102 analyzing if the state described by the covariance matrix is physical or not using the symplectic eigenvalues of $\tilde{V}$ [38] and [39]. A symplectic transformation S preserves the commutation relation of the system operators.

Let us suppose that there is a symplectic transformation that made us able to compute the eigenvalues of $S\tilde{V}S^T + i\Omega$, where $\Omega = S\Omega S^T$. According to Williamson [40], "any covariance matrix 4x4, real, positive and symmetric can be written in a diagonal form under a symplectic transformation".

$$S\tilde{V}S^T + i\Omega = \begin{pmatrix} \nu_1 & 0 & 0 & 0 \\ 0 & \nu_1 & 0 & 0 \\ 0 & 0 & \nu_2 & 0 \\ 0 & 0 & 0 & \nu_2 \end{pmatrix} + i \begin{pmatrix} 0 & 1 & 0 & 0 \\ -1 & 0 & 0 & 0 \\ 0 & 0 & 0 & 1 \\ 0 & 0 & -1 & 0 \end{pmatrix} \geq 0 \tag{1.103}$$

, whose symplectic eigenvalues $\nu_i \geq 1$ to assure the positivy of the eigenvalues of the symplectic transformation 1.103. The eigenvalues ν_k are computed by:

$$\nu_k = \sqrt{Eigenvalues(\mathcal{V})}, \quad \text{where} \quad \mathcal{V} = -(\tilde{V}\Omega)^2. \tag{1.104}$$

It follows from this conditions above that the minimum symplectic eigenvalue needs to be bigger then 1 for the covariance matrix of the system represent a separable system. If this minimum eigenvalue is smaller than 1, the covariance matrix represent a entangled state. And, this is a necessary and sufficient condition to demonstrate entanglement for Gaussian states.

Let us apply this criterion in the following covariance matrix adapted for our system:

$$V = \begin{pmatrix} \Delta^2\hat{p}_1 & 0 & C(\hat{p}_1\hat{p}_2) & 0 \\ 0 & \Delta^2\hat{q}_1 & 0 & C(\hat{q}_1\hat{q}_2) \\ C(\hat{p}_2\hat{p}_1) & 0 & \Delta^2\hat{p}_2 & 0 \\ 0 & C(\hat{q}_2\hat{q}_1) & 0 & \Delta^2\hat{q}_2 \end{pmatrix} = \begin{pmatrix} 1.27 & 0 & 0.8 & 0 \\ 0. & 2.76 & 0 & -2 \\ 0.8 & 0 & 1.99 & 0. \\ 0. & -2 & 0 & 2.53 \end{pmatrix} \tag{1.105}$$

First we will perform the partial transposition in the subsystem 2, so we will apply $\tilde{V} = \Gamma V \Gamma$:

$$V = \begin{pmatrix} 1.27 & 0 & 0.8 & 0 \\ 0. & 2.76 & 0 & 2 \\ 0.8 & 0 & 1.99 & 0. \\ 0. & 2 & 0 & 2.53 \end{pmatrix} \tag{1.106}$$

Now, we need to compute the symplectic eigenvalues. First, we will calculate the matrix $\mathcal{V}$:

$$\mathcal{V} = \begin{pmatrix} 5.12 & 0. & 6.20 & 0. \\ 0. & 5.12 & 0. & 4.57 \\ 4.57 & 0. & 6.65 & 0. \\ 0. & 6.20 & 0. & 6.65 \end{pmatrix} \tag{1.107}$$

and, finally we need to compute the eigenvalues ν_k that are given by $\nu_k = \{11.3, 11.3, 0.50, 0.50\}$, where we can see that the minimum eigenvalues is $\nu_{1(2)} = 0.50$, due this value is smaller than 1, these partitions are entangled.

In this chapter we have shown the principal concepts necessary to understand the development of this thesis. If we know how to characterize the noise spectrum of one and more beams we are able to construct the covariance matrix of our system and from it we can characterize the quantum correlations between the beams using one of the separability criteria presented here. In the next chapter we will present a quantum description of the optical parametrical oscillator using the linearized fluctuations of the eld in the Langevin formalism. Knowing the fluctuations we are able to analyze the noise spectrum of our system in different quadratures

combinations, where we can apply different separability criteria to see if the system is entangled or not.

Chapter 2

Quantum description of the OPO

In this chapter, we will study the physical principles related to the optical parametric oscillator (OPO), the light source used to generate entangled states in this experiment. In general, the OPO is formed by a non-linear medium inserted into an optical cavity, see figure 2.1. In the presented case, the non-linear medium is a Type II PPKTP (Periodically Poled Potassium Titanyl Phosphate) with second order nonlinear susceptibility.

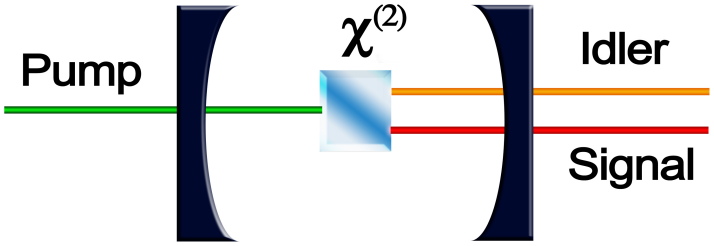

Figure 2.1: OPO schematic representation. Inside the optical cavity there is a non-linear medium with second order nonlinearity. In this system there is the conversion of a photon from the pump beam into signal and idler photo due the interaction with the crystal.

Through interaction with the non-linear medium, there is the conversion of the incident beam, called the pump beam (frequency ω_0) into two other beams, signal (frequency ω_1) and idler (frequency ω_2), such that:

$$\hbar\omega_0 = \hbar\omega_1 + \hbar\omega_2. \tag{2.1}$$

Inside an optical cavity, a nonlinear medium works like a gain medium and the resonant beams are amplified in each interaction with the medium. For a given input power, called threshold power, there is the emission of intense beams (signal and idler) through the output mirror of the cavity.

In the quantum level, the process that describes this phenomenon is the parametric down conversion, where it occurs the annihilation of a pump photon and the creation of a signal and

a idler photons, in a way that energy (2.1) and momentum is conserved:

$$\hbar\mathbf{k_0} = \hbar\mathbf{k_1} + \hbar\mathbf{k_2}. \tag{2.2}$$

The OPO is a very versatile light source. It can be used in spectroscopy [41], optical microscopy [42], biomedicine[43] and metrology[42]. Our group has the expertise in implementation that uses the OPO as a source of entangled states, as the measure of the tripartite entanglement between beams of distinct colors [18]. In this work we aim to use the OPO to generate entangled beams in a quantum communication network that can encode information in atomic media and in light beams at the wavelength used in telecommunications.

We will start in the next section talking about the formalism that describes the dynamics of the field in the OPO. After this, we will describe the principal classical parameters related to the amplitudes of the fields emitted by the OPO. Following we will compute the dynamic of field fluctuations in different subspaces. As we are working with Gaussian states, we will organize the second order momenta fluctuations in a covariance matrix as in 1.5.4, showing its behavior in function of the pump intensity normalized by the power threshold (σ). And, to finish this chapter we will describe the theoretical predictions of entanglement between the beams.

2.1 Quantum Description

In this section we will describe the quantum treatment for the optical parametric oscillator. The modes of the intracavity fields interact with the environment through the mirrors that compose the cavity of the OPO, the transmissions are chosen such that the input mirror transmits the pump beam and the output mirror allows the coupling of the converted beams with the environment. The transmissions of the mirrors are useful losses added to the system, in addition we have losses denominated spurious due intracavity scatterings, absorption of light by the crystal, among others. In this way, the OPO can be seen as an open quantum system. The treatment performed in this section follows the references [26, 28, 44].

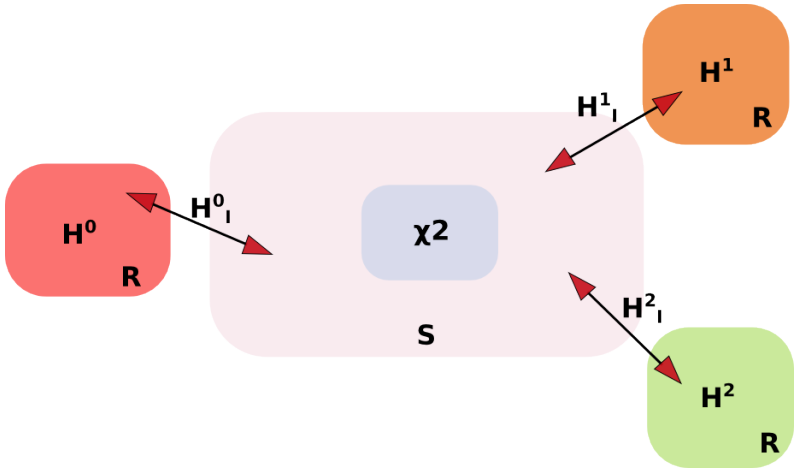

Figure 2.2: Representation of the interactions between the intracavity fields and the environment for the pump, signal and idler fields of the OPO.

The figure 2.2 is a schematic diagram of the process where there are the intracavity field modes generated by the parametric down conversion. These fields interact with the reservoir by means of the input/output mirrors through the hamiltonian $\hat{H}_0^I$, $\hat{H}_1^I$ e $\hat{H}_2^I$. The modes present in the reservoir are described by uncoupled harmonic oscillators and we model the reservoir as a cavity of very large size compared to the OPO.

The following hamiltonian describes the parametric down conversion process:

$$\hat{H}_\chi = 2i\hbar\frac{\chi}{\tau}(\hat{a}_0\hat{a_1}^\dagger\hat{a_2}^\dagger - \hat{a}_0^\dagger\hat{a}_1\hat{a}_2), \tag{2.3}$$

where we have the annihilation of a photon in pump mode and the creation of a photon in the signal mode and a photon in the idler mode. The coefficient χ is related to the second order nonlinear susceptibility term $\chi^{(2)}$ and $\tau = \frac{L}{c}$ is related to the time that a photon takes to make a round trip in the cavity. Furthermore, we have the relation between each intracavity field with the field carrier outside the cavity, as only the pump field carrier is injected into the cavity, we must have:

$$\hat{H}_{in} = i\hbar\frac{\sqrt{2\gamma_0}}{\tau}\alpha_0^{in}(\hat{a}_0^\dagger - \hat{a}_0). \tag{2.4}$$

This hamiltonian represents the injection of a pump field, classical and intense in the cavity. The pump field amplitude α_0^{in} is real, as the phase of the input field is chosen as reference for the other fields.

The hamiltonian that represents the coupling made by the input/output mirror follows the Jaynes-Cummings model and describes the process of absorption (emission) of one photon

outside the cavity with the emission (absorption) of another photon into the cavity.

$$\begin{aligned} \hat{H}_I^i &= \hbar \sum_k (g_i^k \hat{a}_i \hat{b}_i^{\dagger k} + h.c), \\ \hat{H}_I &= \sum_i \hat{H}_I^i \text{ onde i= 0, 1, 2,} \end{aligned} \tag{2.5}$$

the indices $i = 0, 1, 2$ represent the intracavity modes and $k = 0, 1, 2...N$ with $N \to \infty$ represents the indices of the reservoir modes, the coupling constant g_i^k is related to the mirrors transmissions.

In the interaction picture, the free hamiltonians of the intracavity modes of the reservoir are:

$$\begin{aligned} \hat{H}_{cav}^i &= \hbar \frac{\gamma_i^{'}}{\tau} \Delta_i \hat{a}_i^\dagger \hat{a}_i \\ \hat{H}_{res}^i &= \hbar \Delta_i (\hat{b}_i^k)^\dagger \hat{b}_i^k, \end{aligned} \tag{2.6}$$

where the term $\Delta_i = \frac{\omega_i - \omega_{ci}}{\delta \omega_{ci}}$ represents the cavity detuning normalized by the bandwidth and $\delta\omega_{ci} = \frac{2\gamma_i^{'}}{\tau}$. The term $\gamma_i^{'}$ represents the total losses in the cavity $\gamma^{'} = \gamma + \mu$, where 2γ is the transmission coefficient of the coupling mirror and μ are the spurious losses. Thus, the system's total free hamiltonian is given by:

$$\hat{H}_{free} = \Sigma_i (\hat{H}_{cav}^i + \hat{H}_{res}^i). \tag{2.7}$$

The time evolution is obtained making use of the mater equation for the density operator $\hat{\rho}(t)$ of the system:

$$\frac{d\hat{\rho}}{\mathrm{dt}} = \frac{1}{i\hbar} \left[\hat{H}_{\mathrm{in}} + \hat{H}_\chi + \hat{H}_0 + \hat{H}_1 + \hat{H}_2, \hat{\rho} \right] - \Sigma_i \hat{\Lambda}_i(\hat{\rho}), \tag{2.8}$$

where the term $\hat{\Lambda}_i(\hat{\rho})$ refers to the intracavity losses and is described by:

$$\hat{\Lambda}_i(\hat{\rho}) = \frac{\gamma_i^{'}}{\tau} \left(\hat{\rho} \hat{a}_i^\dagger \hat{a}_i + \hat{a}_i^\dagger \hat{a}_i \hat{\rho} - 2 \hat{a}_i \hat{\rho} \hat{a}_i^\dagger \right). \tag{2.9}$$

2.1.1 Fokker-Planck equations

To solve equations 2.8 we must write them in terms of a quasi-probability equation. The usual treatment consists in rewriting it in terms of the Wigner function, due to it's semiclassical description. By using a quasi-probability representation the $\hat{a}$ and $\hat{a}^\dagger$ are replaced by complex field amplitudes α and α^* in a specific reordering through the correspondence rules. The Wigner

function for the density operator is written as [28]:

$$W(\{\alpha_i\}) = \frac{1}{(\pi^2\hbar)^n}\int_{-\infty}^{\infty} d^{2n}\beta e^{-i\Sigma_i(\beta_i^*\alpha_i+\beta_i\alpha_i^*)}\chi(\beta_i,\beta_i^*), \tag{2.10}$$

where $W(\{\alpha_i\})$ is the probability of obtaining the amplitude $\{\alpha_i\} = (\alpha_0, \alpha_0^*, \alpha_1, \alpha_1^*, \alpha_2, \alpha_2^*)$ of the field. The characteristic function $\chi(\{\beta_i\})$ is defined as:

$$\chi(\{\beta_i\}) = Tr[e^{i\beta_i\hat{a}_i^\dagger}e^{i\beta_i^*\hat{a}_i}e^{-\frac{1}{2}|\beta_i|^2}\hat{\rho}]. \tag{2.11}$$

The time derivative of 2.10 gives:

$$\frac{d}{dt}W(\{\alpha_i\}) = \frac{1}{(\pi^2\hbar)^n}\int_{-\infty}^{\infty} d^{2n}\beta e^{-i\Sigma_i(\beta_i^*\alpha_i+\beta_i\alpha_i^*)}Tr[e^{i\beta_i\hat{a}_i^\dagger}e^{i\beta_i^*\hat{a}_i}e^{-\frac{1}{2}|\beta_i|^2}\frac{d}{dt}\hat{\rho}]. \tag{2.12}$$

We will rewrite the above equation using the following correspondence rules for the Wigner function [26]:

$$\begin{aligned}
\hat{a}_i\hat{\rho} &\longleftrightarrow \left(\alpha_i + \frac{1}{2}\frac{\partial}{\partial\alpha_i^*}\right)W,\\
\hat{a}_i^\dagger\hat{\rho} &\longleftrightarrow \left(\alpha_i^* - \frac{1}{2}\frac{\partial}{\partial\alpha_i}\right)W,\\
\hat{\rho}\hat{a}_i &\longleftrightarrow \left(\alpha_i - \frac{1}{2}\frac{\partial}{\partial\alpha_i^*}\right)W,\\
\hat{\rho}\hat{a}_i^\dagger &\longleftrightarrow \left(\alpha_i^* + \frac{1}{2}\frac{\partial}{\partial\alpha_i}\right)W.
\end{aligned}$$

In such way that, after all the substitutions, we arrive in a set of differential equations for the Wigner function:

$$\begin{aligned}
\frac{d}{dt}W(\{\alpha_i\}) &= -\frac{1}{\tau}\sum_i \frac{\partial}{\partial\alpha_i}A_iW(\{\alpha_i\})\\
&+ \frac{1}{\tau}\left(\gamma_0^{'}\frac{\partial^2}{\partial\alpha_0\partial\alpha_0^*} + \gamma_1^{'}\frac{\partial^2}{\partial\alpha_1\partial\alpha_1^*} + \gamma_2^{'}\frac{\partial^2}{\partial\alpha_2\partial\alpha_2^*}\right)W(\{\alpha_i\})\\
&+ \frac{\chi}{2\tau}\left(\frac{\partial}{\partial\alpha_0}\frac{\partial}{\partial\alpha_1^*}\frac{\partial}{\partial\alpha_2^*} + \frac{\partial}{\partial\alpha_0^*}\frac{\partial}{\partial\alpha_1}\frac{\partial}{\partial\alpha_2}\right)W(\{\alpha_i\}).
\end{aligned} \tag{2.13}$$

In the Equation 2.13 we will neglect the third order terms [45]. This is possible due the fact that we are working with a Gaussian approximation, that is valid if we have an intense pump beam and intense signal and idler fields, and if the coupling coefficient $\chi << 1$. If the states in study are non-Gaussian, as for example in a OPO with a χ^3 medium close to the threshold, this kind of approximation is not valid. Doing this approximation, we get a Fokker-Plank equations

as:

$$\frac{\partial p(x)}{\partial t} = \left(-\sum_i \frac{\partial}{\partial x_i} A_i(x) + \frac{1}{2} \sum_{i,j} \frac{\partial}{\partial x_i} \frac{\partial}{\partial x_j} D_{i,j}(x) \right). \tag{2.14}$$

The term A_i is the drift matrix and $D_{i,j}$ is the diffusion matrix of the stochastic process. The explicit form of the drift matrix follows:

$$\mathbf{A} = \begin{pmatrix} -2\chi\alpha_1\alpha_2 - \alpha_0\gamma_0^{'}(1+i\Delta_0) + \sqrt{2\gamma_0}\alpha_0^{in} \\ -2\chi\alpha_1^{*}\alpha_2^{*} - \alpha_0^{*}\gamma_0^{'}(1-i\Delta_0) + \sqrt{2\gamma_0}\alpha_0^{in} \\ 2\chi\alpha_0{\alpha_2}^{*} - \alpha_1\gamma_1^{'}(1+i\Delta_1) \\ 2\chi\alpha_0{}^{*}\alpha_2 - \alpha_1{}^{*}\gamma_1^{'}(1-i\Delta_1) \\ 2\chi\alpha_0{\alpha_1}^{*} - \alpha_2\gamma_2^{'}(1+i\Delta_2) \\ 2\chi\alpha_0{}^{*}\alpha_1 - \alpha_2{}^{*}\gamma_2^{'}(1-i\Delta_2) \end{pmatrix} \tag{2.15}$$

The Fokker-Planck equation is equivalent to a set of Langevin equations:

$$\frac{d\alpha_j}{dt} = A_j + [\mathbf{B}.\sigma(t)]_j, \tag{2.16}$$

where $\sigma(t)$ is a vector of stochastic forces with null average $< \sigma_j(t) >= 0$ with correlation terms of kind:

$$< \sigma_i(t)\sigma_j(t^{'}) >= \delta_{i,j}\delta(t-t^{'}). \tag{2.17}$$

The matrices product $[\mathbf{B}\mathbf{B}^T]$ is the diffusion matrix of the equation 2.14. From the following diffusion matrix:

$$\mathbf{D} = \begin{pmatrix} 0 & 2\gamma_0^{'} & 0 & 0 & 0 & 0 \\ 2\gamma_0^{'} & 0 & 0 & 0 & 0 & 0 \\ 0 & 0 & 0 & 2\gamma_1^{'} & 0 & 0 \\ 0 & 0 & 2\gamma_1^{'} & 0 & 0 & 0 \\ 0 & 0 & 0 & 0 & 0 & 2\gamma_2^{'} \\ 0 & 0 & 0 & 0 & 2\gamma_2^{'} & 0 \end{pmatrix} \tag{2.18}$$

we can identify a possible matrix $\mathbf{B}$, such that $\mathbf{D} = \mathbf{B}.\mathbf{B}^T$:

$$\mathbf{B} = \begin{pmatrix} i\sqrt{\gamma_0^{'}} & \sqrt{\gamma_0^{'}} & 0 & 0 & 0 & 0 \\ -i\sqrt{\gamma_0^{'}} & \sqrt{\gamma_0^{'}} & 0 & 0 & 0 & 0 \\ 0 & 0 & i\sqrt{\gamma_1^{'}} & \sqrt{\gamma_1^{'}} & 0 & 0 \\ 0 & 0 & -i\sqrt{\gamma_1^{'}} & \sqrt{\gamma_1^{'}} & 0 & 0 \\ 0 & 0 & 0 & 0 & i\sqrt{\gamma_2^{'}} & \sqrt{\gamma_2^{'}} \\ 0 & 0 & 0 & 0 & -i\sqrt{\gamma_2^{'}} & \sqrt{\gamma_2^{'}} \end{pmatrix} \tag{2.19}$$

With the knowledge of the matrices **A** and **B**, we are able to write the set of Langevin equations that describes the complex amplitudes dynamics α_i.

2.1.2 Langevin equations for the reflected pump, signal and idler fields

We shall rewrite the equation 2.16 as:

$$\frac{d\alpha_j}{dt} = A_j + \Sigma_i T_{j,i}\delta u_i(t) + \Sigma_i T'_{j,i}\delta v_i(t), \tag{2.20}$$

where the terms $\delta u_i(t) = (0, 0, \delta u_1, \delta u_1^*, \delta u_2, \delta u_2^*)^T$ and $\delta v_i(t) = (\delta v_0, \delta v_0^*, \delta v_1, \delta v_1^*, \delta v_2, \delta v_2^*)^T$ represent the vacuum states that are coupled to the system by the transmission of the mirrors (in the case of the pump, the corresponding terms are replaced by the amplitude α_0^{in} which brings the information concerning the incident pumping beam) of the cavity and the spurious losses. The matrices $T_{j,i}$ and $T'_{j,i}$ represent the transmission and spurious losses, respectively:

$$\begin{aligned} T &= diag(\sqrt{2\gamma_0}, \sqrt{2\gamma_0}, \sqrt{2\gamma_1}, \sqrt{2\gamma_1}, \sqrt{2\gamma_2}, \sqrt{2\gamma_2}) \\ T' &= diag(\sqrt{2\mu_0}, \sqrt{2\mu_0}, \sqrt{2\mu_1},, \sqrt{2\mu_1}, \sqrt{2\mu_2}, \sqrt{2\mu_2}). \end{aligned} \tag{2.21}$$

We will rewrite the field amplitude as the mean value plus a fluctuation term:

$$\alpha = \overline{\alpha} + \delta\alpha. \tag{2.22}$$

By rewriting the Langevin equation in terms of the mean value of the field ($\overline{\alpha}_i = |\overline{\alpha}_i|e^{i\phi_i}$) and its fluctuations ($\delta\alpha_i$), we will be able to study the stationary case, in which $\frac{d}{dt}\overline{\alpha} = 0$ and with the linearized equations in terms of the fluctuations, we may obtain the noise spectrum of the intracavity fields.

We will begin by treating the stationary case that provides us solutions for the input fields equivalent to those obtained for the classical treatment of the OPO.

2.1.3 Classical Equivalence

In terms of the mean values, we have the following set of equations:

$$\frac{d\overline{\alpha}_0}{dt} = -2\chi\overline{\alpha}_1\overline{\alpha}_2 - \overline{\alpha}_0\gamma_0'(1 + i\Delta_0) + \sqrt{2\gamma_0}\overline{\alpha}_0^{in}, \tag{2.23}$$

$$\frac{d\overline{\alpha}_1}{dt} = 2\chi\overline{\alpha}_0\overline{\alpha}_2{}^* - \overline{\alpha}_1\gamma_1'(1 + i\Delta_1), \tag{2.24}$$

$$\frac{d\overline{\alpha}_2}{dt} = 2\chi\overline{\alpha}_0\overline{\alpha}_1{}^* - \overline{\alpha}_2\gamma_2'(1 + i\Delta_2). \tag{2.25}$$

In order to determine which oscillating conditions for the system, we must consider two possible solutions:

1. **Trivial Solution:** $\alpha_1 = \alpha_2 = 0$

   Under these conditions there is no generation of the twin beams and the OPO operates below the oscillation threshold. The amplitude of the reflected beam in this case is given by:

$$\alpha_0 = \sqrt{2\gamma_0}\frac{\overline{\alpha}_0^{in}}{\gamma_0^{'}(1+i\Delta_0)}. \tag{2.26}$$

2. **Solution for** $\alpha \neq 0$**,** $\alpha_1 \neq 0$ **and** $\alpha_2 \neq 0$:

   In this case, we obtain the following relation between the modulus of the fields:

$$|\alpha_0|^2 = \frac{\gamma_1^{'2}(1+\Delta_1^2)}{4\chi^2}\frac{|\alpha_1|^2}{|\alpha_2|^2}, \tag{2.27}$$

   in which the ratio between the intensity of the signal and idler fields is:

$$\frac{|\alpha_1|^2}{|\alpha_2|^2} = \frac{\gamma_2^{'}}{\gamma_1^{'}}\frac{\sqrt{1+\Delta_2^2}}{\sqrt{1+\Delta_1^2}}. \tag{2.28}$$

   Thus, we obtain the amplitude of the reflected pump field above the threshold:

$$|\alpha_0|^2 = \frac{\gamma_1^{'}\gamma_2^{'}\sqrt{1+\Delta_1^2}\sqrt{1+\Delta_2^2}}{4\chi^2} \tag{2.29}$$

   The power of the pump beam from which the twin beam generation process begins is called the threshold power. In the threshold we set $\alpha_1 = \alpha_2 = 0$. Thus:

$$\sqrt{2\gamma_0}(\overline{\alpha}_0^{in})_{th} = (\overline{\alpha}_0)_{limiar}\gamma_0^{'}\left(1+i\Delta_0\right). \tag{2.30}$$

   Calculating the norm of the equation above and replacing $|\overline{\alpha}_0|^2_{th}$ by 2.29, we find the oscillating threshold power:

$$|\overline{\alpha}_0^{in}|^2_{th} = \frac{\gamma_1^{'}\gamma_2^{'}\gamma_0^{'2}}{8\gamma_0\chi^2}(1+\Delta_0^2)\sqrt{1+\Delta_1^2}\sqrt{1+\Delta_2^2}. \tag{2.31}$$

   In the resonance condition for the three fields, $\Delta_0 = \Delta_1 = \Delta_2 = 0$, we get the minimum value for the threshold power:

$$|\overline{\alpha}_0^{in}|^2_{res} = \frac{\gamma_1^{'}\gamma_2^{'}\gamma_0^{'2}}{8\gamma_0\chi^2}. \tag{2.32}$$

   The next step is to obtain the intensities of the twin beams in terms of the incident beam

power and the losses. However, we shall first analyze the relationship between the phases of the fields and their dependence on the detuning of the cavity.

3. Relation between the phases of the fields

Rewriting the equations that relate the modulus of the field amplitudes in terms of the phases, we have:

$$\gamma_1^{'}(1 - i\Delta_1)|\overline{\alpha_1}|e^{i\phi_1} \quad = \quad 2\chi|\overline{\alpha_0}||\overline{\alpha_2}|e^{i(\phi_0-\phi_2)}, \tag{2.33}$$

where ϕ_i are the phases of the intracavity fields. Since signal and idler beams have close wavelengths, we will consider $\Delta_1 = \Delta_2 = \Delta$. We obtain the following relation between the three field phases:

$$e^{i(\phi_0-\phi_1-\phi_2)} = \frac{1 - i\Delta}{\sqrt{1 + \Delta^2}}. \tag{2.34}$$

Given the relation between the field phases, we can compute the amplitude of the output beams.

4. Amplitude of the output fields

We shall rewrite the complex amplitudes in Equation 2.23 in terms of $\overline{\alpha}_i = |\overline{\alpha}_i|e^{i\phi_i}$:

$$\gamma_0^{'}\left(1 + i\Delta_0\right)|\overline{\alpha}_0|e^{i\phi_0} = -2\chi|\overline{\alpha}_1||\overline{\alpha}_2|e^{i(\phi_1+\phi_2)} + \sqrt{2\gamma_0}|\overline{\alpha}_0^{in}|, \tag{2.35}$$

and replacing the relations between the fields by 2.34, we find the following equations related with the output fields:

$$|\overline{\alpha}_1||\overline{\alpha}_2| = \frac{2\gamma_0}{\gamma_0^{'}\sqrt{\gamma_1^{'}\gamma_2^{'}}}|\overline{\alpha}_0^{in}|_{res}^2[(\Delta\Delta_0 - 1) \pm \sqrt{\sigma - (\Delta + \Delta_0)^2}], \tag{2.36}$$

where $\sigma = \frac{|\overline{\alpha}_0^{in}|^2}{|\overline{\alpha}_0^{in}|_{res}^2}$ is the ratio of the power of the pump beam to the threshold power in the resonance condition for the three fields.

Since the difference between the output wavelengths of the OPO is less than 20nm, we can consider that $|\overline{\alpha}_1| = |\overline{\alpha}_2|$ and that the transmission losses and spurious losses for the two beams are equal, $\gamma_1^{'} = \gamma_2^{'} = \gamma^{'}$. In this way, we obtain a final equation for the intensity of the output fields that depends only on the parameters that we have access in the experiment:

$$|\overline{\alpha}|^2 = \frac{2\gamma_0}{\gamma_0^{'}\gamma^{'}}|\overline{\alpha}_0^{in}|_{res}^2[(\Delta\Delta_0 - 1) \pm \sqrt{\sigma - (\Delta + \Delta_0)^2}]. \tag{2.37}$$

2.1.4 Linearized fluctuations in the space of the three fields

The linearized equations in terms of fluctuations are obtained by considering only first order terms of the fluctuations.

$$\begin{aligned}
\frac{d}{dt}\delta\alpha_0 &= -\gamma_0^{'}(1+i\Delta_0)\delta\alpha_0 - \eta(1+i\Delta)(\delta\alpha_1+\delta\alpha_2) + \sqrt{2\gamma_0}\delta\alpha_0^{in} + \delta v_0\sqrt{2\mu_0}, \\
\frac{d}{dt}\delta\alpha_1 &= -\gamma^{'}(1+i\Delta)\delta\alpha_1 + (1-i\Delta)\left(\gamma^{'}\delta{\alpha_2}^{*} + \eta\delta\alpha_0\right) + \sqrt{2\gamma}\delta u_1 + \sqrt{2\mu}\delta v_1, \\
\frac{d}{dt}\delta\alpha_2 &= -\gamma^{'}(1+i\Delta)\delta\alpha_2 + (1-i\Delta)\left(\gamma^{'}\delta{\alpha_1}^{*} + \eta\delta\alpha_0\right) + \sqrt{2\gamma}\delta u_2 + \sqrt{2\mu}\delta v_2. \qquad (2.38)
\end{aligned}$$

To obtain the set of equations above, we rewrite the complex amplitudes using $\overline{\alpha} = |\alpha|^{i\phi}$, keeping in mind that the relations between phases is given by 2.34. The constant η is related with the nonlinear susceptibility tensor and the intensity of the output beams $|\alpha|$ as $\eta = \frac{2\chi|\alpha|}{\sqrt{1+\Delta^2}}$.

Our objective now is to obtain the equations for the fluctuations in terms of the quadratures corresponding to the amplitude and phase fluctuations. For this, we will rewrite the equations 2.38 using our definition of quadratures:

$$\begin{aligned}
\delta p_i &= \delta\alpha_i^{*} + \delta\alpha_i \Rightarrow \text{amplitude quadrature} \\
\delta q_i &= i(\delta\alpha_i^{*} - \delta\alpha_i) \Rightarrow \text{phase quadrature} \qquad (2.39)
\end{aligned}$$

And, we will study the noise spectrum for the fluctuations of the quadratures of the pump, signal and idler beams.

Noise spectrum in the three fields space

In terms of the fluctuations of the amplitude and phase quadratures, we have the new set of equations:

$$\frac{d}{dt}\delta\chi = M\delta\chi + T\delta\beta + T^{'}\delta\epsilon, \qquad (2.40)$$

in which $\delta\chi = (\delta p_0\ \delta q_0\ \delta p_1\ \delta q_1\ \delta p_2\ \delta q_2)^T$ are the vectors that correspond to the fluctuations of the amplitude and phase quadratures, $\delta\beta = (\delta p_0^{in}\ \delta q_0^{in}\ \delta u_{p1}\ \delta u_{q1}\ \delta u_{p2}\ \delta u_{q2})^T$ and $\delta\epsilon = (\delta v_{p0}\ \delta v_{q0}\ \delta v_{p1}\ \delta v_{q1}\ \delta v_{p2}\ \delta v_{q2})^T$ are the vectors that correspond to the fluctuations of the quadratures for the states of vacuum and T and $T^{'}$ are the matrices with terms related to mirror transmissions and spurious losses, such as in 2.21.

In explicit form, the $\mathbf{M}$ matrix:

$$\mathbf{M} = \begin{pmatrix} -\gamma_0^{'} & \gamma_0^{'}\Delta_0 & -\eta & \Delta\eta & -\eta & \Delta\eta \\ \gamma_0\Delta_0 & -\gamma_0^{'} & -\Delta\eta & -\eta & -\Delta\eta & -\eta \\ \eta & \Delta\eta & -\gamma^{'} & \gamma^{'}\Delta & \gamma^{'} & -\gamma^{'}\Delta \\ -\Delta\eta & \eta & -\gamma^{'}\Delta & -\gamma^{'} & -\gamma^{'}\Delta & -\gamma^{'} \\ \eta & \Delta\eta & \gamma^{'} & -\gamma^{'}\Delta & -\gamma^{'} & \gamma\Delta \\ -\Delta\eta & \eta & -\gamma^{'}\Delta & -\gamma^{'} & -\gamma^{'}\Delta & -\gamma^{'} \end{pmatrix} \tag{2.41}$$

To calculate the noise spectrum for these fluctuations, we will work in the frequency domain through the following Fourier transform:

$$\delta\chi(\Omega) \;=\; \int \delta\chi(t)e^{2i\gamma^{'}\Omega t}dt. \tag{2.42}$$

In this way, the equation 2.40 is rewritten:

$$\delta\chi(\Omega) = -\frac{1}{M + 2i\gamma^{'}\Omega}[T\delta\beta(\Omega) + T^{'}\delta\epsilon(\Omega)], \tag{2.43}$$

where $\delta\chi(\Omega)$ is the spectral solution for the intracavity field fluctuations. We look for the spectral solution for the output fields, since they are the fields that we have access (fields measured in each photodetector).

$$\begin{aligned} \delta\chi_s(\Omega) &= T\delta\chi(\Omega) - \delta\epsilon(\Omega), \\ \delta\chi_s(\Omega) &= -\left(T\frac{1}{M + 2i\gamma^{'}\Omega}T + I\right)\delta\beta(\Omega) - T\frac{1}{M + 2i\gamma^{'}\Omega}T^{'}\delta\epsilon(\Omega), \end{aligned} \tag{2.44}$$

where $T\delta\chi(\Omega)$ refers to the intracavity field transmission and $-\delta\epsilon(\Omega)$ to the reflection of the vacuum external to the cavity.

Like in the 1.60, we calculate the noise spectrum matrix for the OPO output:

$$\begin{aligned} 2\pi\delta(\Omega + \Omega^{'})S_s(\Omega) &= \left(TN^{-1}(\Omega)T + I\right)\left(TN^{-1}(\Omega^{'})T + I\right)^T < \delta\beta(\Omega)\delta\beta(\Omega^{'}) > \\ &+ \left(TN^{-1}(\Omega)T^{'}\right)\left(TN^{-1}(\Omega^{'})T^{'}\right)^T < \delta\epsilon(\Omega)\delta\epsilon(\Omega^{'}) > . \end{aligned} \tag{2.45}$$

in which $N(\Omega)^{-1} = \frac{1}{M+2i\gamma^{'}\Omega}$. The terms referring to the vacuum noise spectrum obey the following property:

$$< \delta v_i(\Omega)\delta v_j(\Omega^{'}) >= 2\pi\delta_{ij}\delta(\Omega + \Omega^{'}). \tag{2.46}$$

The matrix $S_s(\Omega)$:

$$S(\Omega) = I + V_{pure} + V_{losses}, \tag{2.47}$$

where the physical meaning of each term is:

- **Identity I**: input noise reflected by the coupling mirror equivalent to the vacuum state for all field modes except in cases where the pump laser shows excess noise in some quadrature;
- the term $\mathbf{V_{pure}}$ is given

$$T.\left(N(\Omega)^{-1}\right)^{T}.T + T.(N(-\Omega)^{-1})^{T}.T + T.\left(N(\Omega)^{-1}\right)^{T}.T^{2}.(N(-\Omega)^{-1})^{T}.T, \tag{2.48}$$

  and represents the noise spectrum of the intracavity fields;

- The term $\mathbf{V_{losses}}$

$$T.N(\Omega)^{-1}.T'^{2}.\left(N(-\Omega)^{-1}\right)^{T}.T, \tag{2.49}$$

  represents the excess of noise coupled to the intracavity fields due to spurious losses.

The theory described thus far agrees experimentally with the results obtained for the fluctuations of intensity (amplitude). However, as for the phase there is excess noise present in the three fields due to the presence of phonons generated by thermal vibrations in the crystalline lattice[46]. The excess noise inserted by this effect may become less noticeable when the nonlinear crystal is cooled. This extra noise added to the phase will be included in the spectral diffusion matrix. For this, we will define a vector of stochastic forces for the phase of each field:

$$\delta q^{ex} = (0, \delta q_0^{ex}, 0, \delta q_1^{ex}, 0, \delta q_2^{ex})^{T}. \tag{2.50}$$

The relationship between the intracavity fields is rewritten by adding the term of excess phase noise:

$$\frac{d}{dt}\delta\chi = M\delta\chi + T\delta\beta + T'\delta\epsilon + \delta q^{ex}. \tag{2.51}$$

The same treatment in terms of the Fourier transform is performed to find the new spectral diffusion matrix, thus obtaining:

$$S_{ex}(\Omega) = S(\Omega) + T.N(\Omega)^{-1}V_Q.(N(-\Omega)^{-1})^{T}.T, \tag{2.52}$$

the V_Q matrix is:

$$\begin{aligned} V_Q &= \langle \delta q_i^{ex}(\Omega)\delta q_j^{ex}(\Omega')\rangle \\ \langle \delta q_i^{ex}(\Omega)\delta q_j^{ex}(\Omega')\rangle &= \eta_{i,j}\sqrt{P_iP_j}, \end{aligned} \tag{2.53}$$

where $\eta_{i,j}$ is a coefficient that represents the coupling between the noises of the fields and it is determined experimentally. P_i, P_j are the powers of the intracavity fields.

For the case where the three fields are resonant to the cavity, that is, when we work in the regime of zero detuning, the noise spectrum matrix is given by:

$$\mathbf{S} = \begin{pmatrix} \mathrm{Sp}_0 & 0 & C^R_{\mathrm{p0p1}} + iC^I_{\mathrm{p0p1}} & 0 & C^R_{\mathrm{p0p2}} + iC^I_{\mathrm{p0p2}} & 0 \\ 0 & \mathrm{Sq}_0 & 0 & C^R_{\mathrm{q0q1}} + iC^I_{\mathrm{q0q1}} & 0 & C^R_{\mathrm{q0q2}} + iC^I_{\mathrm{q0q2}} \\ C^R_{\mathrm{p1p0}} + iC^I_{\mathrm{p1p0}} & 0 & \mathrm{Sp}_1 & 0 & C^R_{\mathrm{p1p2}} + iC^I_{\mathrm{p1p2}} & 0 \\ 0 & C^R_{\mathrm{q1q0}} + iC^I_{\mathrm{q1q0}} & 0 & \mathrm{Sq}_1 & 0 & C^R_{\mathrm{q1q2}} + iC^I_{\mathrm{q1q2}} \\ C^R_{\mathrm{p2p0}} + iC^I_{\mathrm{p2p0}} & 0 & C^R_{\mathrm{p2p1}} + iC^I_{\mathrm{p2p1}} & 0 & \mathrm{Sp}_2 & 0 \\ 0 & C^R_{\mathrm{q2q0}} + iC^I_{\mathrm{q2q0}} & 0 & C^R_{\mathrm{q2q1}} + iC^I_{\mathrm{q2q1}} & 0 & \mathrm{Sq}_2 \end{pmatrix} \tag{2.54}$$

The diagonal terms are the noise spectra referring to the fluctuations in the quadratures of each field. The off-diagonal terms represent the correlations between the fields.

The figure 2.3 shows how the noise spectrum of the pump, signal and idler beams change for different pump intensity σ (pump power normalized by the threshold power, as defined in 2.1.3). The other parameters used were $\gamma_0 = 0.15$, $\gamma = 0.02$, $\mu_0 = 0.02$, $\mu = 0.002$ and $\Omega' = 0.5$ that are compatible with the experimental values we use in the laboratory. We will use this values throughout the text.

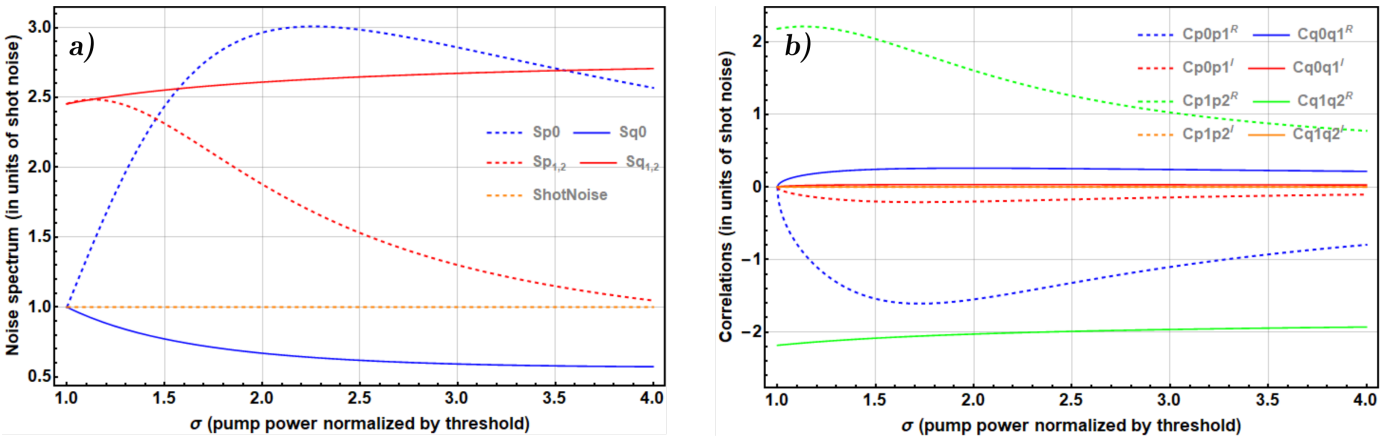

Figure 2.3: a) Spectrum of pump, signal and idler beams normalized by the shot noise. b) Correlations terms between the phases or between field amplitudes quadratures. The correlations between amplitude and phase are zero for all fields.

Looking at a) on the figure 2.3 for the noise spectrum of the pump, signal and idler beams, we notice that, for the noise spectrum of the pump, the quadrature amplitude (Sp_0) shows excess noise when the quadrature phase (Sq_0) show noise compression for any value of σ. There is no difference between the noise spectra for the signal and idler beams. In this way, we express graphically the quantity referring to only one of them. We notice by the figure 2.3 that the phase quadrature ($Sq_{1,2}$) always shows excess noise and the quadrature amplitude ($Sp_{1,2}$)excess noise to lower values than 4σ.

In part b) of the figure 2.3 we have the correlations between the pump, signal and idler

beams. Since the correlation between pump-signal and pump-idler are equal, only one of the correlations was presented. The blue curves represent these correlations, the dashed curve represents the real part of the amplitude correlations (C^R_{p0p1}) between pump and signal and it tells us that these two beams are strongly anticorrelated. For the real part of the quadrature phase (C^R_{q0q1}) there is a small correlation. As for the imaginary part, it is null for the phase quadrature and there is a small anticorrelation with respect to the quadrature amplitude.

As for the existing correlations between signal and idler beams, we noticed that while the amplitude quadrature (C^R_{p1p2}) correlation with the quadrature phase (C^R_{q1q2}) shows anticorrelation.

In figure 2.4, we present the noise spectra and the terms of correlations with the addition of the phonon noise matrix. The data used to construct the covariance matrix for the phonon noise was taken from our experiment and we will present in the chapter 5, the parameters used were $\eta_{00} = 0.066$, and the other coefficents are related with η_{00} in the follow way: $\eta_{12} = \eta_{22} = \eta_{00}/4$, $\eta_{01} = \eta_{02} = 0.27\eta_{00}$, $\eta_{12} = 0.16\eta_{00}$. When we compare the figures without the presence of phonon noise (continuous lines) and with the insertion of phonon noise (dashed lines), we notice that phase quadratures of the pump and signal beams present an excess of noise compared with the figure without phonon noise.

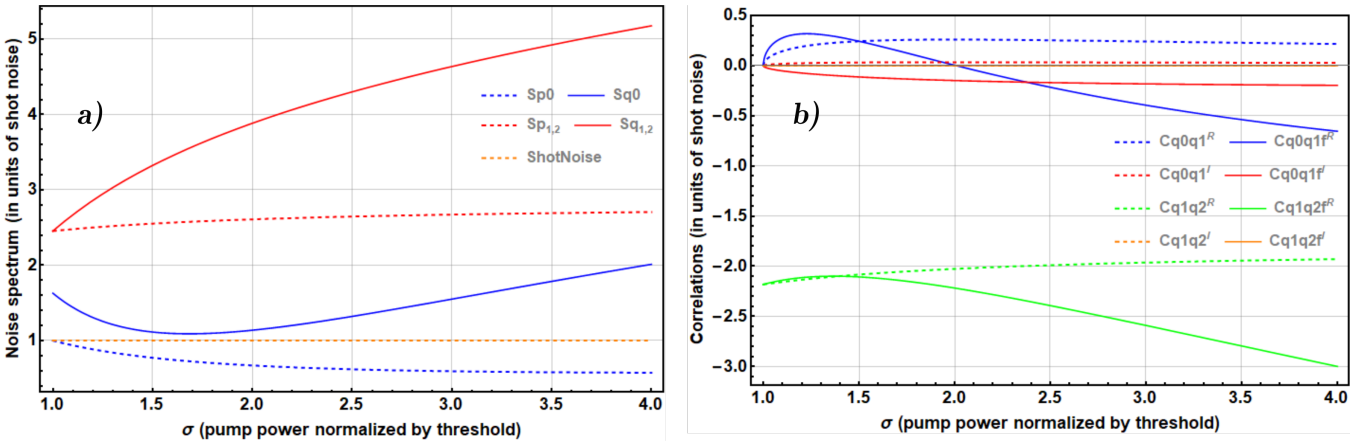

Figure 2.4: a)Noise spectrum of pump, signal and idler beams for phase quadrature fluctuations comparing situations with and without the presence of phonon noise. b)Correlation terms between the phase quadratures, comparing the situations with and without the presence of phonon noise.

The presence of this excess noise made it difficult to measure tripartite entanglement among the three beams of the OPO performed by our group. However, during the investigation, it was found that the coupling of the phonons with the intracavity fields was the source of excess noise in the phase of the three fields. It was noticed that there was a dependence of the excess of phase noise with the temperature, as detailed in the master dissertation [47], in such a way that the lower the system temperature, the lower would be the presence of phase noise. The

first measure of tripartite entanglement was performed [18] and we are currently working on temperatures lower than $-10^0 C$ to avoid the presence of excessive phonon noise.

2.1.5 Pump space, sum and subtraction

We can analyze the noise spectrum of the amplitude and phase quadratures fluctuations of the twin beams generated by the OPO through the following linearization:

$$\begin{aligned} \delta\hat{p}_{\pm} &= \frac{\hat{p}_1 \pm \hat{p}_2}{\sqrt{2}}, \\ \delta\hat{p}_{\pm} &= \frac{\hat{q}_1 \pm \hat{q}_2}{\sqrt{2}}. \end{aligned} \tag{2.55}$$

To write the noise matrix in this new subspace, we must replace the equations 2.55 in the equations of Langevin 2.16 and perform the procedure described in the previous section. The new vector that we analyzed it has the following quadraturas $\delta\zeta = (\delta p_0\ \delta q_0\ \delta p_+\ \delta q_+\ \delta p_-\ \delta q_-)^T$. In this new space, the temporal equation is written as:

$$\frac{d}{dt}\delta\zeta = N\delta\zeta + T\delta\phi + T^{'}\delta\theta, \tag{2.56}$$

in which T and $T^{'}$ are the matrices defined in 2.21, the terms $\delta\phi = (\delta p_0^{in}\ \delta q_0^{in}\ \delta u_+^p\ \delta u_+^q\ \delta u_-^p\ \delta u_-^q)^T$ e $\delta\theta = (\delta v_{p0}\ \delta v_{q0}\ \delta v_+^p\ \delta v_+^q\ \delta v_-^p\ \delta v_-^q)^T$ and the matrix N has the following format:

$$\mathbf{N} = \begin{pmatrix} -\gamma_0 & 0 & -\sqrt{2}\eta & 0 & 0 & 0 \\ 0 & -\gamma_0 & 0 & -\sqrt{2}\eta & 0 & 0 \\ \sqrt{2}\eta & 0 & 0 & 0 & 0 & 0 \\ 0 & \sqrt{2}\eta & 0 & -2\gamma & 0 & 0 \\ 0 & 0 & 0 & 0 & -2\gamma & 0 \\ 0 & 0 & 0 & 0 & 0 & 0 \end{pmatrix} \tag{2.57}$$

We see that the fluctuations referring to the amplitude and phase quadratures of the subtraction subspace are completely decoupled from the other quadratures. In this way we can perform an analysis that consists in separating the part related to the subtraction terms from the part referring to the fluctuations of the sum and pump quadratures.

Fluctuations of the amplitude and phase quadratures in the subtraction space

The noise spectrum for the amplitude and phase fluctuations in the subtraction subspace is independent of the ratio between the pump power and the threshold power. In the Fourier domain, considering the situation of zero detuning, it follows that the terms of the noise spectrum

of these new quadratures:

$$S\hat{p}_{-} = 1 - \frac{\gamma}{\gamma'}\frac{1}{(\Omega'^2+1)}, \tag{2.58}$$

$$S\hat{q}_{-} = 1 + \frac{\gamma}{\gamma'}\frac{1}{\Omega'^2}. \tag{2.59}$$

The figure 2.5 shows the behavior of the quadratures as a function of the frequency Ω (analysis frequency normalized by the OPO bandwidth).

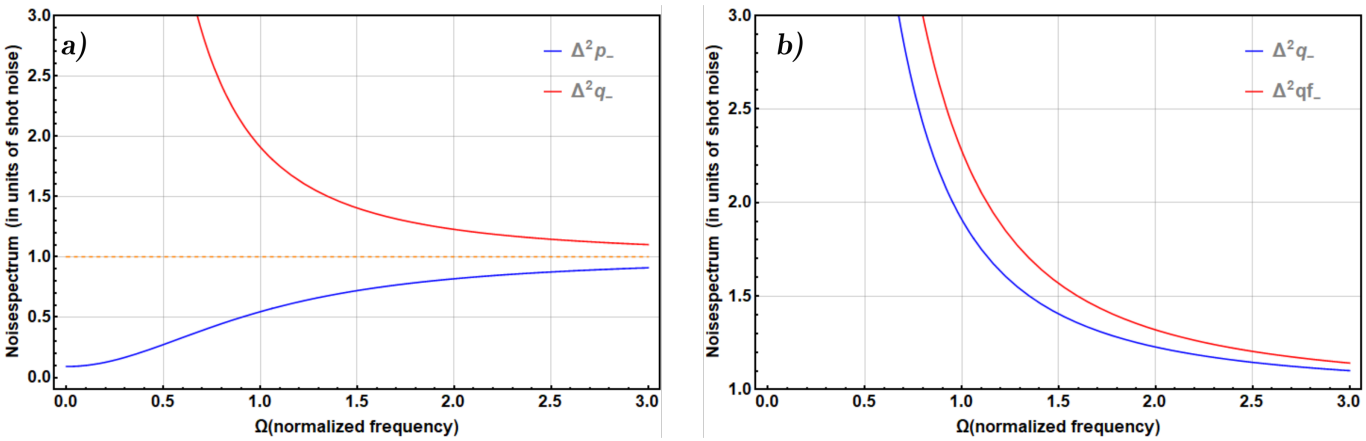

Figure 2.5: Behavior of the noise spectrum of the quadratures $\hat{p}_{-}$ e $\hat{q}_{-}$ as a function of the analysis frequency normalized by the bandwidth($\Omega^{'}$)a) Without the presence of phonon noise b) in blue: in the absence of phonon noise and in red: in the presence of phonon noise.

We can see in the figure 2.5 that the presence of phonon noise increases the excess of noise in the phase difference quadrature. The amplitude subtraction quadrature noise spectrum always presents noise compression [48], while the phase quadrature, excess noise. This relation is in accordance with the principle of uncertainty, because while one of the quadratures always presents noise compression, the conjugate presents excessive noise. For values $\Omega > 1$, the noise in both quadratures tends to shot noise. When we analyze the situation in which we do not have spurious losses in the system, $\gamma^{'} = \gamma$, we have $S\hat{p}_{-}.S\hat{q}_{-} = 1$. This implies that the subtraction subspace has minimal uncertainty.

Amplitude and phase quadratures fluctuations in reflected pump and sum space

When analyzing the 4x4 matrix relative to the subspace of the fluctuations of the amplitude and phase quadratures of the pump and sum we get a new set of equations equivalent to 2.56,

in which the transformation matrix has the following format:

$$\begin{pmatrix} -\gamma_0' & -\sqrt{2}\eta & 0 & 0 \\ \sqrt{2}\eta & 0 & 0 & 0 \\ 0 & 0 & -\gamma_0' & -\sqrt{2}\eta \\ 0 & 0 & \sqrt{2}\eta & -2\gamma' \end{pmatrix} \tag{2.60}$$

The order is given by the vector $(\delta\hat{p}_0\ \delta\hat{p}_+\ \delta\hat{q}_0\ \delta\hat{q}_+)^T$. See in the figure bellow 2.6 the noise spectrum and correlations in this subspaces.

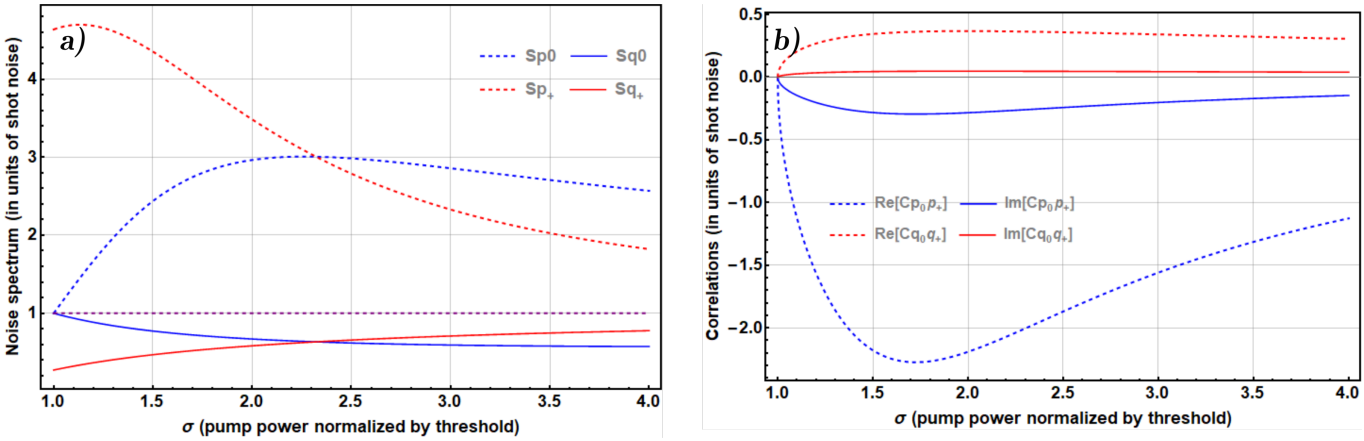

Figure 2.6: a)Noise spectrum for the amplitude and phase quadratures fluctuations for the pump and for the sum combination. b) Correlation terms for the amplitude and phase quadratures for the pump and sum combination.

In these conditions we realize that the fluctuations of the amplitude quadratures present excessive noise, while the fluctuations of the phase quadratures present noise compression for all σ. As for the correlations, there is correlation for the amplitude quadratures and anticorrelation for the phase quadratures the imaginary part are null.

We show in the figure 2.7 the effect of the phonon noise in the phase quadrature of this space. While in the absence of phonon the sum of the phases all have squeezing as demonstrated in the dashed red curve in a) in the presence of phonon noise we have squeezing until $\sigma \approx 1.4$ as we can see in the continuous red curve in the simulation. These effect is very perceptible in experimental result, as we will show in the chapter 5.

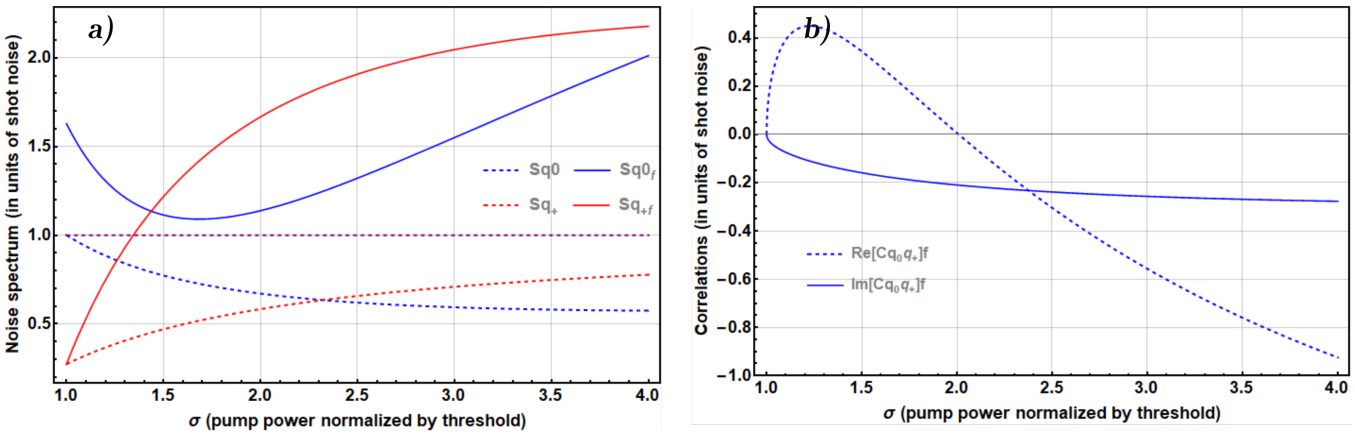

Figure 2.7: a)Noise spectrum for the amplitude and phase quadratures fluctuations for the pump and for the sum combination. b) Correlation terms for the amplitude and phase quadratures for the pump and sum combination. The dashed lines are without phonon noise and the continuous line with presence of phonon noise.

2.1.6 DGCZ Criterion

We have seen that the noise spectrum fluctuations in the amplitude subtraction and in the sum of the phases are squeezed. To verify if there is entanglement between the signal and idler beams in this combination we use the DGCZ criterion as discussed in the section 1.6.1:

$$\langle \Delta^2 \hat{q}_+ \rangle + \langle \Delta^2 \hat{p}_- \rangle \geq 2. \tag{2.61}$$

The figure 2.8 represents the DGCZ inequality criterion.

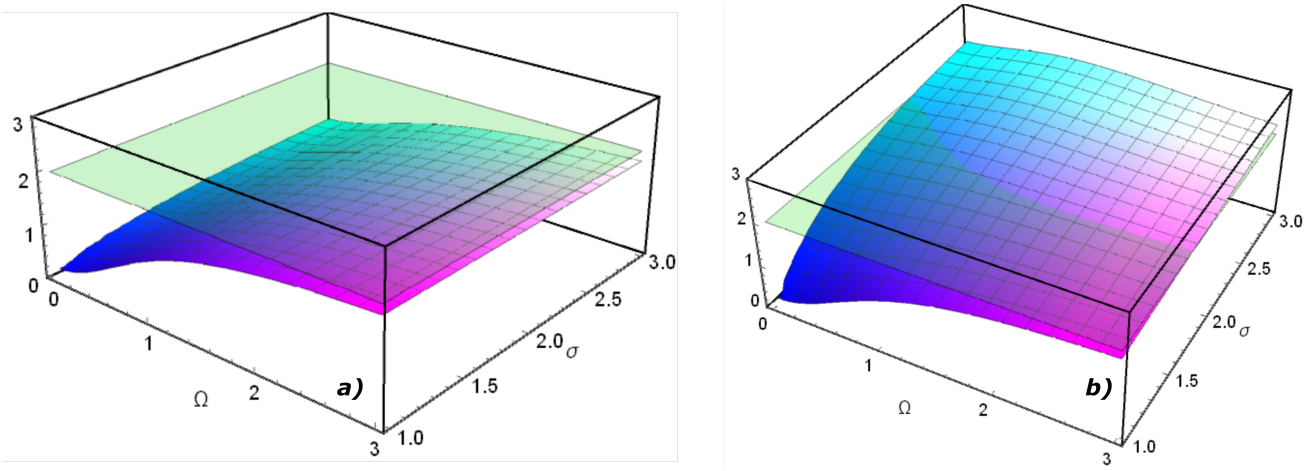

Figure 2.8: a)Sum of noise spectra of fluctuations in the amplitude subtraction fluctuations and phase sum quadrature. b) Same as a) but added Phonon noise.

In both condition on figure 2.8, it is clear that the closer one gets to the threshold and analysis frequencies close to zero stronger is the violation of the inequality witnessing the

entanglement between idler and signal beams. In the case we study in the laboratory we worked with a analysis frequency of $\Omega \approx 0.5$. The figure 2.9 shows us what values we expect to obtain for the bipartite entanglement between the beams generated by our OPO.

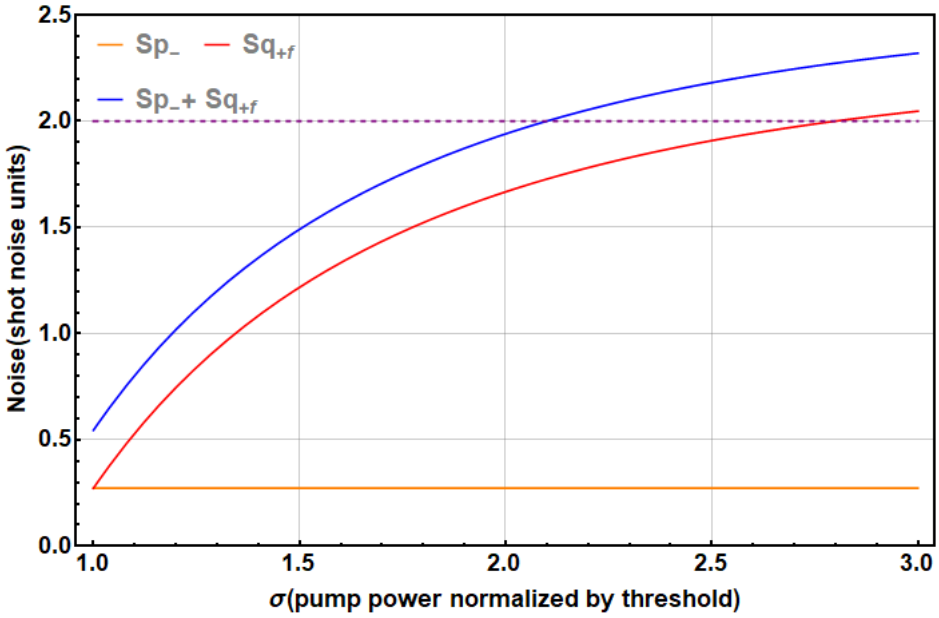

Figure 2.9: Sum of noise spectra of amplitude subtraction fluctuations and phase sum of signal and idler beams considering the phonon noise in the sum of the phase quadratures. $\Omega^{'} = 0.5$.

2.1.7 Pump and sum Bipartition

We will investigate the quantum correlations between the reflected pump and the sum of the quadratures between the signal and idler beams, since as demonstrated in subsection2.1.5 the subtraction subspace is decoupled from this system. The Duan inequality violation in this case allows us to demonstrate if there is entanglement between the reflected pump beam and the combined sum of the twin beams.

Starting from the matrix 2.60 we use the development in 2.1.5 to find the noise spectrum matrix in Fourier, where the following transformation was used to diagonalize this space [49]:

$$\begin{aligned} S_{\hat{p}_0\hat{p}_\pm} &= \frac{S_{\hat{p}_+} + S_{\hat{p}_0}}{2} \pm C_{\hat{p}_0\hat{p}_+}, \\ S_{\hat{q}_0\hat{q}_\pm} &= \frac{S_{\hat{q}_+} + S_{\hat{q}_0}}{2} \pm C_{\hat{q}_0\hat{q}_+}. \end{aligned} \tag{2.62}$$

The figure 2.10 represents the correlation between amplitude quadratures of $\hat{p}_0$ and $\hat{p}_+$ and between the phase quadratures of $\hat{q}_0$ e $\hat{q}_+$:

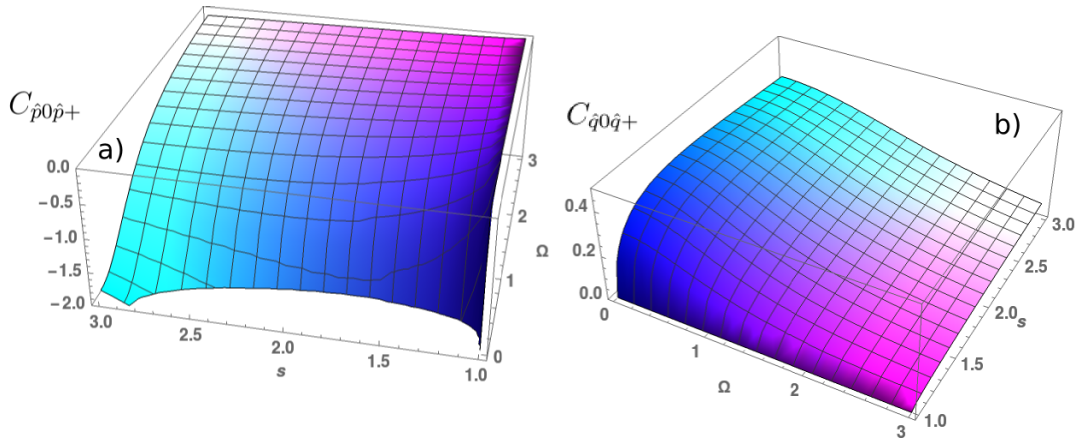

Figure 2.10: a) Anticorrelation between the amplitude quadratures of $\hat{p}_0$ and $\hat{p}_+$. b) Correlation between phase quadratures of $\hat{q}_0$ e $\hat{q}_+$.

We notice that the amplitude quadrature presents anticorrelation while the phase quadrature presents correlation between the pumping and the space sum. As Ω grows the correlation between the beams tends to zero, keeping in mind that the value Ω that is represented in 2.10 corresponds to the value of the analysis frequency normalized by the bandwidth, as Ω grows, the analysis frequency becomes greater than the bandwidth of the OPO and there are no more quantum correlations between the beams.

The noise spectrum corresponding to the quadratures $S_{\hat{p}_0\hat{p}_+}$ and $S_{\hat{p}_0\hat{p}_-}$ are represented in the figure 2.11.

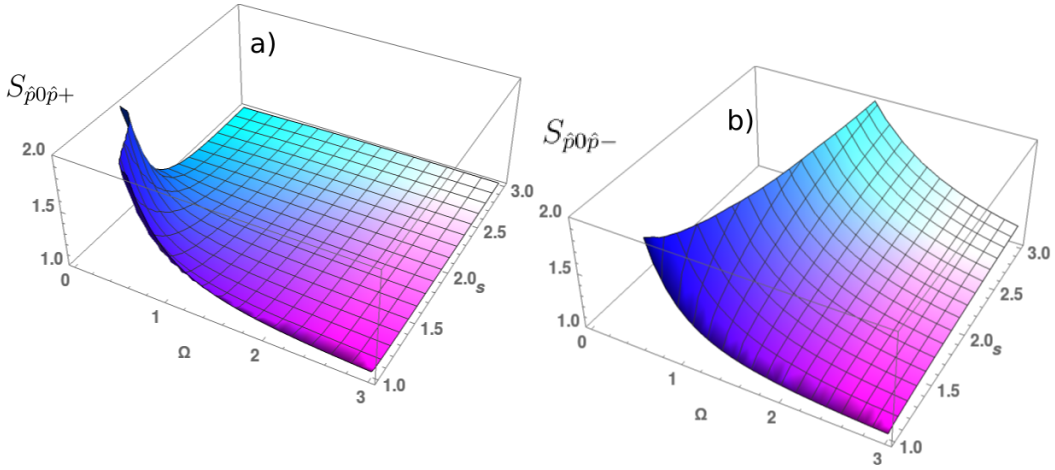

Figure 2.11: a) Noise spectrum $S_{\hat{p}_0\hat{p}_+}$. b) Noise spectrum $S_{\hat{p}_0\hat{p}_-}$.

In part a) of the figure 2.11 its noticeable that as Ω gets close to zero and for σ values that are in $1 < \sigma < 2.2$ this quadrature shows excess of noise. As we increase the value of σ, the noise gets close to the shot-noise. For part b) there is excess of noise for a large interval of values, specially in the region $\Omega < 1.5$.

For the phase quadrature, the corresponding noise spectrum is shown in figure 2.12.

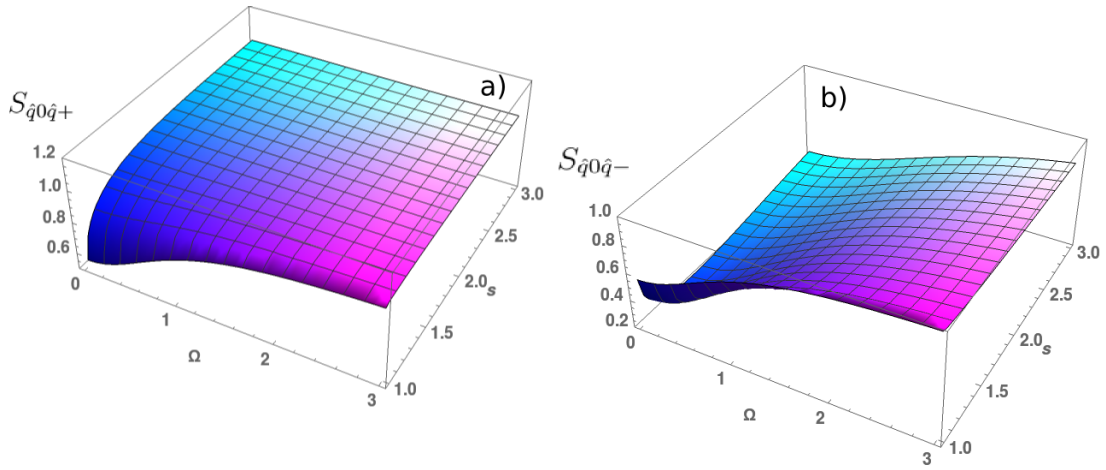

Figure 2.12: a) Noise spectrum $S_{\hat{q}_0\hat{q}_+}$. b) Noise spectrum $S_{\hat{q}_0\hat{q}_-}$.

In part a) of the figure 2.12 we notice that as Ω gets close to zero and for values for σ close to 1 there is a maximal noise compression, surpassing the shot-noise level for valuer of σ greater than 1.5 and analysis frequencies close to zero. For part b) we notice that for values Ω and σ analyzed there always is noise compression for this quadrature, with minimum value for σ close to 1.5.

In order to show entanglement in this bipartition, we will use the DGCZ criterion [2] which as explained in the course of the text, if the value found for the variance is smaller than 2, the criterion is violated and there is entanglement in bipartition. As $S_{\hat{q}_0\hat{q}_-}$ present noise compression for all the region analyzed and $S_{\hat{p}_0\hat{p}_+}$ shows noise excess in a favorable region for the parameters we use, to verify if there is entanglement in the bipartition sum and pump we will use this configuration.

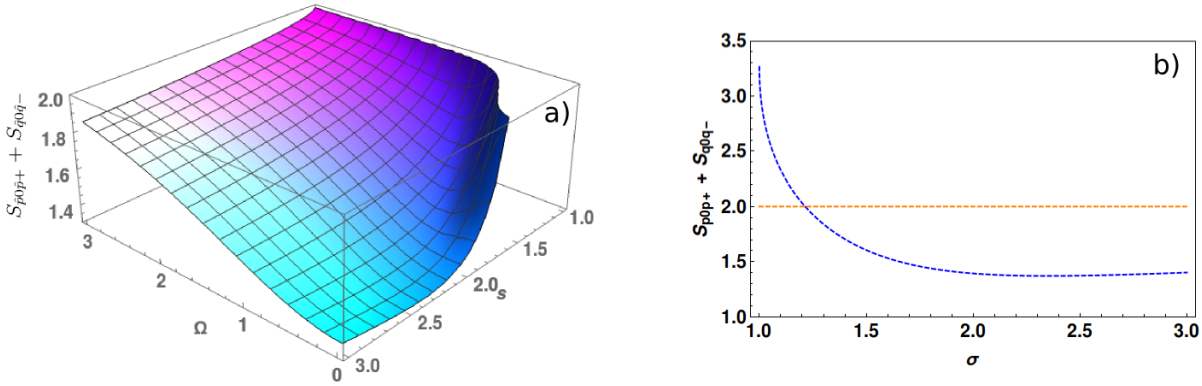

Figure 2.13: a) Noise spectrum sum of the quadratures $\hat{p}_0\hat{p}_+$ and $\hat{q}_0\hat{q}_-$ for different values of σ and Ω. b) Same as a) analyzed for $\Omega = 0.53$.

We notice that just as in sum and subtraction space, in the sum and pump space there is a violation of the inequality of the DGCZ criterion. It is a clear indication that there is

entanglement between the three beams.

Chapter 3

Steering

Einstein, Podolsky and Rosen (EPR) introduced in their famous paper [9] that entangled particles have correlations between position and momenta that it is not possible to be predicted classically. It became known as EPR paradox and can be evidenced by EPR steering tests [5] as a form to confirm entanglement between two [50] or more systems [51]. Despite the fact that other methods to witness entanglement require less stringent limits, like Duan et al. [2] and Simon, [4], Steering test is used to validate quantum communication protocols based on entanglement, e.g., quantify the capacity of quantum-information channel in a dense coding protocol [52] or secure bit rate in a quantum key distribution [53].

3.1 Steering criterion

We will introduce the EPR-steering criterion based on Reid proposal (1989)[5, 54]. Let us consider a bipartite system where Alice and Bob share a unknown quantum state $\hat{\rho}_{AB}$ of a two-mode continuous variable system, where $\{\hat{p}_a, \hat{q}_a\}$ and $\{\hat{p}_b, \hat{q}_b\}$ correspond to the pair of canonically conjugate observables of the subsystem A and B, respectively. The part A measure $\hat{q}_a$ and try to infer the measurement outcome $\hat{q}_b$ of the part B, denote $\hat{q}_b^{est} = \sigma_q \hat{q}_a$ as can be seen in the figure 3.1.

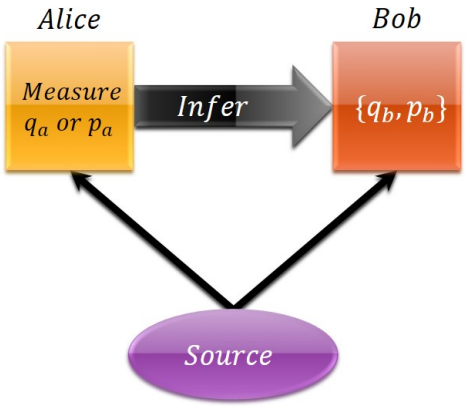

Figure 3.1: Schematic representation of the steering process, we have a source that produces a unknown state $\hat{\rho}_{AB}$ shared by Alice and Bob, Alice does a measurement in his own subsystem and try to infer the measurement outcome in the Bob subsystem.

The inferred variance of $\hat{q}_b$ given estimate $\hat{q}_b^{est}(\hat{q}_a)$ is:

$$\begin{aligned} \Delta^2_{inf}\hat{q}_b &= \Delta^2(\hat{q}_b - \hat{q}_b^{est}) \\ &= \langle(\hat{q}_b - \sigma_q\hat{q}_a)^2\rangle - \langle(\hat{q}_b - \sigma_q\hat{q}_a)\rangle^2. \end{aligned} \tag{3.1}$$

The closer the deviation of $\hat{q}_b^{est}$ from $\hat{q}_b$, the greater $\Delta^2_{inf}\hat{q}_b$ will be determined at a distance by the determination of $\hat{q}_a$. The inferred conjugated quadrature is $\Delta^2_{inf}\hat{p}_b = \Delta^2(\hat{p}_b - \hat{p}_b^{est})$ where $\hat{p}_b^{est} = \sigma_p\hat{p}_a$.

We have to find the best σ_q (σ_p) parameter in a way to minimize $\Delta^2_{inf}q_b$ ($\Delta^2_{inf}p_b$). In the OPO context we are interested in bipartite Gaussian state, and the minimum inference variance correspond to the mean value of the conditional variance [55]. Computing the $\frac{\partial\Delta^2_{inf}\hat{q}_b}{\partial\sigma_q} = 0$ and $\frac{\partial\Delta^2_{inf}\hat{p}_b}{\partial\sigma_p} = 0$, we find:

$$\sigma_q = \frac{\langle\Delta\hat{q}_b\Delta\hat{q}_a\rangle}{\Delta^2\hat{q}_a^2} \qquad \sigma_p = \frac{\langle\Delta\hat{p}_b\Delta\hat{p}_a\rangle}{\Delta^2\hat{p}_a^2}. \tag{3.2}$$

Now, we apply the value of σ_q in Equation 3.2 in the Equation 3.1 and we obtain:

$$\begin{aligned} \Delta^2_{inf}\hat{q}_b &= \Delta^2(\hat{q}_b - \frac{\langle\Delta\hat{q}_b\Delta\hat{q}_a\rangle}{\Delta^2\hat{q}_a}\hat{q}_a) \\ &= \Delta^2\hat{q}_b\left(1 - \frac{\langle\hat{q}_b\hat{q}_a\rangle^2}{\Delta^2\hat{q}_b\Delta^2\hat{q}_a}\right). \end{aligned} \tag{3.3}$$

For the conjugated quadrature, we have:

$$\Delta^2_{inf}\hat{p}_b = \Delta^2\hat{p}_b\left(1 - \frac{\langle\hat{p}_b\hat{p}_a\rangle^2}{\Delta^2\hat{p}_b\Delta^2\hat{p}_a}\right). \tag{3.4}$$

The minimum inferred variance is also known as conditional variance $\Delta^2\hat{q}_{bcond}$ and $\Delta^2\hat{p}_{bcond}$, a

measure of the noise degradation of correlations between two modes. Thus, in the case that we are inferring a result in the subsystem B doing a measurement in the subsystem A, the state has steering if:

$$\Delta^2_{inf}\hat{q}_b\Delta^2_{inf}\hat{p}_b < 1. \tag{3.5}$$

In the case that the part B does a measurement and try to infer the measurement outcome in the subsystem A, we have the following inequality:

$$\Delta^2_{inf}\hat{q}_a\Delta^2_{inf}\hat{p}_a < 1. \tag{3.6}$$

The inferred quadrature is not an observable, it is a correlation parameter. Therefore, it does not violate the principle of uncertainty. Unlike entanglement that is defined symmetrically with respect to both observables, steering is asymmetric with respect to subsystems A and B, so:

$$\Delta^2_{inf}\hat{q}_b\Delta^2_{inf}\hat{p}_b \neq \Delta^2_{inf}\hat{q}_a\Delta^2_{inf}\hat{p}_a, \tag{3.7}$$

to infer the canonical pair $\{\hat{q}_b, \hat{p}_b\}$ measuring $\{\hat{q}_a, \hat{p}_a\}$ is different of to infer the canonical pair $\{\hat{q}_a, \hat{p}_a\}$ measuring $\{\hat{q}_b, \hat{p}_b\}$. Each direction independently can present steering.

Using the Equation 3.5 and Equation 3.6 is possible to witness steering between two-OPO modes: between twin-beams [50] or between one down-converted beam and the pump beam as we will present in the next section 3.2. However this can also be used to analyze a three mode steerability where a measurement in one mode, $\hat{q}_a$ ($\hat{p}_a$) is used to infer a composed canonical observable:

$$\hat{q}_b = c\hat{q}_{b'} + c'\hat{q}_{b''} \qquad \hat{p}_b = c\hat{p}_{b'} + c'\hat{p}_{b''}, \tag{3.8}$$

where mode b is a mode combination of b' and b''. Note that we need to find the right mode combination to minimize the inference variance. This happen when complementary conjugate mode $\tilde{b}$, with quadratures

$$\hat{q}_{\tilde{b}} = c'\hat{q}_{b'} - c\hat{q}_{b''} \qquad \hat{p}_{\tilde{b}} = c'\hat{p}_{b'} - c\hat{p}_{b''}, \tag{3.9}$$

does not have any correlation with modes a and b. In twin-photon case produced by OPO this happen with twin-beam combination when $c = c' = 1/\sqrt{2}$ where we have the mode b, known as mode sum, which maximize the correlation with pump mode and the $\tilde{b}$, known as mode difference, that has no correlation with modes a and b.

3.2 Steering in the Optical Parametrical Oscillator

The optical parametrical oscillator is a source of entangled states of light, the emitted beams are represented by Gaussian states and their quantum correlations can be used in different quantum

information protocols. In the future, we would like to use the OPO studied in this thesis as a source of quantum correlations for different quantum protocols. Teleportation protocol requires entanglement [56], we have seen in the chapter 2 that is expected entanglement in different bipartition and tripartite combination between the beams. Steering is a figure of merit of quantum secret sharing protocols [57], for example. It is important, in this scenario, to know in what combination we have steering in our system and how this change for different configurations. In this way, we will perform the steering criterion for different bipartition and may find one that is more suitable to work experimentally.

We have seen that knowing the covariance matrix of the three beams, we have a tomography of our state. We will apply the steering criterion using the language that we used to construct the covariance matrix. The canonical quadratures that are present in equation Equation 3.5 will be written as:

$$\begin{aligned} \Delta^2\hat{X}_{ij} &= \Delta^2\hat{p}_i - \frac{C(\hat{p}_i\hat{p}_j)^2}{\Delta^2\hat{p}_j} \\ \Delta^2\hat{Y}_{ij} &= \Delta^2\hat{q}_i - \frac{C(\hat{q}_i\hat{q}_j)^2}{\Delta^2\hat{q}_j} \end{aligned} \tag{3.10}$$

If the bipartition presents steering, the follow inequality needs to be fulfilled:

$$\Delta^2\hat{X}_{ij}\Delta^2\hat{Y}_{ij} < 1 \qquad \Delta^2\hat{X}_{ji}\Delta^2\hat{Y}_{ji} < 1. \tag{3.11}$$

It is not necessary that both inequalities are satisfied at the same time, if only one is satisfied this mean that in that direction that we have steering.

To perform the simulations that will follow we have used an analysis frequency normalized by OPO bandwidth $\Omega = 0.5$, spurious losses for the pump beam of $\mu_0 = 0.02$ and for twin beams of $\mu = 0.002$, a phonon parameter (more about in the section 2.1.4) from the pump $\eta_{00} = 0.07$ for $T = 18^0C$ as we have measured for our system, the pump beam for $\Omega = 0.5$ presents a phase noise of 1.30 above the shot noise that was considered too.

3.2.1 Bipartition pump and idler (or signal) beams

We will first analyze the inference between the reflected pump and one of the twin beams. In this case the index in the Equation 3.11 will be replaced for i=0 and j=1. The figure 3.2 shows the behavior of the inferred quadratures when we change σ (intensity of the pump normalized by the OPO threshold) and Ω (analysis frequency normalized by the bandwidth of the OPO).

There isn't any steering in this bipartition for any configuration of the OPO.

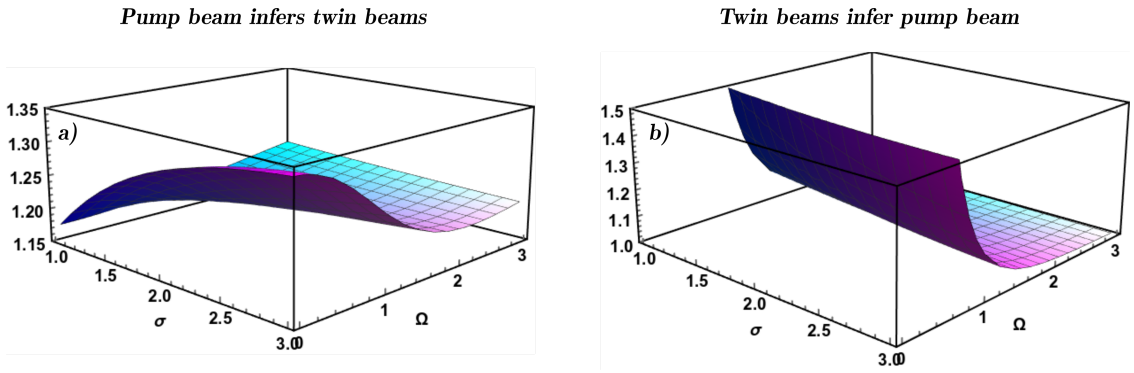

Figure 3.2: a) Steering test of the reflected pump inferring one of the twin beams; b) and the opposite inference when we change the analysis frequency (Ω) and the power normalized by the threshold (σ).

3.2.2 Bipartition signal and idler beams

If we analyze the inference between the signal and idler combination, it is indifferent if we compute the inference from signal to idler or vice-versa, because we use the approximation that the OPO losses for both beams are equal.

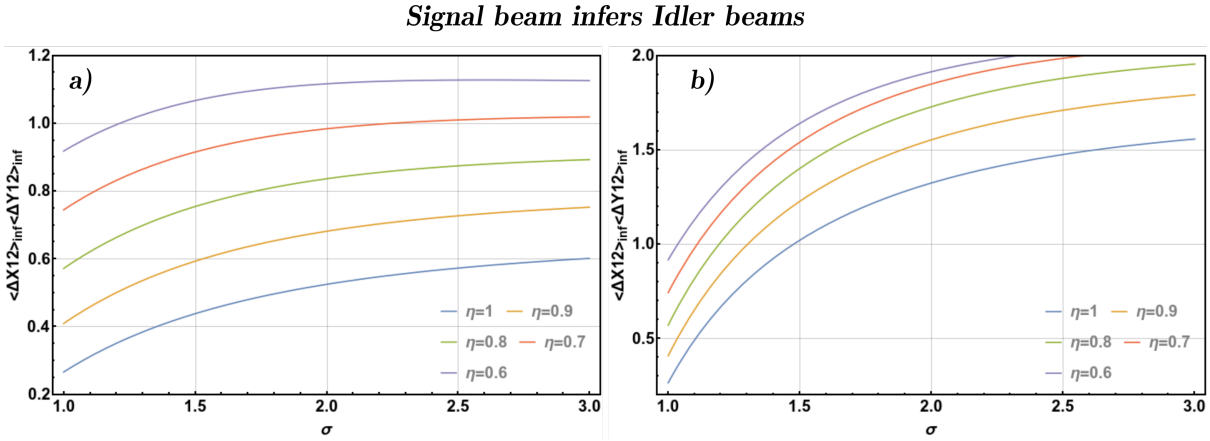

Figure 3.3: In part a) we have that signal beam infer idler beam and vice-versa. In b) the same that in a) but now with the phonon noise effect applied. In both cases the different line colors are representing different detection efficiency of the system.

In the part a) of the figure 3.3 we analyze the inference varying the detection efficiency of the system. In the absence of losses, we expected for all the region analyzed that the inequality 3.11 is violated. In this simulation, we need to input several losses in the detection efficiency for the system no more present steering.

As we discussed in the chapter 2 the presence of the phonon noise in the system degrades the quantum correlations because this "extra noise" increases the noise in the phase quadrature of each beam. If we perform the simulation in the presence of phonon noise as in part b) of the figure 3.3, what is more close of the real system situation, it is perceptible that the inference

between the twin beams in very sensible to this noise. Differently from the situation a) now, considering the better efficiency $\eta = 100\%$, we have steering between the signal and idler beams until $\sigma = 1.5$.

3.2.3 Bipartition pump and sum combination of twin beams

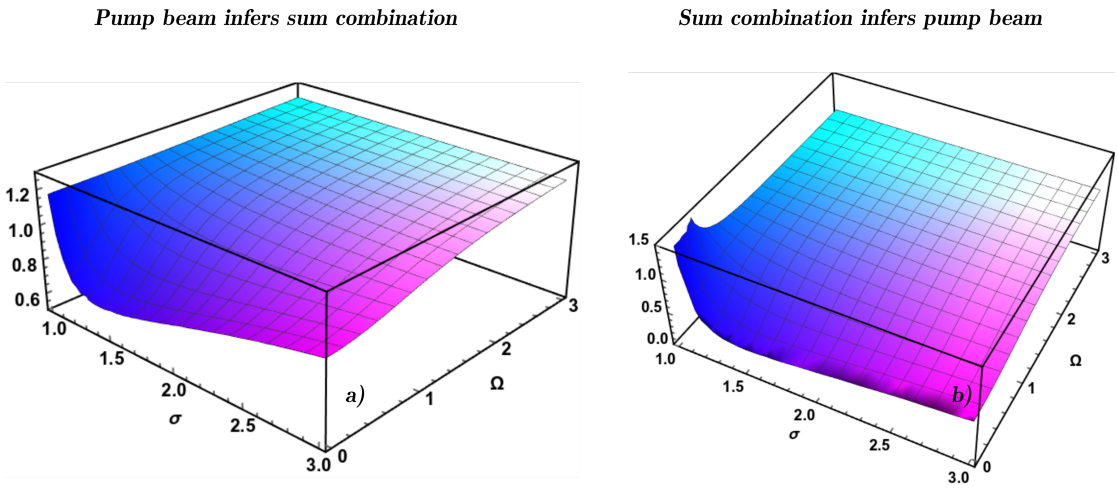

Figure 3.4: a) Pump infers sum combination b) sum combination infers pump beam.

Another bipartition that is interesting to analyze is the pump and sum combination (quadrature sum between the twin beams), in this situation in terms of σ and Ω, we have a region of parameters where there are inference from the pump to sum combination and from sum to pump. We can see in the figure 3.4 that close to $\sigma = 1.7$ we have the better inference in both combinations to $\Omega \approx 0.5$.

In the figure 3.5 we are analyzing the effect of the detection efficiency in each side of the inference. We choose a $\Omega = 0.5$ to perform the analysis and we can see that the better inference in this bipartition is close to $\sigma = 1.7$, where we have a better entanglement in the bipartition pump and sum quadratures as in the figure 2.13.

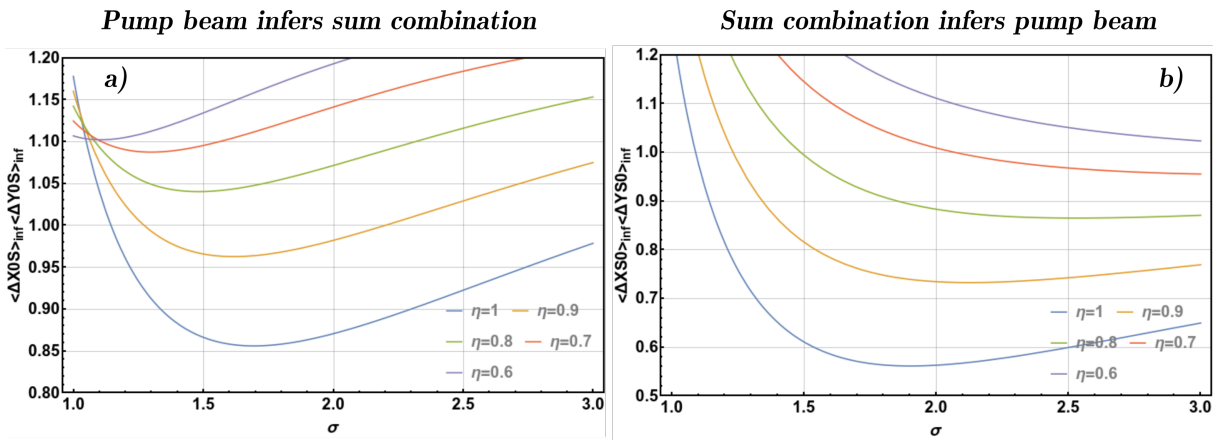

Figure 3.5: a) Inference between pump and sum combination and b) sum combination and pump varying the detection efficiency of the system.

A better simulation of the experimental setup is including the phonon noise, in this case we have the behavior represented in the figure 3.6. There is no steering in this situation considering the measurement in room temperature. In this case, to avoid the presence of phonon noise to measure steering in this combination and to perform this we need to cool down the system down to $-30°C$.

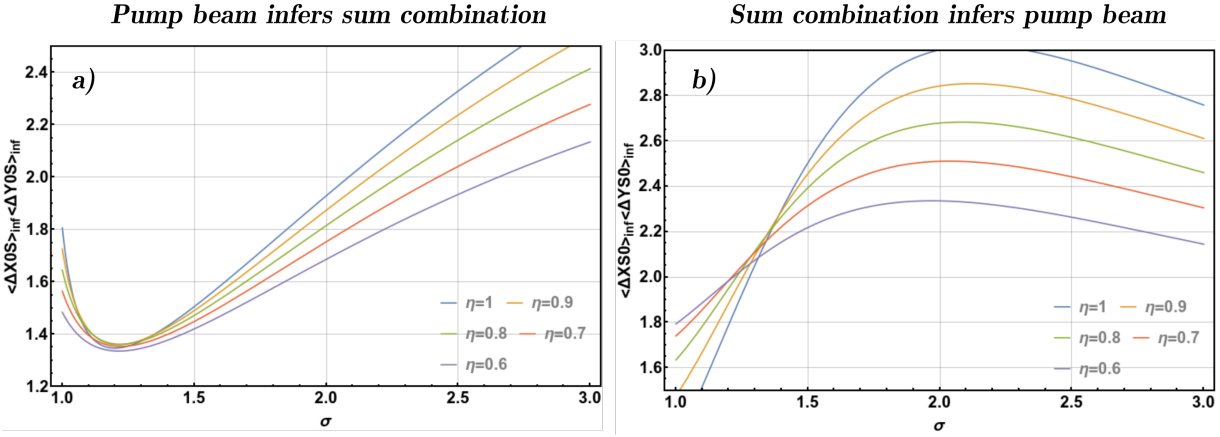

Figure 3.6: a) Inference between pump and sum combination and b) sum combination and pump varying the detection efficiency of the system and considering the phonon noise.

After our analysis we can conclude that it is possible to experimentally measure the steering between the reflected pumping and the twin beams, where the correlation is maximized when the pumping beam has intensity of $\sigma \approx 1.7$.

Chapter 4

Teleportation Protocol

In this chapter we will make a proposal of a continuous variable quantum teleportation protocol using tripartite entanglement generated by the OPO as the quantum resource in teleportation. This protocol is very interesting because it consists, in terms of frequency, of teleporting an input state in a region of wavelengths completely different from the sending station. The wavelength of the beam that will form the input state is $780nm$ which is compatible with the D2 line of Rb that will be teleported to a station in which the wavelength is around $1560nm$. Here it will be presented a first set of ideas showing how this teleportation can be carried out.

In the previous chapter, we have studied several possibilities of analysis of the noise spectrum matrix generated by different combinations of the quadratures of the pump, signal and idler beams. Most of the experimental data used to construct the analysis were based on the parameters we use in the OPO pumped by the titanium sapphire laser. In this way, we obtain predictions about the values of the variances of these quadratures. In this context, we will use these values to verify the possibility of accomplishing the proposal that follows.

In the next section, we will briefly describe the theory of quantum teleportation and what happens in each protocol station. Soon after, we will describe the proposed model and the results we hope to achieve with this protocol.

4.1 Quantum Teleportation

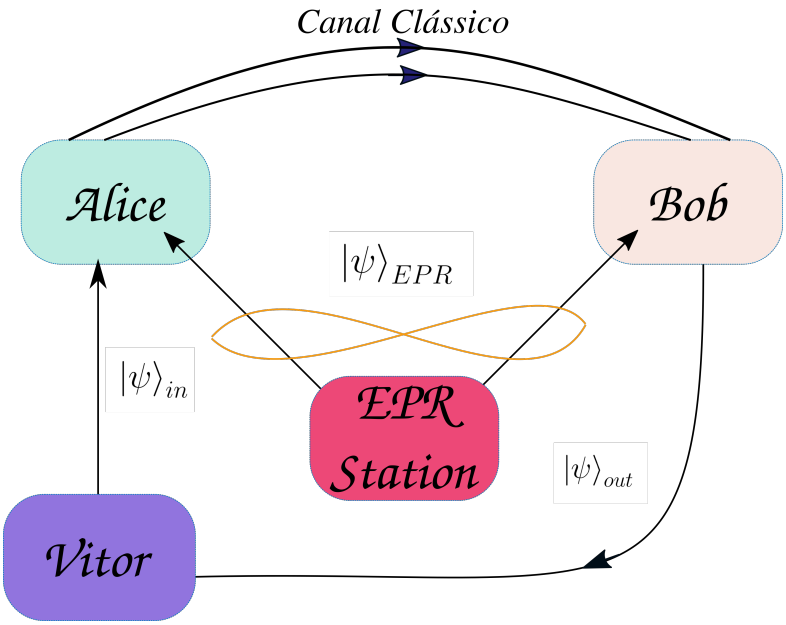

Figure 4.1: General description of a quantum teleportation process.

The process of teleportation of an unknown quantum state is based on the following protocol represented in figure 4.1. An entangled state is generated at the EPR station and shared between stations Alice and Bob. Vitor prepares the input state that will be teleported and sends it to Alice who performs Bell measurements in that state. Through a classical communication channel this result is sent to Bob station that operates on his received field. Since Alice and Bob share an entangled state, Bob is able to operate on his subsystem using the information sent by Alice to obtain a state analogous to Vitor's initial state. After this procedure, the state is sent to the station that produced the input state where the conference will be will be done to know the fidelity between the initial and teleported state. In this context, the figure 4.1 shows a simplified scheme of the teleportation process where the following aspects should be considered[58]:

- the incoming state that is unknown to Alice and Bob remains unknown throughout the teleportation process. If Alice gains some information during Bell's measurement of the input state, Bob will not get a perfect replica of that state;
- the input state does not remain in its initial state due to Bell's measurement, thus ensuring that the non-cloning theorem is not violated;
- the classical communication channel that exists between Alice and Bob is restricted to the speed of light, which precludes a contradiction with the theory of special relativity;

- The teleportation success depends on how the shared state between Alice and Bob is matched.

In the regime of discrete variables, the teleportation of an unknown spin $\frac{1}{2}$ state was firstly proposed by Bennet [56]. The experimental implementation of this protocol is quite complex. The first attempt to perform the teleportation in this scheme was performed by Zeilinger [59] and the protocol was based on the post-selection technique, which consists of selecting experimental data from the set of collected data that meets certain pre-established criteria, that is, a conditional process of measurement that will only work in a quarter of cases, when the necessary operation is identity. Following the description of the teleportation process, Bennet, Vaidman [60] analyzed the process of teleportation of the wave function of a particle at a distance in a variation of the original EPR paradox, in which case the state entangled by Alice and Bob is a EPR state with perfect position and momentum correlations. Soon after, Braustein [61] proposed a quantum teleportation protocol in the regime of continuous variables where the process in non-conditional. The proposal was experimentally performed for the first time by Furusawa [7], where they teleported a coherent state using a source of entangled squeezed states.

In the following sections we will describe each step of the teleportation process separately. We will start describing how we compute the fidelity between two states in section 4.2. The fidelity will be used to characterize the success of the teleportation protocol that we will propose in section 4.3 for the system in study.

4.2 Fidelity

The fidelity can be used to certify information from one station to another. Following the Uhlmann's theorem, we have that the overlap between two states represented by their density matrix $\hat{\rho}_1$ and $\hat{\rho}_2$ is given by:

$$F(\hat{\rho}_1, \hat{\rho}_2) = Tr\left(\sqrt{\sqrt{\hat{\rho}_2}\hat{\rho}_1\sqrt{\hat{\rho}_2}}\right), \tag{4.1}$$

if density matrices $\hat{\rho}_1$ and $\hat{\rho}_2$ represent pure states defined as $\hat{\rho}_1 = |\psi\rangle\langle\psi|$ and $\hat{\rho}_2 = |\phi\rangle\langle\phi|$ the overlap can be rewritten as:

$$F(\hat{\rho}_1, \hat{\rho}_2) = |\langle\psi|\phi\rangle|. \tag{4.2}$$

The overlap has the boundaries $0 \leq F \leq 1$ where the inferior limit of the inequality occurs when the input and output states are orthogonal and the superior limit is achieved when the input state is equal the output state. The fidelity is defined as the square of the overlap in 4.2:

$$\mathcal{F} = |\langle\psi|\phi\rangle|^2. \tag{4.3}$$

Another way to write the fidelity is exposing the equation above in term of the output density matrix:

$$\mathcal{F} = \langle\psi|\,\hat{\rho}_{out}\,|\psi\rangle\,. \tag{4.4}$$

In our case we are teleporting an input coherent state and all noise statistics are Gaussian, so the fidelity is calculated by the following expression [62]:

$$\mathcal{F} = \frac{2e^{-\kappa^{+}-\kappa^{-}}}{\sqrt{(1+V_{out}^{Q})(1+V_{out}^{P})}}, \tag{4.5}$$

where $\kappa_{\pm} = \alpha_{in}^{\pm}(1-g^{\pm})/(1+\Delta^2 X_{out}^{\pm})$ are the gains applied to the classic channels when the signal is sent from Alice station to Bob station, the terms V_{out}^{Q} e V_{out}^{P} are the variances of the quadratures fluctuations of the teleported state measured by Vitor.

There are two main values of fidelity that need to be analyzed, the classical limit and the non-cloning limit. The classic limit defines the maximum value from which entanglement was necessarily used in the teleportation process [63].

$$F_{classic} = \frac{1}{2}, \tag{4.6}$$

in this case the variance of each output quadratures have the value of the vacuum variance, considering a unitary gain in Equation 4.5. To achieve better fidelity than 1/2 is necessary to use an entangled source.

The limit of no-cloning proposed by [64] for coherent states defines the limit of

$$F_{nclo} = \frac{2}{3}, \tag{4.7}$$

where above this limit it is ensured that not only the teleportation process used the entanglement feature but also implies that no copy of the input state was made during the process.

4.3 Proposal of quantum teleportation

In this section we will describe two different quantum teleportation proposals of a coherent state. In the first one we will teleport a coherent state for the sidebands of the fields emitted by the OPO, where the input state has a wavelength of $780nm$ and the station that will receive the teleported state in the region of $1560nm$.

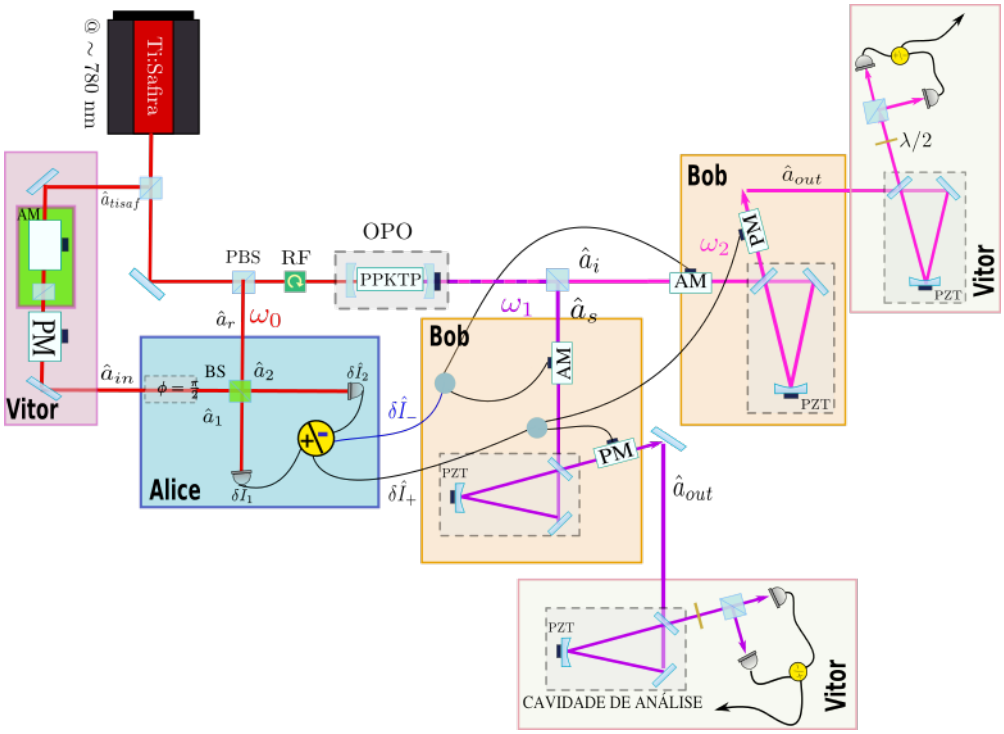

Figure 4.2: Schematics of the teleportation process.

In the process described in the figure 4.2 an unknown state ($\hat{a}_{in}$) prepared in Vitor station is sent to Alice's system who will perform a Bell analysis in this state using as like "EPR-entangled state" the pump beam reflected ($\hat{a}_r$) by the OPO (the source of entangle states), the result will be sent by classical channels to Bob station. The classical result sent to Bob are sum ($\delta\hat{I}_+$) and difference ($\delta\hat{I}_-$) between the photocurrents measured in Alice's photodetectors. Each photocurrent combination will be required to operate a modulation in Bob station. The result of this process $\hat{a}_{out}$ will be sent to Vitor station who will perform a overlap with the input state in order to compute the fidelity of the teleportation protocol.

The second model that we will propose is described in figure 4.8, the main difference in this case is that one of the twin beams will act as an auxiliary in the teleportation process in order to increase the fidelity of the process.

In each subsection that follow we will describe each station that compose the system. Whenever necessary we will separate the two models proposed and expose their main difference.

4.3.1 Vitor - Input state preparation

The input state is prepared at Vitor station, without the knowledge of Alice and Bob. We would like to teleport a coherent state to Bob station, as we discussed before our pump laser generates a coherent beam. To prepare the input state, part of the titanium sapphire beam will be directed to Vitor station where we will perform modifications in this beam in order to

have excess of noise in its sidebands. This excess of noise will be created in two steps, first the beam will undergo an amplitude modulation and then a phase modulation.

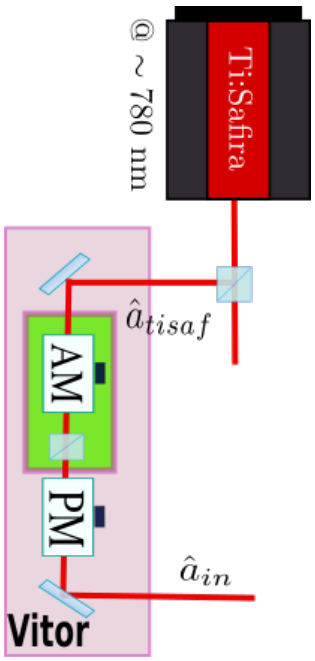

Figure 4.3: Preparing the input state.

We will describe below how these modulations occur.

Amplitude Modulation

Amplitude modulation consists on rewriting the amplitude of the field in the form:

$$\begin{aligned} \alpha(t) &\rightarrow \alpha(t)e^{\gamma_{am}(t)}, \text{ where } \gamma_{am}(t) \ll 1, \\ e^{\gamma_{am}(t)} &\approx 1 + \gamma_{am}(t), \end{aligned} \tag{4.8}$$

this modulation is inserted experimentally by means of an amplitude modulator that could be done by an electro-optics modulator, for instance. With this, we can rewrite the quadrature fluctuations in terms of this modulation.

Using the semiclassical picture, the annihilation operator can be replaced by the complex amplitude α that can be write as a mean value ($\langle\alpha\rangle = \alpha_0$) plus a fluctuation term: $\alpha = \alpha_0 + \delta\alpha$. Where the fluctuations $\delta\alpha = \frac{\delta p(t) + i\delta q(t)}{2}$ are related with the amplitude and phase fluctuations quadratures of the field. Applying the amplitude modulation in the complex amplitude α, we

get:

$$\begin{aligned}\alpha(t)e^{\gamma_{am}(t)} &= \alpha_0 + \frac{\delta p(t) + i\delta q(t)}{2} + \alpha_0\gamma_{am}(t) + \mathcal{O} \\ &\approx \alpha_0 + \left(\frac{\delta p(t) + 2\alpha_0\gamma_{am}(t) + i\delta q(t)}{2}\right),\end{aligned} \tag{4.9}$$

where terms with quadratic dependence in fluctuations were neglected. In the equation above, the amplitude quadrature fluctuations modified by the amplitude modulation will generate the amplitude quadrature $\delta p_{am}(t)$, where:

$$\delta p_{am}(t) \to \delta p(t) + 2\alpha_0\gamma_{am}(t). \tag{4.10}$$

Replacing this term in Equation 4.9, we obtain the transformation in the mean value of the field when it undergoes an amplitude modulation:

$$\alpha(t)e^{\gamma_{am}(t)} = \alpha_0 + \left(\frac{\delta p_{am}(t) + i\delta q(t)}{2}\right). \tag{4.11}$$

Phase modulation

The phase modulation consists of performing the following transformation:

$$\alpha(t) \to \alpha(t)e^{i\phi_{pm}(t)}, \text{ where } \phi_{pm}(t) \ll 1, \tag{4.12}$$

$$e^{i\phi_{pm}(t)} \approx 1 + i\phi_{pm}(t). \tag{4.13}$$

In terms of the field quadratures:

$$\alpha(t)e^{i\phi_{pm}(t)} = \alpha_0 + \frac{\delta p(t)}{2} + i\left(\frac{\delta q(t) + 2\phi_{pm}(t)\alpha_0}{2}\right). \tag{4.14}$$

Where we will replaced the term in parentheses for the phase quadrature $\delta q_{pm}(t)$ that contains the phase modulation term:

$$\delta q_{pm}(t) \to \delta q(t) + 2\alpha_0\phi_{pm}(t) \tag{4.15}$$

When the field undergoes a phase modulation, the complex amplitude becomes:

$$\alpha(t)e^{i\phi_{pm}(t)} = \alpha_0 + \left(\frac{\delta\hat{p}(t) + i\delta\hat{q}_{pm}(t)}{2}\right). \tag{4.16}$$

Input state

The coherent field of titanium sapphire will then undergo the following modifications:

$$\hat{a}_{in} = PM(AM)\hat{a}_{tisaf}. \tag{4.17}$$

where PM is the phase modulation process and AM the amplitude modulation. Knowing how amplitude and phase modulations affect the amplitude of the field, the input state is given by:

$$\hat{a}_{in} = \alpha_{tisaf} + \left(\frac{\delta p_{am}(t) + i\delta q_{pm}(t)}{2}\right), \tag{4.18}$$

where $\delta p_{am}(t)$ and $\delta q_{pm}(t)$ are the quadratures of the field after undergo the modulation process and α_{tisaf} is the mean value of the pump beam that generates the input state.

$$\begin{aligned} \delta p_{am}(t) &= \delta p(t) + 2\alpha_{tisaf}\gamma_{am}(t), \\ \delta q_{pm}(t) &= \delta q(t) + 2\alpha_{tisaf}\phi_{pm}(t). \end{aligned} \tag{4.19}$$

The modulation is a displacement unitary operation that generates a state that can be a statical mixture of coherent states. It may, however, be replaced for any process that generates light in this range of frequency, that can be non-classical states as squeezing states or even states with negative Wigner function, as cat states or Fock states. The type of state produced it will depend on the modulation format applied, if $\gamma_{am}(t)$ and $\phi_{pm}(t)$ were a periodic function of time, the input state will be a displaced vacuum state, therefore, a coherent state. If these modulations were a white noise, the input state will be a thermal state. We will work with a coherent input state.

4.3.2 EPR station

In order to implement the quantum teleportation protocol we need to generate the entangled state that will be shared by Alice and Bob.

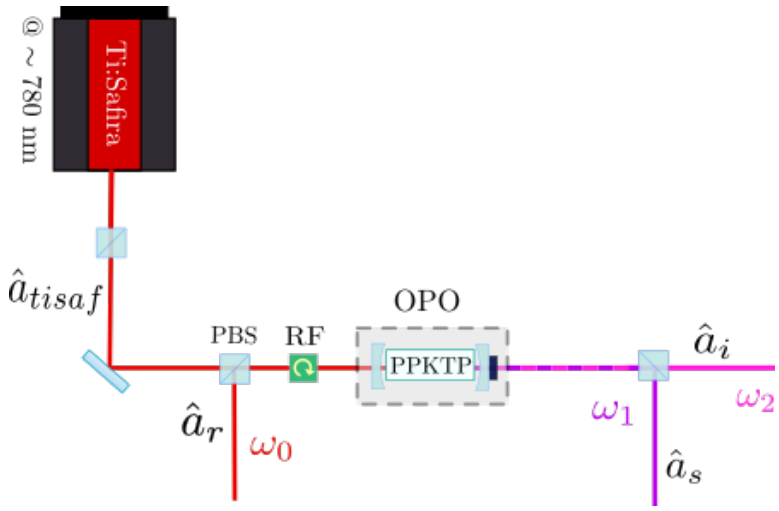

Figure 4.4: Schematic representation of EPR station.

We will use the OPO as a source of entangled states. Above the oscillation threshold, our source emits three beams with distinct colors that are entangled, the reflected pump, signal and idler beams. The emitted beams can be described by the operators:

$$\hat{a}_j = \delta\hat{a}_j + \alpha_j, \tag{4.20}$$

where $j = \{r, s, i\}$ represent the reflected pump, signal and idler beam, respectively. The quadratures fluctuations are given by:

$$\delta\hat{p}_j = \delta\hat{a}_j + \delta\hat{a}_j^\dagger \qquad \delta\hat{q}_j = i\left(\delta\hat{a}_j^\dagger - \delta\hat{a}_j\right). \tag{4.21}$$

One of our purpose is to teleport an input state related to the pump field into the sidebands of the twin beams generated by the OPO. We will rewrite here the Furusawa inequalities so that we keep in mind the possible combinations that must be violated to have the entanglement between the reflected pump, signal and idler beams, and which combinations of quadratures we should keep in mind while preparing the teleportation process:

$$V_0 = \Delta^2\left(\frac{\hat{p}_1 - \hat{p}_2}{\sqrt{2}}\right) + \Delta^2\left(\frac{\hat{q}_1 + \hat{q}_2}{\sqrt{2}} - \kappa_0\hat{q}_0\right) \geq 2, \tag{4.22}$$

$$V_1 = \Delta^2\left(\frac{\hat{p}_0 + \hat{p}_1}{\sqrt{2}}\right) + \Delta^2\left(\frac{\hat{q}_1 - \hat{q}_0}{\sqrt{2}} + \kappa_2\hat{q}_2\right) \geq 2, \tag{4.23}$$

$$V_2 = \Delta^2\left(\frac{\hat{p}_0 + \hat{p}_2}{\sqrt{2}}\right) + \Delta^2\left(\frac{\hat{q}_2 - \hat{q}_0}{\sqrt{2}} + \kappa_1\hat{q}_1\right) \geq 2. \tag{4.24}$$

4.3.3 Alice - Bell measurement

At Alice station we will carry out the Bell measurement which will consist of using the reflected pump beam, represented by $\hat{a}_r$, by the OPO with the input state prepared by Vitor.

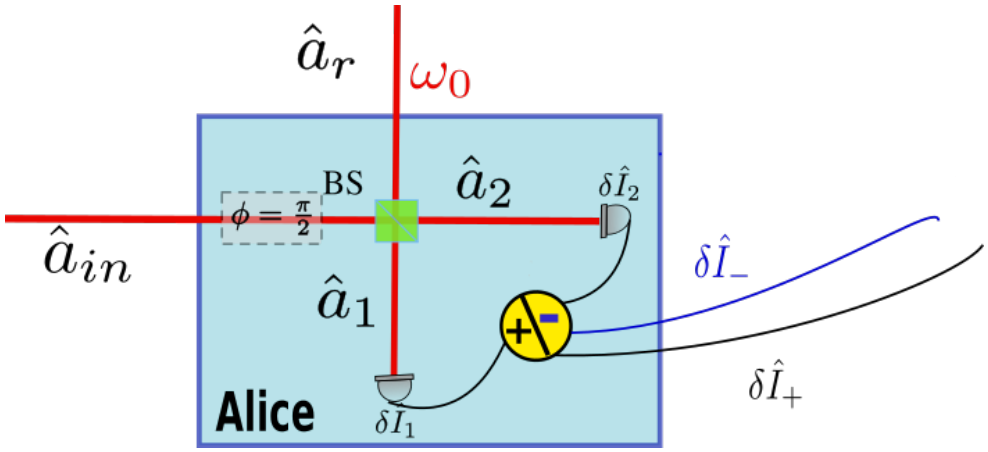

Figure 4.5: Alice station diagram where the Bell measurement will be carried out.

We will make this mixture through a beam splitter(BS) that performs the following operation:

$$\begin{aligned} \hat{a}_1 &= \frac{\hat{a}_r + e^{i\phi}\hat{a}_{in}}{\sqrt{2}}, \\ \hat{a}_2 &= \frac{\hat{a}_r - e^{i\phi}\hat{a}_{in}}{\sqrt{2}}, \end{aligned} \tag{4.25}$$

where $\hat{a}_1$ is the transmitted field and $\hat{a}_2$ the reflected field by the BS and ϕ is a phase added to the input beam. We will impose a phase shift of $\frac{\pi}{2}$ between the pump reflected and the input beams and the intensity of both beams will be adjusted to be the same. In this way we will perform a Bell measurement in Alice's stations as in [65]. The intensity acquired in each photodetector is given by $\hat{I} = \hat{a}^\dagger\hat{a}$ and the combination of the photocurrents acquired will give us the quadratures fluctuations. First, we will compute the photocurrent in each photodetector:

$$\begin{aligned} \hat{I}_1 &= \frac{1}{2}\left[\hat{I}_r + \hat{I}_{in} - i(\hat{a}_{in}^\dagger\hat{a}_r - \hat{a}_r^\dagger\hat{a}_{in})\right] \\ \hat{I}_2 &= \frac{1}{2}\left[\hat{I}_r + \hat{I}_{in} + i(\hat{a}_{in}^\dagger\hat{a}_r - \hat{a}_r^\dagger\hat{a}_{in})\right] \end{aligned} \tag{4.26}$$

We are interested in the combination between these two photocurrents, we would like to know in terms of the quadratures fluctuations the value of $\hat{I}_\pm = \hat{I}_1 \pm \hat{I}_2$:

$$\begin{aligned} \hat{I}_+ &= \hat{I}_r + \hat{I}_{in}, \\ \hat{I}_- &= i(\hat{a}_{in}^\dagger\hat{a}_r - \hat{a}_r^\dagger\hat{a}_{in}) \end{aligned} \tag{4.27}$$

The equation above will be computed remembering that the field operator can be written as $\hat{a} = \alpha + \left(\frac{\delta\hat{p}+i\delta\hat{q}}{2}\right)$. The photocurrent combination in terms of the amplitude and phase quadratures is given by:

$$\begin{aligned} \hat{I}_+ &= \alpha_r^2 + \alpha_{in}^2 + \alpha_r\delta\hat{p}_r + \alpha_{in}\delta\hat{p}_{in}, \\ \hat{I}_- &= -\alpha_r\delta\hat{q}_{in} + \alpha_{in}\delta\hat{q}_r, \end{aligned} \tag{4.28}$$

where the mean value $\alpha_{in} = \alpha_r = \alpha$ and we will acquire separately the DC part related to the mean field and the HF part related to the fluctuations of the field will be send to Bob station:

$$\begin{aligned} \delta\hat{I}_+ &= \alpha(\delta\hat{p}_r + \delta\hat{p}_{tisaf}), \\ \delta\hat{I}_- &= \alpha(\delta\hat{q}_r - \delta\hat{q}_{tisaf}). \end{aligned} \tag{4.29}$$

4.3.4 Bob - Received station

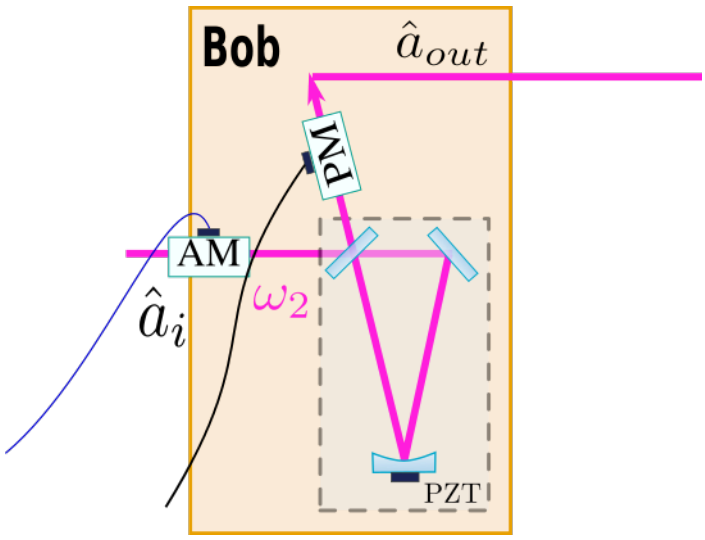

Figure 4.6: Input state destination station.

After the Bell measurement in Alice station, the classical signals are sent to Bob station, as shown in figure 4.6. Each photocurrent combination will pass for an amplification system whose electronic gains are adjustable.

$$\begin{aligned} \delta\hat{I}_+ &= g_+\alpha(\delta\hat{p}_r + \delta\hat{p}_{tisaf}), \\ \delta\hat{I}_- &= g_-\alpha(\delta\hat{q}_r - \delta\hat{q}_{tisaf}). \end{aligned} \tag{4.30}$$

Teleport model 1

In the protocol proposed here, we will work with classical signals generated after the Bell measurement in each beam of the EPR pair separately. Each beam of the EPR pair will have its own Bob station and its Vitor conference station. The procedure that we will describe below will be performed on both the signal and idler beams. The classical signal will be split electronically to perform EPR pair amplitude modulation.

Initially, we will modulate the phase of the beams by applying a classical signal proportional to $\delta\hat{I}_-$:

$$\begin{aligned}\hat{a}^{pm1}_{(s,i)} &= \langle\hat{a}\rangle_{(s,i)} + \delta\hat{a}_{(s,i)} + i\delta\hat{I}_- \\ \hat{a}^{pm1}_{(s,i)} &= \alpha_{(s,i)} + \left(\frac{\delta\hat{p}_{(s,i)} + i\delta\hat{q}_{(s,i)}}{2}\right) + ig_-\alpha(\delta\hat{q}_r - \delta\hat{q}_{tisaf}).\end{aligned} \tag{4.31}$$

we are working with phase modulations because phase modulators have less experimental losses then amplitude modulators. Experimentally g_- will be adjusted to maximize the fidelity of the teleportation process. For now, let's rewrite the equation above for each signal and idler fields and rewrite the quantity $\alpha g^l_- = \epsilon^l_-$, where $l = \{s, i\}$:

$$\begin{aligned}\hat{a}^i_{pm1} &= i(\epsilon^i_-\delta\hat{q}_r + \frac{\delta\hat{q}_i}{2}) - i\epsilon^i_-\delta\hat{q}_{tisaf} + \frac{\delta\hat{p}_i}{2} + \alpha_i, \\ \hat{a}^s_{pm1} &= i(\epsilon^s_-\delta\hat{q}_r + \frac{\delta\hat{q}_s}{2}) - i\epsilon^s_-\delta\hat{q}_{tisaf} + \frac{\delta\hat{p}_s}{2} + \alpha_s.\end{aligned} \tag{4.32}$$

After the above step, the beam is sent to an analysis cavity locked on the side of the resonance peak. The aim is to ensure that a $\theta = \frac{\pi}{2}$ phase will be added to the field allowing the conversion of phase to amplitude fluctuations. The reflected field will be:

$$\hat{a}_{reflected} = e^{i\frac{\pi}{2}}\delta\hat{a}_{pm1}. \tag{4.33}$$

Thus, the reflected signal and idler fields are:

$$\begin{aligned}\hat{a}^i_{ref} &= -(\epsilon^i_-\delta\hat{q}_r + \frac{\delta\hat{q}_i}{2}) + \epsilon^i_-\delta\hat{q}_{tisaf} + i\frac{\delta\hat{p}_i}{2} + i\alpha_i, \\ \hat{a}^s_{ref} &= -(\epsilon^s_-\delta\hat{q}_r + \frac{\delta\hat{q}_s}{2}) + \epsilon^s_-\delta\hat{q}_{tisaf} + i\frac{\delta\hat{p}_s}{2} + i\alpha_s.\end{aligned} \tag{4.34}$$

The beam reflected by the analysis cavity will undergo another phase modulation proportional to the classical signal $\delta\hat{I}_+$:

$$\hat{a}^{(s,i)}_{pm2} = \hat{a}^{(s,i)}_{ref} + i\delta\hat{I}_+. \tag{4.35}$$

Replacing the quantity $\alpha g+^{l} = \epsilon_{+}^{l}$, where $l = \{s, i\}$:

$$\begin{aligned}
\hat{a}_{pm2}^{i} &= i[(\frac{\delta\hat{p}_i}{2} + \epsilon_{+}^{i}\delta\hat{p}_r) + i(\epsilon_{-}^{i}\delta\hat{q}_r + \frac{\delta\hat{q}_i}{2}) + (\epsilon_{+}^{i}\delta\hat{p}_{tisaf} - i\epsilon_{-}^{i}\delta\hat{q}_{tisaf}) + \alpha_i], \\
\hat{a}_{pm2}^{s} &= i[(\frac{\delta\hat{p}_s}{2} + \epsilon_{+}^{s}\delta\hat{p}_r) + i(\epsilon_{-}^{s}\delta\hat{q}_r + \frac{\delta\hat{q}_s}{2}) + (\epsilon_{+}^{s}\delta\hat{p}_{tisaf} - i\epsilon_{-}^{s}\delta\hat{q}_{tisaf}) + \alpha_s]. \qquad (4.36)
\end{aligned}$$

The variances of the amplitude and phase quadratures related to each signal and idler beams are given by:

$$\begin{aligned}
\Delta^2\hat{p}_{(s,i)}^{out} &= \Delta^2(2\epsilon_{-}^{(s,i)}\delta\hat{q}_r + \delta\hat{q}_{(s,i)}) + 4(\epsilon_{-}^{(s,i)})^2\Delta^2\delta\hat{q}_{tisaf} \\
\Delta^2\hat{q}_{(s,i)}^{out} &= \Delta^2(2\epsilon_{+}^{(s,i)}\delta\hat{p}_r + \delta\hat{p}_{(s,i)}) + 4(\epsilon_{+}^{(s,i)})^2\Delta^2\delta\hat{p}_{tisaf} \qquad (4.37)
\end{aligned}$$

in this case, as we are applying a phase modulation in the output field of the cavity we will rotate the output quadratures of the field that is clear in the Equation 4.37, where the out amplitude quadrature are related with the phase quadrature of the input beam, and the out phase quadrature are related with the amplitude quadrature of the input beam.

In order for the fluctuation spectra of the above components be equivalent to that of the input state, the quadrature fluctuations related to the terms $\Delta^2(2\epsilon_{-}^{(s,i)}\delta\hat{q}_r + \delta\hat{q}_{(s,i)})$ and $\Delta^2(2\epsilon_{+}^{(s,i)}\delta\hat{p}_r + \delta\hat{p}_{(s,i)})$ must be maximally entangled, which means that their values tend to zero and the gain must be adjusted in a way that $\epsilon_{-}^{i,s} = -\frac{1}{2}$ and $\epsilon_{+}^{i,s} = \frac{1}{2}$. If we have this condition being obeyed, the output state is:

$$\begin{aligned}
\Delta^2\hat{p}_{(s,i)}^{out} &= \Delta^2\delta\hat{q}_{tisaf} \\
\Delta^2\hat{q}_{(s,i)}^{out} &= \Delta^2\delta\hat{p}_{tisaf}. \qquad (4.38)
\end{aligned}$$

This ensures that the incoming state was teleported.

But, not necessarily we have the states maximally entangled, in this situation adjusting the electronic gain to have the best fidelity, the output variances are given by:

$$\begin{aligned}
\Delta^2\hat{p}_{(s,i)}^{out} &= \Delta^2(-\delta\hat{q}_r + \delta\hat{q}_{(s,i)}) + \Delta^2\delta\hat{q}_{tisaf} \\
\Delta^2\hat{q}_{(s,i)}^{out} &= \Delta^2(\delta\hat{p}_r + \delta\hat{p}_{(s,i)}) + \Delta^2\delta\hat{p}_{tisaf}, \qquad (4.39)
\end{aligned}$$

where we can recognize the Furusawa inequality Equation 4.24, wherein the term $\kappa_2 = 0$ in this case. Considering the $\Delta^2\delta\hat{q}_{tisaf}$ and $\Delta^2\delta\hat{p}_{tisaf}$ the noise of a coherent state, the fidelity of this system can be written as:

$$\mathcal{F} = \frac{2}{\sqrt{(1+V_q+1)(1+V_p+1)}}, \qquad (4.40)$$

where $V_p = \Delta^2(-\delta\hat{q}_r + \delta\hat{q}_{(s,i)})$ and $V_q = \Delta^2(\delta\hat{p}_r + \delta\hat{p}_{(s,i)})$. In this case, the fidelity will change with the input power normalized by the threshold as in the figure below:

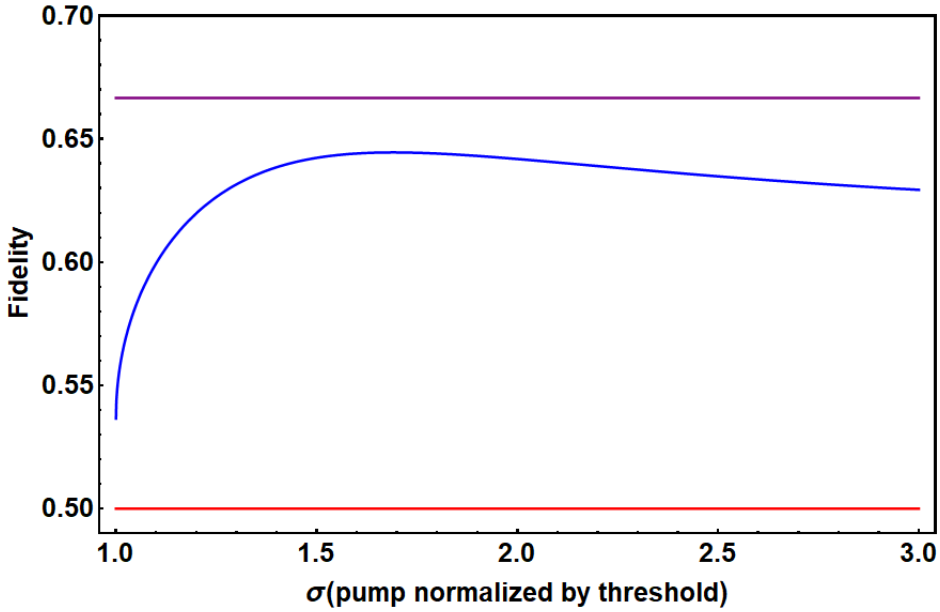

Figure 4.7: Fidelity of the system in blue. The red line represents the classical limit and the purple line the non-cloning limit.

In the figure 4.7 the blue line represents the result of the fidelity in terms of the system parameters. The classical limit (red line) is superpass for all the region being analyzed. But, as we are send the same input state to two Bob stations, the non-cloning limit is not achieved. What implies that Bob doesn't reconstructed the input state in a higher fidelity way.

Teleport model 2

Another teleport protocol that we developed is using one of the twin beams as an auxiliar in the teleportation process. Now, instead of we teleport the input state to idler and signal Bob stations, we will use Charlie station as a support in the teleportation process with the purpose to increase the fidelity of the process.

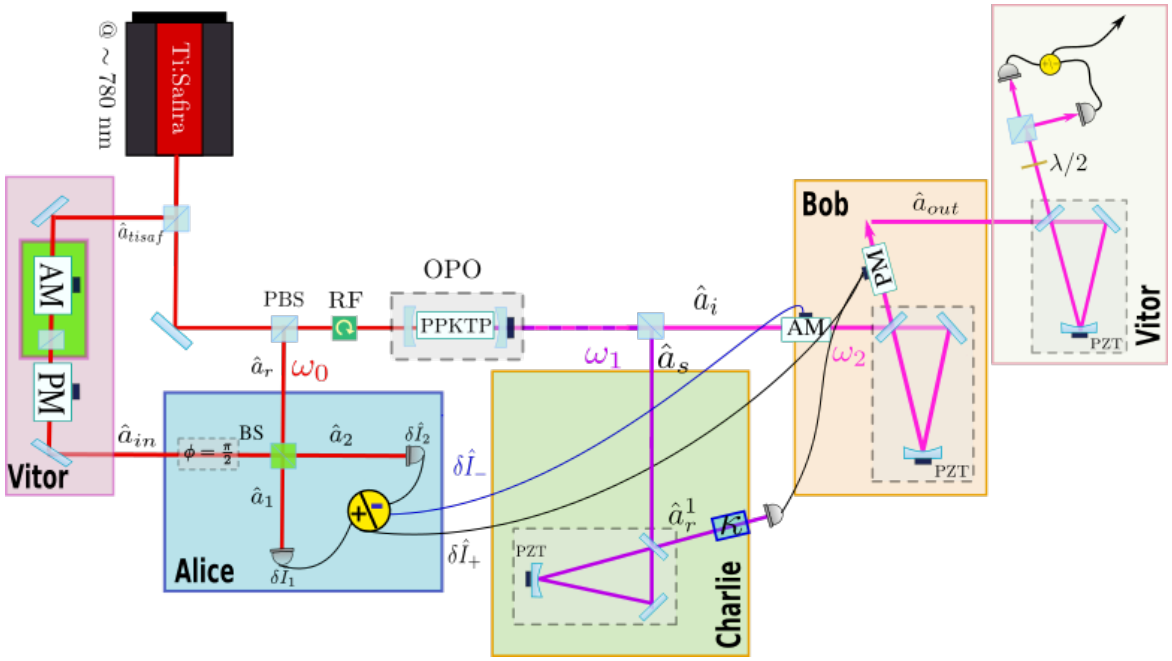

Figure 4.8: Diagram of the teleportation process.

In the figure 4.8 in Charlie station, the signal beam represented by the annihilation operator $\hat{a}_s$ will pass through an analysis cavity locked in the side of fringe, what implies that the sidebands of the reflected field will undergo:

$$\begin{aligned} \hat{a}^s_{ref} &= \alpha_s + e^{i\frac{\pi}{2}}\delta\hat{a}_s \\ &= \left[\alpha_s + i\left(\frac{\delta\hat{p}_s + i\delta\hat{q}_s}{2}\right)\right] \end{aligned} \tag{4.41}$$

The photocurrent acquired by the photodetector in Charlie station is given by $\hat{I}_c = \hat{a}^{s\dagger}_{ref}\hat{a}^s_{ref}$:

$$\begin{aligned} \hat{I}_c &= \alpha_s^2 - \alpha_s\delta\hat{q}_s \\ \delta\hat{I}_c &= -\alpha_s\varsigma\delta\hat{q}_s \end{aligned} \tag{4.42}$$

where we see that the quadrature acquired by the photodetector contains information about the phase quadrature and $\kappa = \alpha_s\varsigma$ is a controllable electronic gain. We will modulate the Bob field with this term in a way that the Equation 4.36 will becomes:

$$\begin{aligned} \hat{a}^i_{pm2} &= i(\frac{\delta\hat{p}_i}{2} + \epsilon^i_+\delta\hat{p}_r) - (\epsilon^i_-\delta\hat{q}_r + \frac{\delta\hat{q}_i}{2}) \\ &+ i(\epsilon^i_+\delta\hat{p}_{tisaf} - i\epsilon^i_-\delta\hat{q}_{tisaf}) + i\alpha_i - \kappa\alpha_s\delta\hat{q}_s \end{aligned} \tag{4.43}$$

And, the variances of the output field in Bob station is given by:

$$\begin{aligned}\Delta^2\hat{p}_i^{out} &= \Delta^2(2\epsilon_-^i\delta\hat{q}_r + \delta\hat{q}_i - \kappa\delta\hat{q}_s) + 4(\epsilon_-^i)^2\Delta^2\delta\hat{q}_{tisaf} \\ \Delta^2\hat{q}_i^{out} &= \Delta^2(2\epsilon_+^i\delta\hat{p}_r + \delta\hat{p}_i) + 4(\epsilon_+^i)^2\Delta^2\delta\hat{p}_{tisaf}\end{aligned} \tag{4.44}$$

Where we can identify that if adjustable electronic gains $\epsilon_+^s = -\epsilon_-^s = \frac{1}{2}$ we will have in the variance of the output amplitude quadrature one term associated with the second Furusawa inequality:

$$\begin{aligned}\Delta^2\hat{p}_i^{out} &= \Delta^2(-\delta\hat{q}_r + \delta\hat{q}_i - \kappa\delta\hat{q}_s) + \Delta^2\delta\hat{q}_{tisaf} \\ \Delta^2\hat{q}_i^{out} &= \Delta^2(\delta\hat{p}_r + \delta\hat{p}_i) + \Delta^2\delta\hat{p}_{tisaf}\end{aligned} \tag{4.45}$$

In the limit that the first variance in each output quadrature tends to zero, we achieve a perfect teleportation process of the optical field.

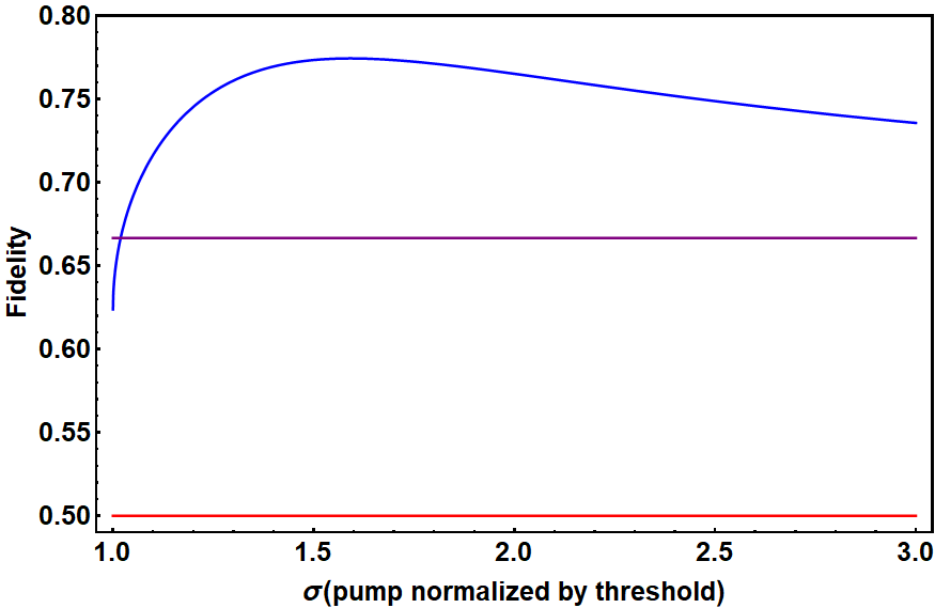

Figure 4.9: Fidelity of the system in red. The purple line represents the classical limit and the orange line the non-cloning limit. The blue line represents the fidelity computed in the first model analyzed.

The fidelity in this case is represented in the figure 4.9 in which we can see that using Charlie station we increase the fidelity of the system to superpass the non-cloning limit for almost all σ unless in a region very close to the threshold power, because there is not entanglement between pump and twin-beam close $\sigma = 1$.

4.3.5 Vitor - Analysis station

Since Alice and Bob do not have information about the incoming state, Vitor performs the conference process because it is where the state was created.

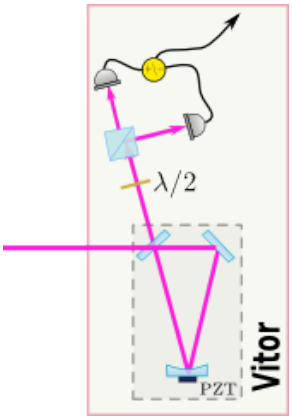

Figure 4.10: Vitor analysis station.

In the figure 4.10 we have a representation of Vitor station. Vitor receives the input state sent by Bob and through an analysis cavity characterizes the state in terms of the fluctuations of the amplitude and phase quadratures. In this way there are the conference between the teleported state and the initial state.

We have seen in this section two different ways to teleport an input state prepared with the pump beam frequency to the telecom region. In the model 1 the fidelity of the system is below than $\frac{2}{3}$. When we use the idler beam as an auxiliary in the teleportation protocol this limit is exceeded.

Chapter 5

Experimental Results

In this chapter we will describe the first experimental results obtained with the OPO pumped by a Titanium Sapphire laser in resonance with the D2 line of rubidium. We will start describing each part of the experimental apparatus, the noise characterization of our pump beam and a phonon noise characterization of the system. To finalize, we will show the first result of the correlations between the pump, signal and idler beams using this OPO as the resource of entangled states.

5.1 Experimental Setup

In the figure 5.1 we see a schematic representation of the setup. We have a Titanium Saphire homemade laser as a pump beam, a linear OPO with a type II PPKTP crystal acting as gain medium inside the cavity. The type II configuration of the crystal enable us to separate the twin beams generated by the OPO with a polarizing beam splitter(PBS), due they twin beams have different polarizations. The pump beam reflected by the cavity is sent to a Faraday rotator (FR) and we acquire its signal in the analysis cavity 0. The generated twin beams are separated in the PBS and each one (represented in the figure by ω_1 and ω_2) are sent to the respectively analysis cavity, where label 1 refers to the signal beam and 2 to the idler beam. Associated with each analysis cavity, we have a balanced detection system, where each beam will be split equally in two by the set of half waveplates and PBS. Finally, the beams are sent to photodetectors connected with the electronic acquisition system.

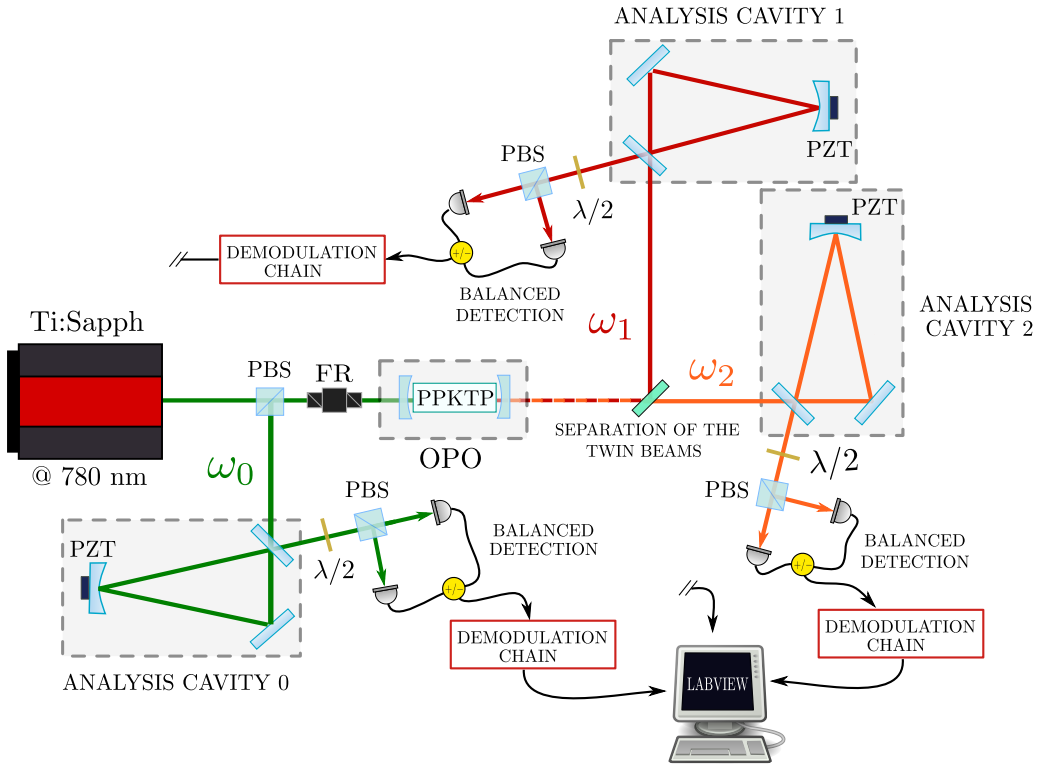

Figure 5.1: Schematic representation of the experimental setup.

In the following subsections we will describe in details each part of the system and in the section 5.3 the principal results acquired in this project.

5.1.1 Titanium Sapphire Laser

The titanium sapphire laser is pumped by a Verdi-V10 (Coherent company) and it operates between 730 nm and 800 nm region, that can be extended by changing the mirrors of the cavity containing the gain medium. Operating around 780 nm and pumped with 5W, the output power is close to 1.3W, with an efficiency of 26%, close to the efficiency of we found in literature [66, 67]. The linewidth of the laser is less than $0,2$ MHz. We also verified that the transverse profile of the laser corresponds to a Gaussian profile no noticeable of astigmatism. This laser was first mounted by the colleague Flavio C. D. de Moraes as part of his masters[16] and since then has been continuously improved.

The titanium sapphire laser is used in our experiment as a pump source of the OPO, because it generates an approximately coherent state. We work with the laser locked in line D2 of *Rb*. Thus, we have a pump source that makes us able to perform a quantum communication network where one of the nodes of the network can be a process performed with an atomic media. Other of the uses of this laser is in a four wave mixing (FWM) process to generate squeezing states of light, for example. Furthermore, it enables the process of teleportation that we envisage accomplishing in this project. It can be used in conjunction with the reflected pump to form

the state that we wish to teleport to the twin beams. We would teleport a coherent state to one of the beams generated by the OPO in a region distinct from the electromagnetic spectrum. Thus, the titanium sapphire laser provides us several possibilities of experiments that can be performed, using it as a pump source in a OPO.

Firstly we need to characterize the noise of the fluctuations of its quadratures. The noise spectrum of a laser will have different behaviors for different analysis frequencies. An illustrative example is in the figure 5.2, that we can see for the analysis of the Laser $RIO@1560\ nm$ that the amplitude quadrature is with the same amount of noise than the shot noise and the phase quadrature has an excess of noise, in both case the fluctuation in the quadratures have different values for the range of analysis frequency measured[1].

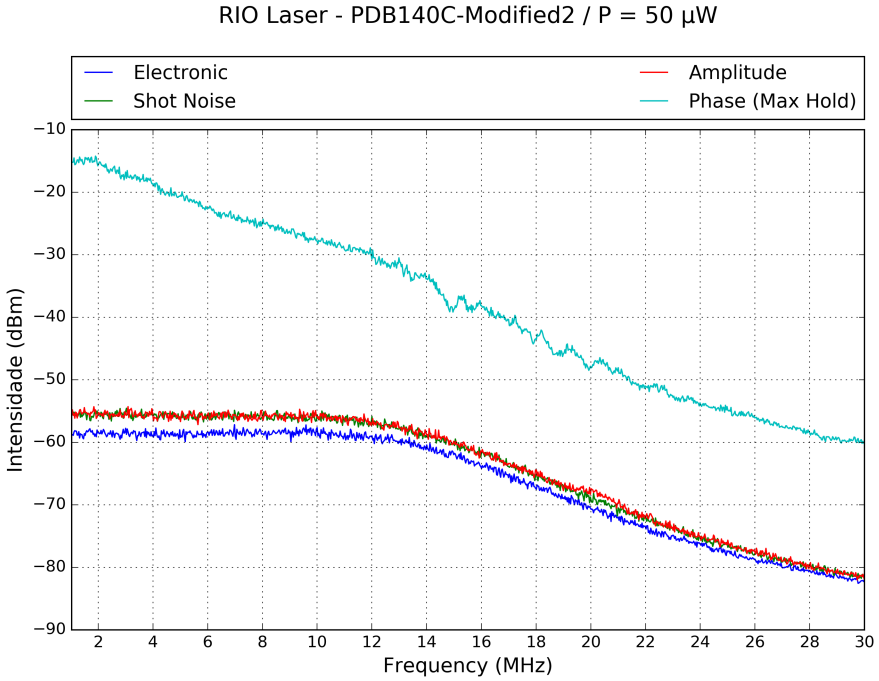

Figure 5.2: Laser RIO@1560nm - Fluctuations of the noise quadratures for a power of $50\mu W$.

To perform the measurement we will use the self-homodyne technique described in the section 1.5.3. The analysis cavity that we used is like in the figure 5.4 (in the subsection 5.1.2 we will give more details about this kind of cavity). The input mirror is partially transmissor from LAYERTEC company and the other two are high reflected produced by ATFilms. In the table 5.1.1 we have the technical characteristics of the cavity.

The fluctuations analysis of the pump beam is required because the extra pump noise degradate the correlation between the OPO output beams. We measured this noise in different frequencies as we show in the figure 5.3. We can see that the phase noise decreases when the analysis frequency increase. The amplitude quadrature is close to the shot noise independently

[1]Due the gain of the amplifier detector PDB140C, the shot noise is flat until approximately 14 Mhz and after this the signal decreases with the frequency.

Parameters	@780(nm)	Rc=200mm
M_{in}	T=5(1)%	F= 160
M_{out}	HR	BW= 4.3MHz
M_c	HR	V=96%

Table 5.1: Characteristics of the mirrors that form the analysis cavity of the pump beam.

of the analysis frequency. We can conclude that above 9MHz the titanium sapphire laser can be described by a coherent state.

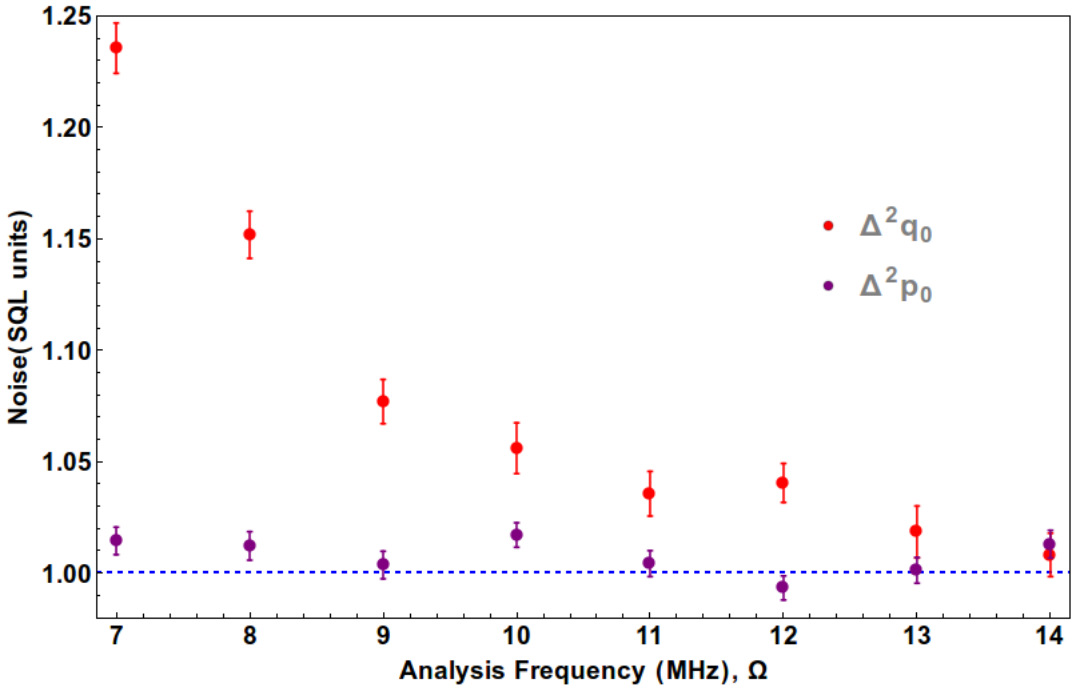

Figure 5.3: Spectrum noise of the titanium sapphire laser in terms of the analysis frequency of the system. The input pump power was 90mW. Measurement performed when the Titatinum Sapphire laser was pumped with a Verdi-V18 (Coherent company).

5.1.2 Analysis cavity - technical characteristics

In general, the analysis cavities that we use in the laboratory have the following schematic drawing 5.4.

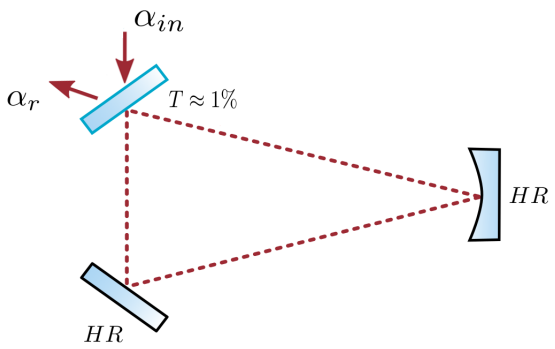

Figure 5.4: Representation of the analysis cavity model that we used in the experiment. The cavity is composed of two flat mirrors and one curved mirror. Associated with the curved mirror we have a PZT used to perform the cavity scan. The mirrors M2 and M3 are highly reflective and the mirror M1 has transmissivity close to 4%.

The analysis cavity has no gain medium and its main purpose is to perform the rotation of the phase quadrature, as discussed in the section 1.5.3, into amplitude quadrature. In this way we have access to the entire spectrum of noise needed to characterize the correlations between the beams emitted by the OPO.

Parameters	Pump beam	Twin beams
F	160	200
$L_g(mm)$	400	400
BW(MHz)	4,3	4
$R_c(mm)$	200	200

Table 5.2: Analysis cavities parameters.

Because of the OPO configuration, the bandwidth of its is approximately 15MHz. The analysis frequency that we performed measurements is 7MHz (approximately $\frac{1}{3}$ of the OPO bandwidth). This analysis frequency limits the upper access region for bandwidth of the analysis cavity. The bandwidth of the analysis cavity is computed from the equation $\Omega \leq \sqrt{2}\delta\omega$ [49], where Ω is the analysis frequency and $\delta\omega$ is the OPO bandwidth. In the table 5.1.2 we have the parameters of each analysis cavity that we use in our system.

5.1.3 Balanced detection system

Each beam generated by the OPO is reflected by an analysis cavity. The reflected beam is sent to a balanced detection scheme that consist of a $\lambda/2$ (half waveplate) plus one PBS (polarizing beam splitter) and two photodetectors as in the figure 5.1. With this acquisition system we are

able to perform the noise analysis of the system. The balanced detection setup is explicit in the figure 5.5. We consider that we have two beams that are represented by the annihilation operators $\hat{a}$ and $\hat{b}$, that will be combined in a beam splitter (BS) and each output of the BS will be sent to a photodetector.

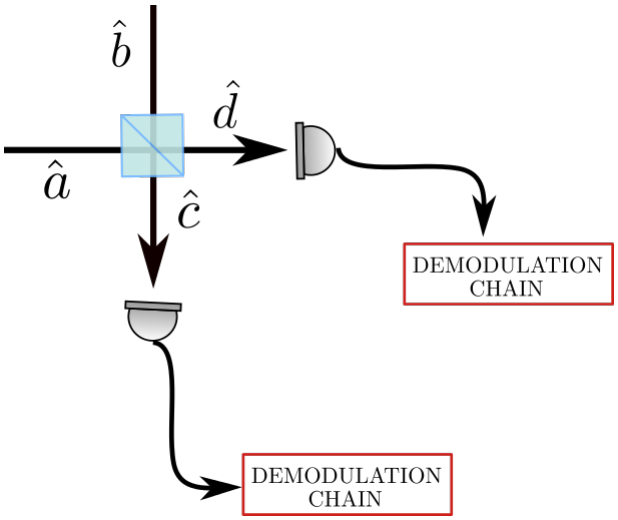

Figure 5.5: Balanced detection system.

The BS will perform a combination of the input fields $\hat{a}$ and $\hat{b}$ and in the output we will have the modes $\hat{c}$ and $\hat{d}$ given by:

$$\hat{c} = |r|\hat{b} + |t|\hat{a} \qquad \hat{d} = |t|\hat{b} - |r|\hat{a}, \tag{5.1}$$

where $r = |r|e^{i\theta_r}$, $t = |t|e^{i\theta_t}$, $|r| = \sqrt{1-T}$ and $|t| = \sqrt{T}$. The phase difference between the reflected and transmitted fields is π in order to satisfy energy conservation and because of this the minus sign appears in the $\hat{d}$ combination. The photocurrent measured in each detector is computed by the number operator of each mode:

$$\hat{I}_c = \hat{c}^\dagger\hat{c} = \frac{1}{2}\left[\hat{I}_a + \hat{I}_b + \hat{a}^\dagger\hat{b} + \hat{a}\hat{b}^\dagger\right], \tag{5.2}$$

$$\hat{I}_d = \hat{d}^\dagger\hat{d} = \frac{1}{2}\left[\hat{I}_a + \hat{I}_b - \hat{a}^\dagger\hat{b} - \hat{a}\hat{b}^\dagger\right], \tag{5.3}$$

where we used $R = T = \frac{1}{2}$, because we are performing a balanced detection process. With the sum and subtraction of the photocurrents we will have information about the input noise in the acquisition system. The subtraction noise will characterize the shot noise and the sum is equivalent to acquire all the noise of the beam, similar of an single photodetector. The sum

and subtraction photocurrents are given by:

$$\hat{I}_+ = \hat{I}_c + \hat{I}_d = \hat{a}^\dagger\hat{a} + \hat{b}^\dagger\hat{b}, \tag{5.4}$$

$$\hat{I}_- = \hat{I}_c - \hat{I}_d = \hat{a}^\dagger\hat{b} + \hat{b}^\dagger\hat{a}. \tag{5.5}$$

The mean value and the variances associated with the sum and subtraction of the photocurrents are $\Delta^2\hat{I}_\pm = \langle\hat{I}_\pm^2\rangle - \langle\hat{I}_\pm\rangle^2$:

$$\begin{aligned}
\Delta^2\hat{I}_- &= \langle(\hat{a}^\dagger\hat{b} + \hat{b}^\dagger\hat{a})^2\rangle - \langle\hat{a}^\dagger\hat{b} + \hat{b}^\dagger\hat{a}\rangle^2 \\
&= \langle\hat{I}_a\rangle + \langle\hat{I}_b\rangle + 2\langle\hat{I}_b\rangle\langle\hat{I}_a\rangle + \langle\hat{b}\hat{b}\rangle\langle\hat{a}^\dagger\hat{a}^\dagger\rangle + \langle\hat{b}^\dagger\hat{b}^\dagger\rangle\langle\hat{a}\hat{a}\rangle \\
&- (\langle\hat{b}\rangle^2\langle\hat{a}^\dagger\rangle^2 + \langle\hat{b}^\dagger\rangle^2\langle\hat{a}\rangle^2 + 2\langle\hat{a}^\dagger\hat{b}\rangle\langle\hat{a}\hat{b}^\dagger\rangle, \qquad (5.6) \\
\Delta^2\hat{I}_+ &= \langle(\hat{a}^\dagger\hat{a} + \hat{b}^\dagger\hat{b})^2\rangle - \langle\hat{a}^\dagger\hat{a} + \hat{b}^\dagger\hat{b}\rangle^2 \\
&= \langle:\Delta^2\hat{I}_a:\rangle + \langle\hat{I}_a\rangle + \langle:\Delta^2\hat{I}_b:\rangle + \langle\hat{I}_b\rangle. \qquad (5.7)
\end{aligned}$$

We will consider that the $\hat{b}$ field operator acts on a coherent state in such a way that $\hat{b}|\alpha\rangle = \beta|\alpha\rangle$, where $\beta = |\beta|e^{i\theta}$, and that the operator $\hat{a}$ acts in the state $|\phi\rangle$. The general state of the system is the product $|\Psi\rangle = |\alpha\rangle \otimes |\phi\rangle$. Let us compute the variance of the combination of the photocurrents in these states:

$$\begin{aligned}
\Delta^2\hat{I}_- &= \langle\hat{a}^\dagger\hat{a}\rangle + 2|\beta|^2\langle\hat{a}^\dagger\hat{a}\rangle + |\beta|^2 + \beta^2\langle\hat{a}^\dagger\hat{a}^\dagger\rangle + \beta^{*2}\langle\hat{a}\hat{a}\rangle - (\beta^2\langle a^\dagger\rangle^2 + \beta^{*2}\langle a\rangle^2 + 2|\beta|^2\langle\hat{a}^\dagger\rangle\langle\hat{a}\rangle) \\
&= \langle\hat{a}^\dagger\hat{a}\rangle + |\beta|^2\langle(e^{i\theta}\hat{a}^\dagger + e^{-i\theta}\hat{a})^2\rangle - |\beta|^2(e^{i\theta}\langle\hat{a}^\dagger\rangle + e^{-i\theta}\langle\hat{a}\rangle)^2 \\
&= \langle\hat{I}_a\rangle + |\beta|^2\Delta^2\hat{X}_\theta, \qquad (5.8) \\
\Delta^2\hat{I}_+ &= \langle:\Delta^2\hat{n_a}:\rangle + \langle\hat{I}_a\rangle + \langle:\Delta^2\hat{n_b}:\rangle + \langle\hat{I}_b\rangle \\
&= \langle:\Delta^2\hat{I}_a:\rangle + \langle\hat{I}_a\rangle + \langle\hat{I}_b\rangle, \qquad (5.9)
\end{aligned}$$

where the notation $\langle:\hat{O}:\rangle$ means that the operator $\hat{O}$ is written in the normal ordering (first creation operators followed by annihilation operators). We can see in equations 5.8 and 5.9 that the variance of the subtraction of the photocurrents are proportional to the noise quadratures amplified by the carrier and the number of photons in the state $\hat{a}$ in a linear form. If we look for the sum, we see a quadratic dependence in the number of photons in the $\hat{a}$ state. A more interesting analysis is to consider the coherent state in a vacuum state $|\alpha\rangle = |0\rangle$. In this case the variances become:

$$\Delta^2\hat{I}_- = \langle\hat{I}_a\rangle, \tag{5.10}$$

$$\Delta^2\hat{I}_+ = \langle:\Delta^2\hat{I}_a:\rangle + \langle\hat{I}_a\rangle, \tag{5.11}$$

where the variance related with the difference of the photocurrents is equal to the mean value

of the input field, that is compatible with a Poission statistics that characterizes the standard quantum noise limit. If we analyse the sum combination, we have a linear contribution due the shot noise limit of the incoming field and a quadratic contribution.

There are two commons way to calibrate the shot noise. The usual is to measure for different input powers the subtraction of the photocurrents, with this we will have a linear response. Acquiring the angular coefficient we can normalized the noise of one measurement by this coefficient times the mean value of the field being analyzed. Another way is the method that we use in this experiment where we acquire the noise of each detector independently in a balanced detection setup and in an analysis program normalize each measurement by the shot noise. With this approach is possible to avoid nonlinearity due the photodiodes and circuit electronics.

What happens when one attenuates the noise?

Suppose that we attenuate the beam using a BS as in the figure 5.5, what happens with the output mode $\hat{c}$:

$$\begin{aligned} \delta\hat{c}(\Omega) &= t\delta\hat{a} + r\delta\hat{b} \\ \delta\hat{X}(\Omega) &= \delta\hat{c}(\Omega)e^{-i\theta} + \delta\hat{c}^{\dagger}(\Omega)e^{i\theta} \end{aligned} \tag{5.12}$$

where $\hat{X}(\Omega)$ is the fluctuation related with mode quadrature. Computing the variance of this quadrature we have:

$$\begin{aligned} \Delta^2\hat{X}(\Omega) &= \langle\hat{X}(\Omega)\hat{X}(\Omega)\rangle - \langle\hat{X}(\Omega)\rangle^2 \\ &= T\Delta\hat{X}_a^2(\Omega) + (1-T)\Delta^2\hat{X}_{shotnoise}, \end{aligned} \tag{5.13}$$

where we can see that the noise is linearly dependent with the attenuation. When T is going to zero the noise tends to the shot noise limit. In the case that we are close to complete attenuation, $T \approx 0$, we have the shot noise in the output because only the vacuum states are interacting with the photodetector.

5.1.4 OPO cavity - description

The OPO is composed by an optical cavity with a second-order nonlinear susceptibility crystal as the gain medium in the interior. The optical cavity is in a linear configuration, where the input mirror is partially transmitting the pump beam and the output mirror is partially transmitting the twin beams. The mirrors used in the experiment were manufactured by *ATFilms* and in the table 5.1.4, there are the measured transmittances for each mirror as well as the expected cavity finesse for each wavelength. The data of the mirrors supplied by the

manufacturer are given in the appendix of A. The output mirror is coupled to a PZT (an

Rc=25mm	@780(nm)	@1560(nm)
M_{in}	T=29,6(0,4)%	HR
M_{out}	HR	T=3,84(0,04)%
F	18	160

Table 5.3: Characteristics of the mirrors that form the cavity of the OPO. M_{in} refers to the input mirror and M_{out} to the output mirror. The ray of curvature of each mirror is R_c equal to 25 mm and the finesses were estimated based on the transmissivity of each mirror.

abbreviation for its chemical formula $Pb[Zr_{(x)}Ti_{(1-x)}]O_3$). The PZT is a perovskite ceramic material characterized by the piezoelectric effect, whose function is to control the size of the cavity. The mirrors are mounted on a kinematic mount (Polaris 1") manufactured by Thorlabs chosen for their high mechanical stability. The supports are mounted in an aluminium block in U format to guarantee the minimum degrees of freedom, which guarantees a robust assembly, reducing its sensitivity to mechanical vibrations.

In the center of the cavity we have a type II PPKT crystal (*Periodically Poled Potassium Titanyl Phosphate*) manufactured by Raicol company. The crystal has 15 mm of length, an expected degeneracy temperature between -25^0C e -75^0C, period $\Lambda = 45\mu m$ refraction index of $1,75$ for 780nm and $1,81$ for 1560 nm[2] and antireflector treatment for both wavelengths (1560 *and* 780 nm). The crystal is fixed in a five axis mount (model 9082-M of Newport company), which allows the meticulous positioning of the crystal.

The next step is to determine the cavity size that we will use. For this we use Rayleigh length (z_R) optimized to determine the cavity length and better efficiency in the parametric down conversion process. The Rayleigh length is determined[69]:

$$\begin{aligned} l &= 5,6 z_R, \\ z_R &= \pi w_0^2 \frac{n_0}{\lambda}, \end{aligned} \tag{5.14}$$

where l is the length of the crystal and n_0 the refractive index of the crystal for the wavelength of pump beam. The optimum waist determined in this process is approximately $19\mu m$. In order to minimize the losses by diffraction we must have the radius of curvature of the wave front of the beam must be lower or equal to the radius of curvature of the mirror. This leads us to a condition also related to the Rayleigh parameter for determining cavity length:

$$z_R = \frac{\sqrt{(2R_E - L_{cav})L_{cav}}}{2}. \tag{5.15}$$

[2]Values obtained on the site $http://refractiveindex.info$, more details can be found in the reference[68].

In this way, we obtain a cavity size (considering the diffraction) of approximately 56mm, region close to concentricity. After determining the length of the cavity, we need to adjust the mode of the input beam to the mode that oscillates in the cavity. For this, a set of lenses is used that allows us to realize the mode matching of the beam emitted by the Ti:Saf with waist w_{tisaf} to the mode of the OPO cavity with waist w_0. The theoretical development of this work is through the formalism for ABCD matrices and Gaussian bundles described in detail in the reference [70].

In order to measure the tripartite entanglement in the OPO is necessary to have the crystal operating in temperatures below -10^0C, since it was predicted and measured that the excess of noise in the phase of the three fields caused by the presence of phonon noise generated by mechanical vibrations in the crystal has less effect than in ambient temperature (more details in the references [46]). In this experimental setup, the OPO is inside a vacuum chamber and we pump out any humidity, needed to work below $10°C$ without condensation in the mirror and crystal interfaces, that can be seen by the increase of spurious losses. However, there are misalignment when the OPO is at low pressure atmosphere. To avoid this problem, we pump out the air using an mechanical vacuum pump (SD40 - Varian company) and introduce synthetic air (80% N_2 and 20% 0_2) to have an standard atmospheric pressure inside the chamber, but with low humidity.

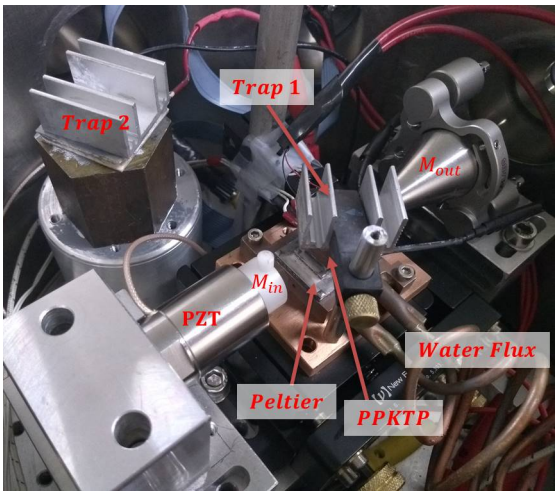

Figure 5.6: Elements inside the vacuum chamber.

Even with the synthetic air, when the temperature is below $0°C$ we see condensation. To decrease the temperature further we use a cryogenic trap above the crystal mounting with a peltier with a continuous current, in the way that the crystal is always at a higher temperature than the trap, $\Delta T \approx 5°C$. In the figure 5.6 we can see the apparatus inside the vaccum chamber. Below the crystal, there are a three layer peltier that is used to set the temperature. The heat is dissipated in a copper basis with an water flux pumped by an chiller with temperature set at $10°C$.

Locking System

We have two principal locking systems in our setup: the stabilization of the pump laser and the locking of the OPO. To stabilize the pump beam in frequency we first lock the titanium sapphire laser. To lock this laser we first control the etalon electronically in a way that only one mode oscillate in titanium sapphire cavity (more details about this system, please see in the reference [16]). After, part of the beam is sent to a saturated absorption scheme using a rubidium cell. Part of that beam passes directly through the rubidium (pump) vapor cell and the other part (probe) is used to saturate the atoms. The emitted beam is resonant with the rubidium D2 line and it has the following spectrum:

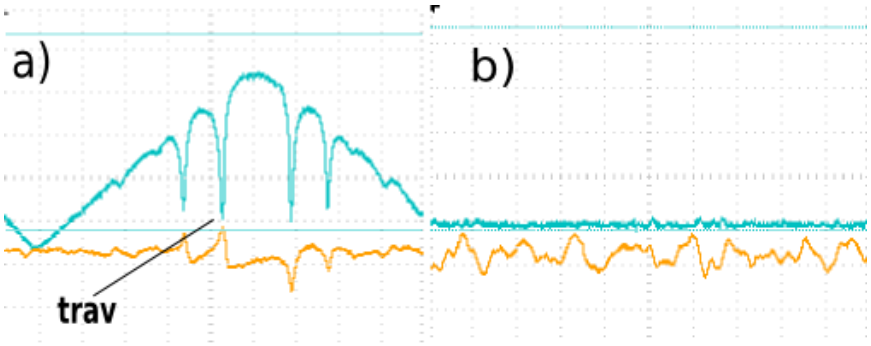

Figure 5.7: a) In blue, saturation absorption signal using a vapor cell with *Rb*. The peak represented by (trav) is what we use to perform the locking and it is resonant with the D2 line of *Rb* atoms. The yellow signal is the error signal generated by the Lock-in. b) Locking signal using the PID system.

We used the absorption output to generate the error signal in a Lock-in system, the error signal generated was sent to a locking system using a proportional, integral and differential system (PID). The output signal of this system is used to perform the control of PZT associated with Titanium Sapphire 5.7. After adjusting the main parameters of the PID we are able to stabilize the laser in the resonant frequency of line D2 of *Rb* (as in the b) part of the figure 5.7.

With the guarantee that the pump beam is stabilized, we need to perform the OPO cavity locking in its resonance. For this we use *Dither & Locking* technique plus a PID system. We use part of the pump signal that is reflected by the OPO as input signal in the locking system that feeds the PID system. The PID output is used to control the PZT that is coupled to the input mirror of the OPO [71]. When this modulation is done in the cavity, we turn on the locking system and at the output of the OPO we will have a continuous light beam.

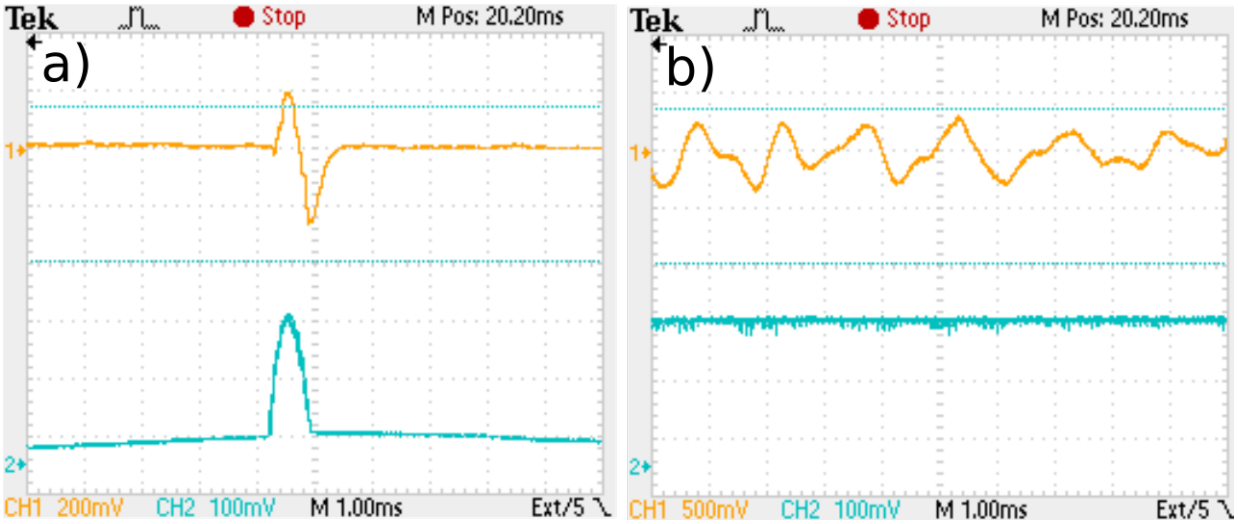

Figure 5.8: a) In yellow, the pump signal transmitted by the OPO above the oscillation threshold. The peak in blue is what we use to perform the locking. The yellow signal is the error signal generated by the *Dither & Locking*. b) Locking signal using the PID system.

We have achieved stable and robust locking for the OPO. We performed an attempt to measure bipartite entanglement and, for the first time, we obtained a signal that is already similar to what we expect to characterize the entanglement between the beams emitted by the OPO.

Detection system

The photodetectors that we used in our system measure the light intensity based in photoelectric effect. In the photodectector there is a photodiode that converts the photons in electric current. The current produced in the photodiode is converted in voltage by an amplification circuit and is separated in two components. A low frequency component, called DC component, and a high frequency (above KHz) component, called HF. The DC component is proportional to the mean intensity of light and is related with the carrier of the field detected. The HF frequency is proportional to the sidebands of the beam detected. After this, the HF signals pass through amplifier circuits and they are demodulated. In the demodulation part we perform a beat between HF signal and a sinusoidal frequency generated by an voltage controlled oscillator (VCO). The resultant signal are decomposed in low frequencies(300KHz) around the analysis frequency being analyzed. The resultant signal is sent to a board from National Instruments Co, (model PCI-6110) an analog/digital converter board from the same company. After this, the signal is sent to the computer and acquired in a rate of 600 KHz and treated in the Lab View program. The measurements are done in a 750ms range, which totalize 450 thousand point by acquisition.

To acquire the pump beam we used a FND-100 photodiode with a measured efficiency of 70%. The twin beams are acquired with ETX-500 from EPITAXX with mean efficiency of 95%.

The total efficiency of the system considering the propagation losses are:

@780 nm	@1560 nm
$\eta_{det} = 80\%$	$\eta_{det} = 95\%$
$\eta_{tot} = 56\%$	$\eta_{tot} = 90\%$

5.2 Phonon-noise characterization

To characterize the excess of noise due the phonon noise generated by the crystal, we measure the matrix V_Q, as given in Equation 2.53. This measurement is performed following the reference [46]. The OPO is pumped below the threshold and we analyze the reflected field by the OPO cavity. The noise spectrum of the amplitude and phase quadratures in terms of the incident pump power is represented in the figure 5.9, the noise of the phase quadrature increases with the incident pump power, while the noise of the amplitude quadrature keeps the same in this process.

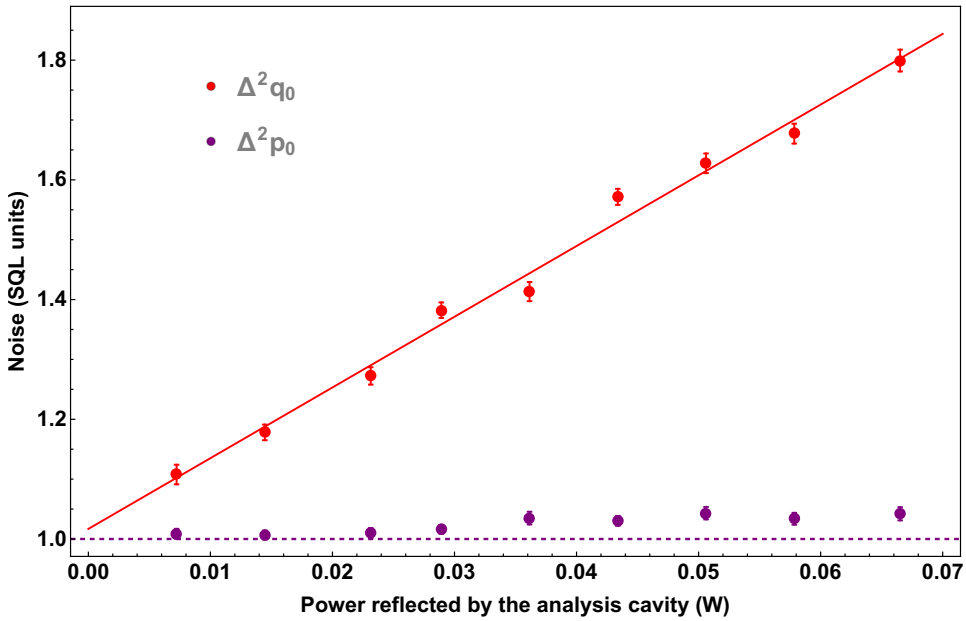

Figure 5.9: Amplitude and phase noise for the pump beam. Measurement performed for a $T = 16^0C$.

In terms of the power, for a temperature of $T = 16^0C$ the phase covariance matrix is given by:

$$\Delta^2 Q_{0int} = 0.118205 P_{intr}(W) \tag{5.16}$$

Following the reference [46], we also measured the effect of the temperature in the system for the pump beam. The behavior of the coupling coefficient η_{00} given in the Equation 2.53 in function of the temperature is shown in the figure 5.10.

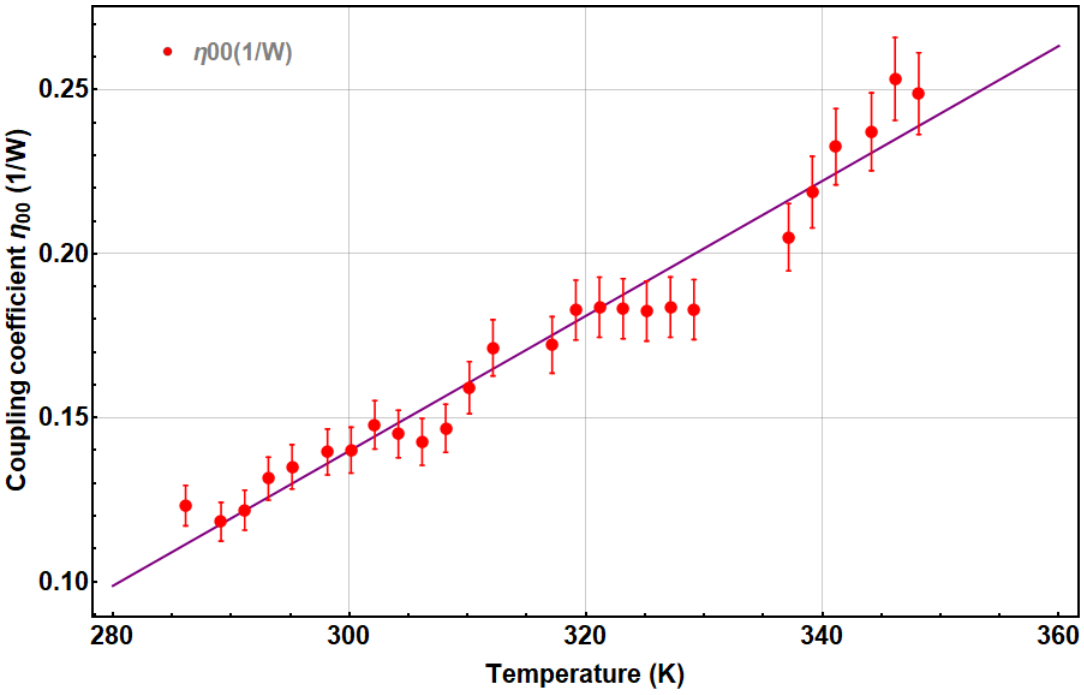

Figure 5.10: Temperature dependence of the noise coupling.

The coupling coefficient η_{00} can be estimated for each analysis temperature by the equation:

$$\eta_{00} = 0.002059T(K) - 0.477953 \tag{5.17}$$

The absence of phonon noise in our system is estimated for temperatures below -40^0C.

It was not possible to measure the same coefficients for the signal and idler beams due the fact that we didn't have a laser with sufficient power around 1560 nm at this time. To estimate these values we used the relation given in the paper [46] between the coupling coefficient for the pump and the coupling coefficient for signal and idler beams, as well as for the correlation between the beams.

$$\eta_{11} = \eta_{22} = \eta_{00}/4 \qquad \eta_{01} = \eta_{02} = 0.27\eta_{00} \qquad \eta_{12} = 0.16\eta_{00} \tag{5.18}$$

We used these relation to perform the theoretical simulations of the OPO.

However, when we did the measurements concerning entanglement between the three beams, explained in detail in section 5.3, we noticed that the noise in the phase quadrature was larger than expected. Trying to understand why this excess of noise excess, we performed the characterization of the phase noise of the pump as a function of the frequency of analysis based

on the references [72, 73]. We observed the presence of structures in the region of we perform the analysis, which suppose that originate from resonances due to boundary conditions in the crystal. Such structures were not observed in the crystal which is used in the article herein taken as reference [46]. Besides the dimensions, the main difference between the two crystals is the way they are made. The crystal used in the reference [46] is a bulk high gray-tracking resistant potassium titanyl phosphate (HGTR-KTP, by Raicol Crystals) cut for type-II phase matching, with length l=12 mm the area is 4mmx4mm, and antireflective coating for both wavelengths, while the crystal used in this thesis is a periodically poled potassium titanyl phosphate (PP-KTP, by Raicol Crystals) with length l=15mm the area is 1mmx2mm, and antireflective coating for both wavelengths. The difference between the bulk and the periodic poled crystal may cause the effect shown in the figure 5.11.

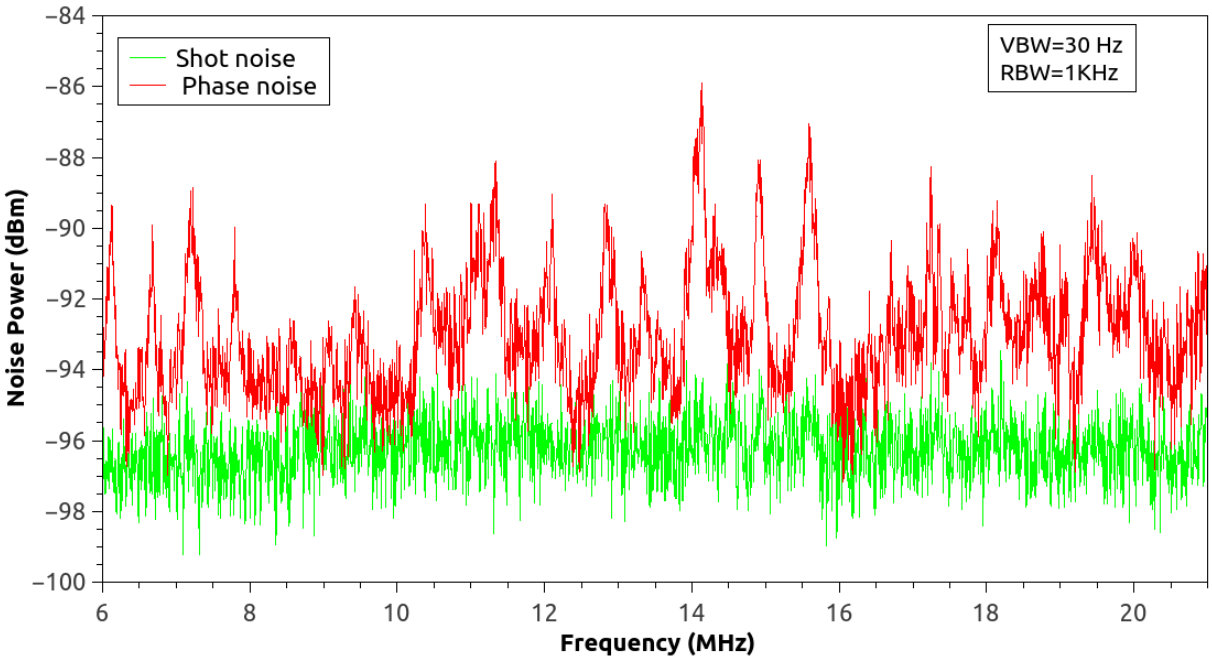

Figure 5.11: Phase noise in function of the frequency. We can see in the figure that close to 9MHz less structures are presented. This measurement was performed with a pump power of 56 mW, using a spectrum analyser with a video bandwidth (VBW) equal to 30HZ and a resolution bandwidth (RBW) equal to 1KHz.

We performed the measurement using a spectrum analyser (model E4401B Agilent company) with the parameters video bandwidth equal to 30 Hz and a resolution bandwidth of 1KHz, the main point here is not integrate the signal during the measurement. In our actual detection system, the bandwidth is 600KHz, what implies that we are acquiring a region between 6.7 MHz and 7.3 MHz when we measure with an analysis frequency of 7MHz.

5.3 Correlations between the pump, idler and signal beams

In this section we analyze the first correlation measurement between the beams emitted by the OPO pumped by the Titanium Sapphire laser. We start by showing the typical result of a measure, how the data analysis is done and how we applied the entanglement criteria studied in the section 1.6. As discussed, we studied the fluctuations of the OPO generated fields that are described by gaussian statistics (for more details read [1]). The acquisition process consists in a data of 450 thousand points in a 750ms window, see subsection 5.1.4. The data used in this section as example was obtained using the measure parameters: analysis frequency of 7MHz, temperature of 18^0C and pump power normalized by the threshold $\sigma = 1.36$. The analysis cavities that were used have characteristics described in table 5.1.2. The DC signal reflected by the analysis cavities and the HF signals are acquired after the demodulation process and have the following format:

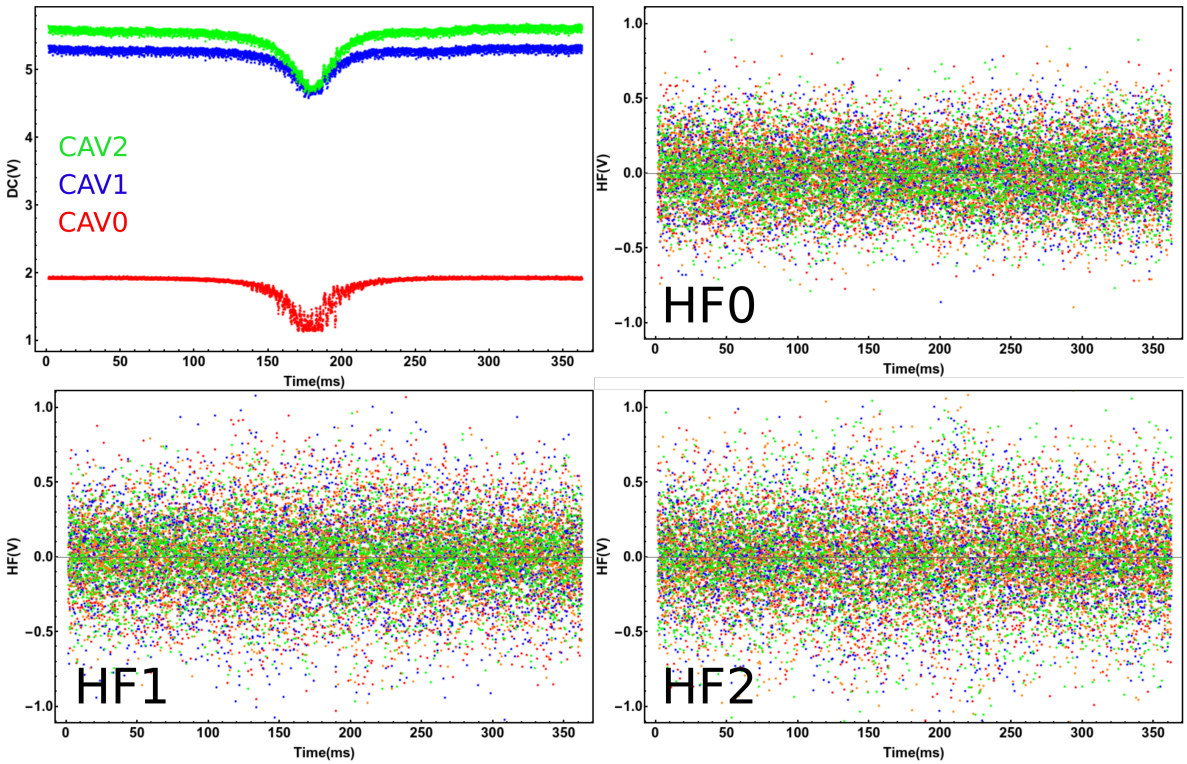

Figure 5.12: Raw data acquired for the 1st measure. For each HF combination we have 4 (2 detectors by analysis cavity) graphs, referring to the current measures in the sine and cosine configuration in each detector. The DC signal acquired is the reflected on each analysis cavity.

The data analysis process of raw data consists in construct the measured covariance matrix by using the noise data and the correlation obtained between the beams in the sine and cosine configuration. For us to have access to every matrix element we make measurements in the following steps:

- **Scan the three cavities through their resonances:** put on this configuration we are

able to acquire the parameters referring to the correlations between the amplitude and phase quadratures. In terms of the parameters described in section 1.5.4, we get from this setup the parameters $\{\mu_{ij}\ \nu_{ij}\ \kappa_{ij}\ \eta_{ij}\}$, where $\{i,j\} = \{0,1,2\}$ with $i \neq j$. ;

- **Scan two cavities through their resonances (CAV1 and CAV0) and one cavity out of resonance (CAV2):** in this setup we want to acquire the correlation between a beam in resonance the other beam out of resonance. For instance, suppose CAV1 in resonance and CAV2 out of resonance, as such we may acquire the correlations between the phase cavity 1 and amplitude cavity 2 quadratures. The parameters related to this setup are $\{\zeta_{12}\ \lambda_{12}\}$;

- **Scan two cavities through their resonances (CAV2 e CAV0) and one cavity out of resonance (CAV1):** suppose now that CAV1 is out of resonance and CAV2 is in resonance, than we may acquire the correlation between the cavity 1 amplitude and cavity 2 phase quadratures. The parameters related to this setup are $\{\epsilon_{12}\ \kappa_{12}\}$;

In graph showed in figure 5.13, we show an example of how these measurements are made and the noise signals of each beam individually and of the corresponding correlations to the analyzed setups, we will focus in the signal and idler beams to explain the analysis:

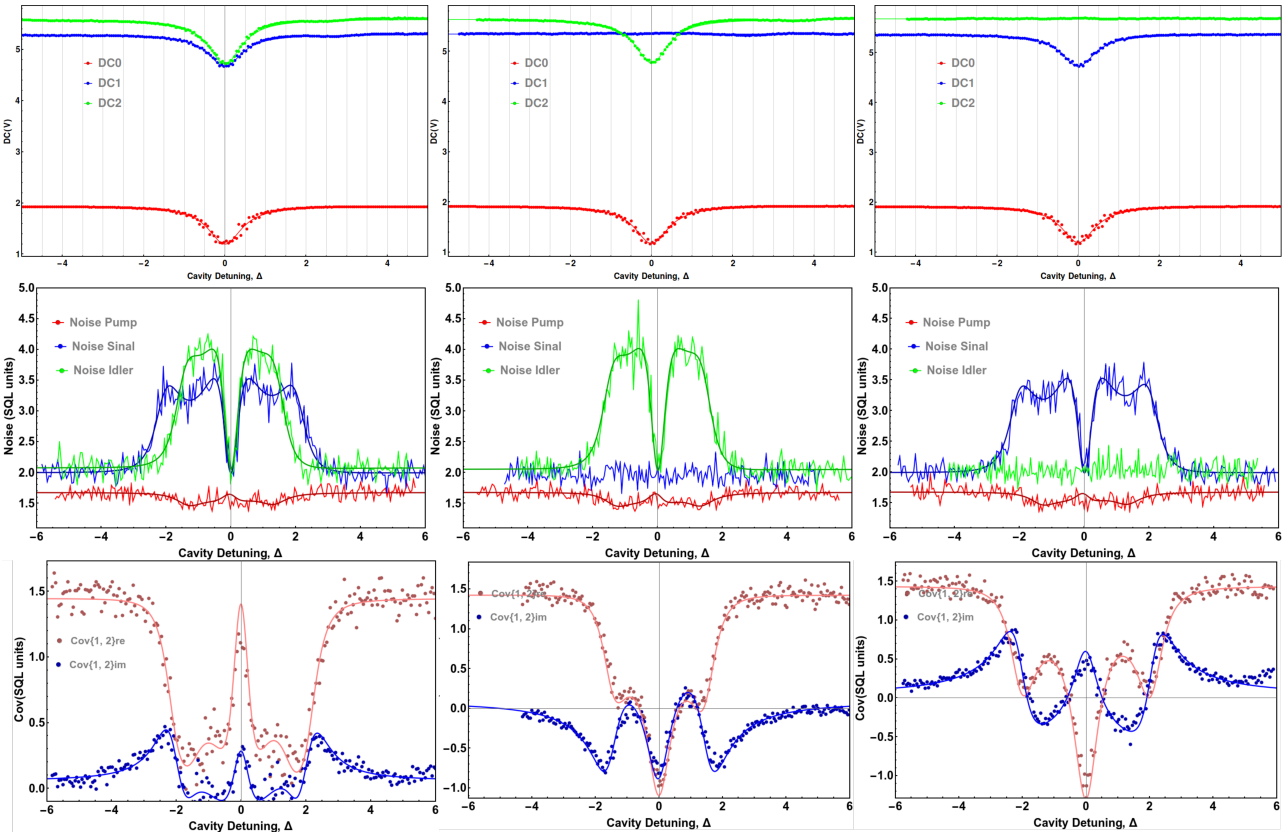

Figure 5.13: Example of a set of data fittings. In the upper part of the figure we have the reflection signals referring to the analysis cavities. In the intermediate part, the noises of the individual beams for studied configuration. In the bottom, we show examples of correlations of the real and imaginary part of the photocurrent given in 1.82 between the signal beam (CAV1) and idler (CAV2) beam.

To make the fit in figure 5.13, we first fit the DC curves of each beam. From this fit, we have the information referring to R_{min} for each cavity. This parameter is necessary to feed the coefficient in equations 1.68. In a first fit for the individual noise, we introduce the fixed value R_{min} for each cavity and then we search the parameter Ω' (analysis frequency normalized by the cavity bandwidth). Having R_{min} and Ω' for each beam, we start the fitting for individual noise and the correlations between the beams. The fit of the individual noise gives us the diagonal entries of the covariance matrix 1.72, the terms α_i and β_i that correspond to the variances of amplitude $\Delta^2 p_i$ and phase $\Delta^2 q_i$, respectively. From the same fit, we obtain the parameters γ_i corresponding the correlation between amplitude and phase in symmetric configuration of each beam, $Cp_{si}q_{si}$ and the parameter δ_i, that is the correlation $Cp_{si}p_{ai}$. These two parameters are close to zero.

The correlation fitting gives us the remaining parameter of the covariance matrix. In the situation that we have cavities 1 and 2 synchronous, we have access to the parameters $\{\mu_{12}\ \nu_{12}\ \eta_{12}\ \tau_{12}\}$ that correspond the following correlations $\{Cp_{s1}p_{s2},\ Cq_{s1}q_{s2},\ Cp_{s1}q_{a2},\ Cq_{s1}p_{a2}\}$ respectively. With these parameters on hand, we feed the analysis fitting in which the cavity

1 is out of resonance and cavity 2 is in resonance. In this case, we are interested in the terms $\{\epsilon_{12}\ \kappa_{12}\}$ that correspond to the correlations $\{Cp_{s1}q_{s2},\ Cp_{s1}p_{a2}\}$. And, finally, the analysis of the system when cavity 1 is in resonance and cavity 2 is out of resonance allows us to have access to the terms $\{\zeta_{12}\ \lambda_{12}\}$ that are the same then the correlations $\{Cp_{s1}p_{s2}\ , Cq_{s1}q_{a2}\}$.

Performing this procedure for the different combinations between the 2 beams, we are able to construct the complete covariance matrix of the system and, with this, we have the tomography of the state under study. As an example, let the covariance matrix for the above system be, considering only cavities 1 and 2:

$$\mathbf{V}_{s}^{(12)} = \begin{pmatrix} 2.07 & -0.05 & 1.45 & -0.046 \\ -0.051 & 3.54 & -0.055 & 0.30 \\ 1.45 & -0.055 & 2.09 & -0.078 \\ -0.046 & 0.30 & -0.078 & 4. \end{pmatrix} \qquad \mathbf{C}_{s/a'}^{(12)} = \begin{pmatrix} 0. & -0.10 & 0.13 & 0.014 \\ 0.10 & 0. & -0.002 & -0.11 \\ -0.13 & 0.002 & 0. & -0.10 \\ -0.014 & 0.11 & 0.10 & 0. \end{pmatrix}$$

We can see that the correlation between the symmetric and antisymmetric basis are close to zero for almost all the parameters, the presence of non zero terms may be caused by a detuning that coupling the phase and amplitude quadratures inside the cavity. The term $C_{s/a'}^{(12)}$ corresponds to the correlation in Equation 1.76 with a rotation of $\pi/2$ in the antisymmetric basis in the sense that this part now is the same that the imaginary part of the matrix Equation 2.54. With the covariance matrix, we are able to apply one criteria to see if there are entanglement or steering in the system. For the example above, Duan criterion has the value of 4.74(2) and the inference between the twin beams are 4.09(1) if we are inferring signal to idler and 4.67(2) if we are inferring idler to signal. Following the procedure described in this section we will now study the tripartite correlations.

5.3.1 Tripartite analysis

In this section, we will present the most important results obtained until now. We start showing a data set for the noise spectrum of amplitude and phase quadratures and their correlations between all three fields. In the figure 5.14, we have the behavior of amplitude and phase quadratures. These data were obtained in a temperature of 18^0C and an analysis frequency of 7MHz.

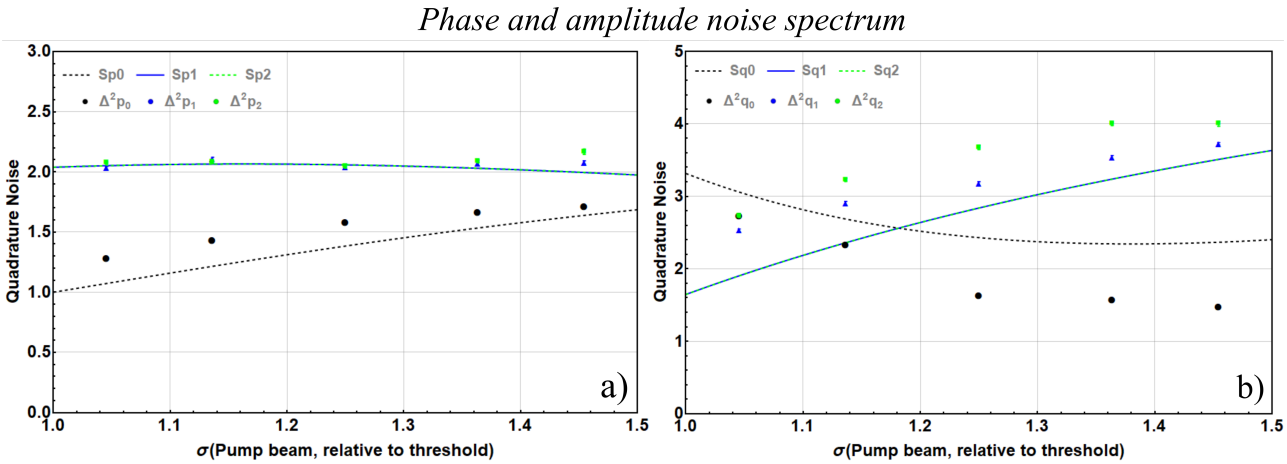

Figure 5.14: This figure show us the symmetric part of the correlation between the twin beams, in a) we have the amplitude correlations and in b) the phase correlations for each beam.

The fit simulation were performed using the theory developed in the chapter 2, and the parameters used were $\Omega^{'} = 0.55$, $\Delta^2\hat{q}_{0in} = 1.30$, $\mu = 0.002$ and $\mu_0 = 0.02$. To perform the fit of the phase quadratures, we needed to multiply the phonon parameters in Equation 5.18 for a factor as in the Equation 5.19:

$$\eta_{00} = p_0\eta_{00}^{fit} \qquad \eta_{01} = \eta_{02} = p_{01}\eta_{02}^{fit} \qquad \eta_{11} = \eta_{22} = p_{11}\eta_{11}^{fit} \qquad \eta_{12} = p_{12}\eta_{12}^{fit}, \tag{5.19}$$

where the parameters $p_0 = 3.5, p_{01} = 1.2, p_{11} = 1.3$ and $p_{12} = 2$ were added to compensate the excess of phonon noise due the presence of different structures in our crystal more explained in the section 5.2, and due the fact that it was not possible to determine the excess of noise due the twin beams because we didn't have a source to measure it. The parameters η_{ij}^{fit} are the same that we shown in the Equation 5.18. We used these parameters to perform the fit simulations in all the figures presented in this chapter.

The correlation between the symmetric part of the amplitude quadratures and phase quadratures between the different beams are in the part a) of the figure 5.15. The symmetric correlation between the different combinations C_{pipj} and C_{qiqj} correspond to the real part of the correlations in the spectral matrix Equation 2.54, and the behavior of these correlations follow what is expected from the theory. The cross-correlation between the symmetric and antisymmetric part correspond to the imaginary part of the spectral matrix and they are presented in the part b) of the figure 5.15 and the presence of a small correlation may come due a detuning that coupling the phase and amplitude quadratures inside the cavity.

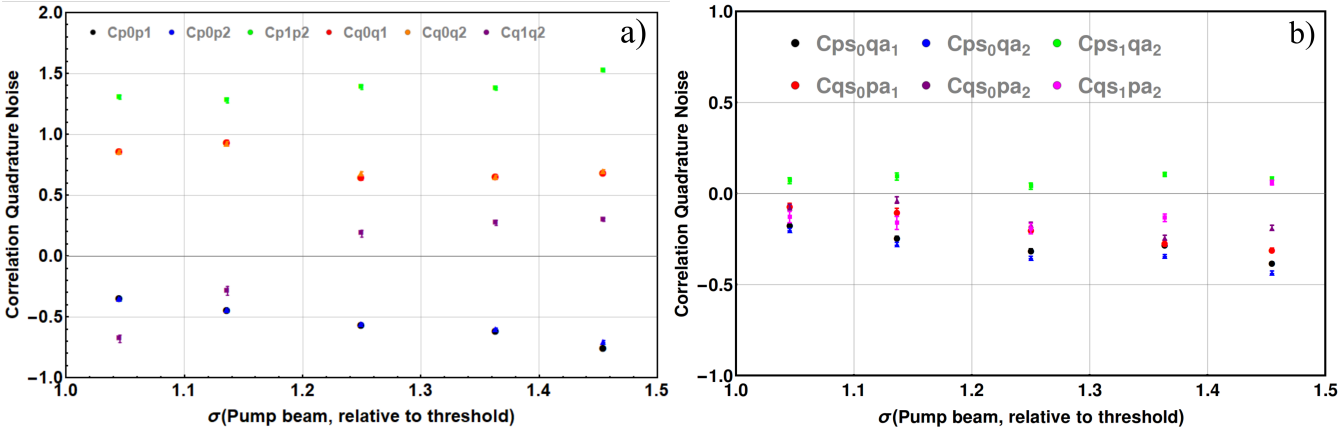

Figure 5.15: In part a) of this figure we have the behavior of symmetric part of the correlation between the twin beams, as described in the covariance matrix 1.76. The part b) of the figure contains the combination between amplitude and phase in the symmetric and antisymmetric basis that we wait be close of zero.

To study the entanglement between the three beams we applied the PPT criterion in the covariance matrix of our system, where the measurements were performed in the temperatures of $T = 18^0C$ and $T = 0^0C$ [3]. Analyzing the PPT criterion in figure 5.16, in both cases the points corresponding to ν_1 and ν_2 represents the partial transposition of the signal and idler beams, and the points corresponding to the eigenvalue ν_0 to the partial transposition of the reflected pump. Comparing the two data, we can see an expressive improvement in the entanglement between the twin beam at $T = 0^0C$, due ν_1 and ν_2 be less than 1 until $\sigma = 1.25$ in this case, while for $T = 18^0C$ these eigenvalues is larger than 1 for $\sigma = 1.1$. In both cases it was not possible see the entanglement between the twin beams and the reflected pump, although that there is an improvement in the symplectic eigenvalue ν_0 in $T = 0^0C$ but these combination stays separated for the twin beams.

We can see that the way to achieve the entanglement between the three beams is to cool down further the system, as predicted in the reference [46]. The interaction of the fields with the phonons present in the crystal lattice generates an excess of spurious losses present in the phase quadrature. As we discussed in the section 5.2, to avoid this noise we need to cool down the crystal close to -40^0C, and this became very challenge in our setup. When we try to cool down the system for temperatures below 0^0C the lock stabilization of the OPO became very sensitive to the small fluctuations in temperature which makes it difficult to proceed with the measurement. The better way to cool down the system is to perform vacuum in the chamber and to proceed with measurement. The problem in our case with this is that when one evacuates the chamber the system suffers a misalignment that, in our case, is very difficult to fix because of the dimensions of our crystal. For this reason we have injected synthetic air

[3] The measurement in $T = 0^0C$ was performed for an analysis frequency of 7.4MHz, and the fit simulations parameters are the same that we used to analyze the other graphics with the change in the phonon parameter that is necessary due the change in the temperature, see figure 5.10.

(as described in 5.1.4) in the system. When we did this the system alignment was recovered making possible the measurement. But, using the synthetic air it was not possible until the present moment to cool down more than 0^0C. More than the phonon noise effect, if we lower the cavity size we will increase the bandwidth of the OPO which allows the measurement in an analysis frequency where the pump beam is more coherent than in 7.0 MHz. In this case the phase noise introduced by the pump beam will not influence in the system and may it might be able to see the correlations between the three beams in temperatures above -40^0C.

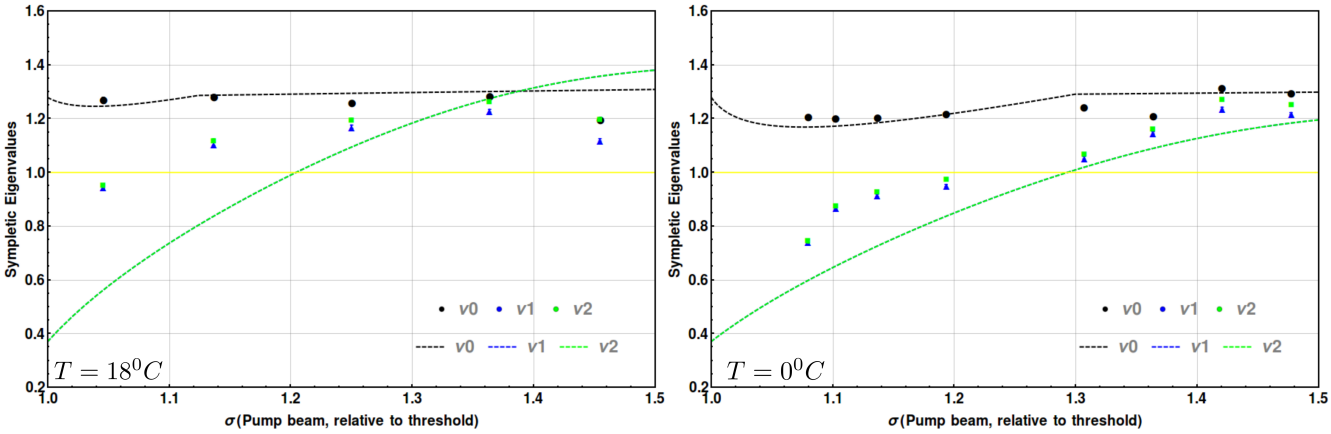

Figure 5.16: Minimum symplectic eigenvalues ν_k obtained by the partial transposition of the subsystem k in function of σ. If ν_k is less then 1, so the bipartition is entangled. In part a) we have the behavior of the symplectic eigenvalues for $T = 18^0C$, in this case we have entanglement between the twin beams for $\sigma \approx 1.05$ for all other cases the subsystem are separated. In b) we can see a huge improvement in the entanglement between the twin beams, the system are entangled until $\sigma \approx 1.2$, but the pump still separated of the system.

Our better result achieved until know is the correlation between the twin beams. For $\sigma \approx 1.07$, Duan inequality is 1.75(3) and we violate the first Van Look-Furusawa inequality as well given in Equation 4.24 where V0=1.57(2), if each one of the Van Look-Furusawa inequality is less then 2, this confirm the tripartite entanglement in the system, in this case the second and third inequality were not violate and they have the values V1=2.58(2) and V2=2.56(1). Considering the PPT criterion, that is necessary and sufficient to demonstrate entanglement for Gaussian system, we saw in the figure 5.16 part b) that for a range until $\sigma \approx 1.2$ we have entanglement between the twin beams.

Chapter 6

Conclusions

In this thesis, we performed a complete analysis of an optical parametric oscillator pumped by a titanium sapphire laser beam. The analysis of this system is of extreme utility when considering a quantum communication network, where we need means of storing information and transmitting it information with minimal losses. The titanium sapphire, the pump beam of the system is tunable in a range between 730 and 800 nm [16]. This region is compatible with the line D1(794.98 nm) and D2(780.24 nm) of Rb. We used the locked laser, using a saturated absorption system, in line D2 of the Rb^{87}. One of the main characteristics of this laser is the fact that the noise generated by it is at the shot-noise level, so we have a coherent pump source that can be used both in a process of integration with atomic systems and in the formation of a input state in a teleportation protocol. The signal and idler twin beams generated by the OPO have wavelengths around 1560nm, in telecommunications region (*C-band*) which allows the use of optical fibers to transport the light generated by the OPO.

Furthermore, we presented many theoretical predictions expected for this system. We studied the behavior of the quadratures of each beam individually and their correlations among different combinations of quadratures. With this data on hand, we constructed the system's covariance matrix that allows us to organize the second order fluctuations terms. From the covariance matrix values we made predictions of entanglement for different bipartitions. For such we used the PPT criterion, that is necessary and sufficient to attest entanglement for Gaussian states, using the Duan criterion, as the usual way to demonstrate entanglement between the amplitude subtraction quadrature and phase sum quadrature. At last, we used the Furusawa criterion as figure of merit in the teleportation process.

We described theoretically the steering criterion for this system, where it was shown which possible bipartitions steering is expected. We saw that there is no steering between the bipartition made by pump mode and one of the twins. Nonetheless, steering is expected to exist between the bipartition made by the twin beams up to $\sigma > 3$. We studied this system considering detection losses and added the noise of phonons in the system. Finally, we analyzed the steering criterion between the bipartition made by the combination of the sum quadrature of

twin beams and the pump beam. In this situation, we have seen that steering is very sensitive to the added losses, there are no steering in the presence of phonon noise. This is one of the main results shown in this thesis.

We developed two multicolor quantum teleportation protocols of the system. In both we will use the pump beam to create the input state. The entangled state necessary for the teleportation process is the three beam entanglement involving reflected pump, signal and idler. The Bell measurement in the Alice station is done using the input state and the reflected pump by the OPO. In the first model, the measurement result is sent by classical channels for the signal and idler beams, each representing a BOB station and checked by Victor station. The fidelity result of the process is bellow the non-cloning limit. With the goal of improving the fidelity, we introduced the signal beam as auxiliary in the process of teleportation, were we introduced the Charlie station, the idler beam will be the only BOB station in this case. In the second model, the fidelity goes beyond the non-cloning limit a proposal develop by our group.

In order to perform the experimental implementation of the steering criterion and the quantum teleportation protocol we need to have a source of quantum correlated states, that is the OPO. The results obtained until now show us the way that we need to follow to achieve the main purpose. For the first time, we demonstrated the squeezing in the amplitude combination of the twin beams in our system. That is consistent in all the measurements performed. The squeezing in the sum of the phases has shown itself to be a huge experimental challenge to be achieved, which we hope will be solved very soon.

We performed the quantum tomography of the system for different input pump power and temperature. With the covariance matrix of each configuration studied, applying different entanglement criteria, we try to understand what we need to improve the system in order in other to have success in the experimental implementation of this source.

In the near future, we expect to perform a quantum communication protocol in this system, either, using to implement the teleportation protocol, or in an interface with atomic medium.

Appendix A

Dados ATFilms

Espelho de entrada

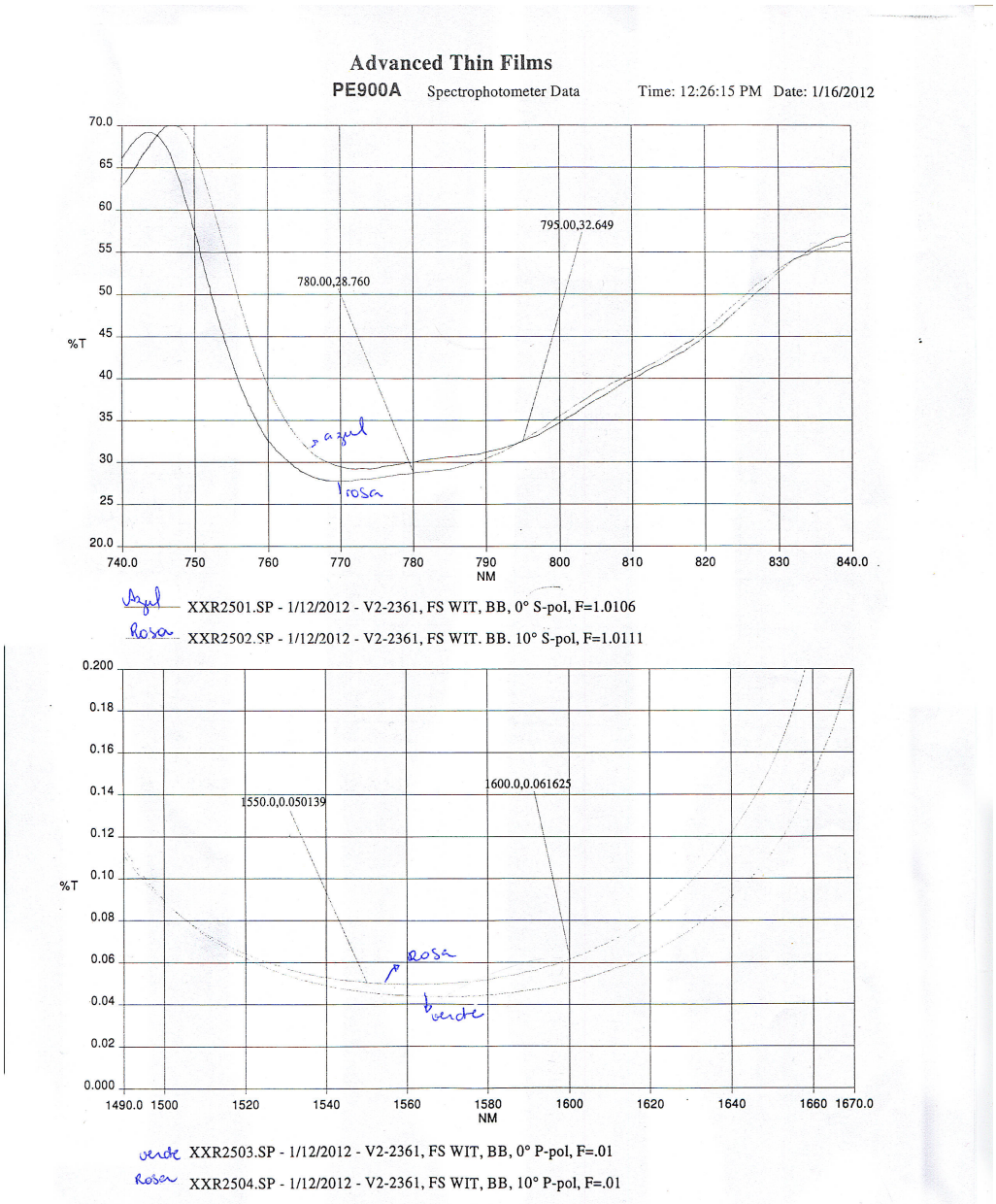

Espelho de saída

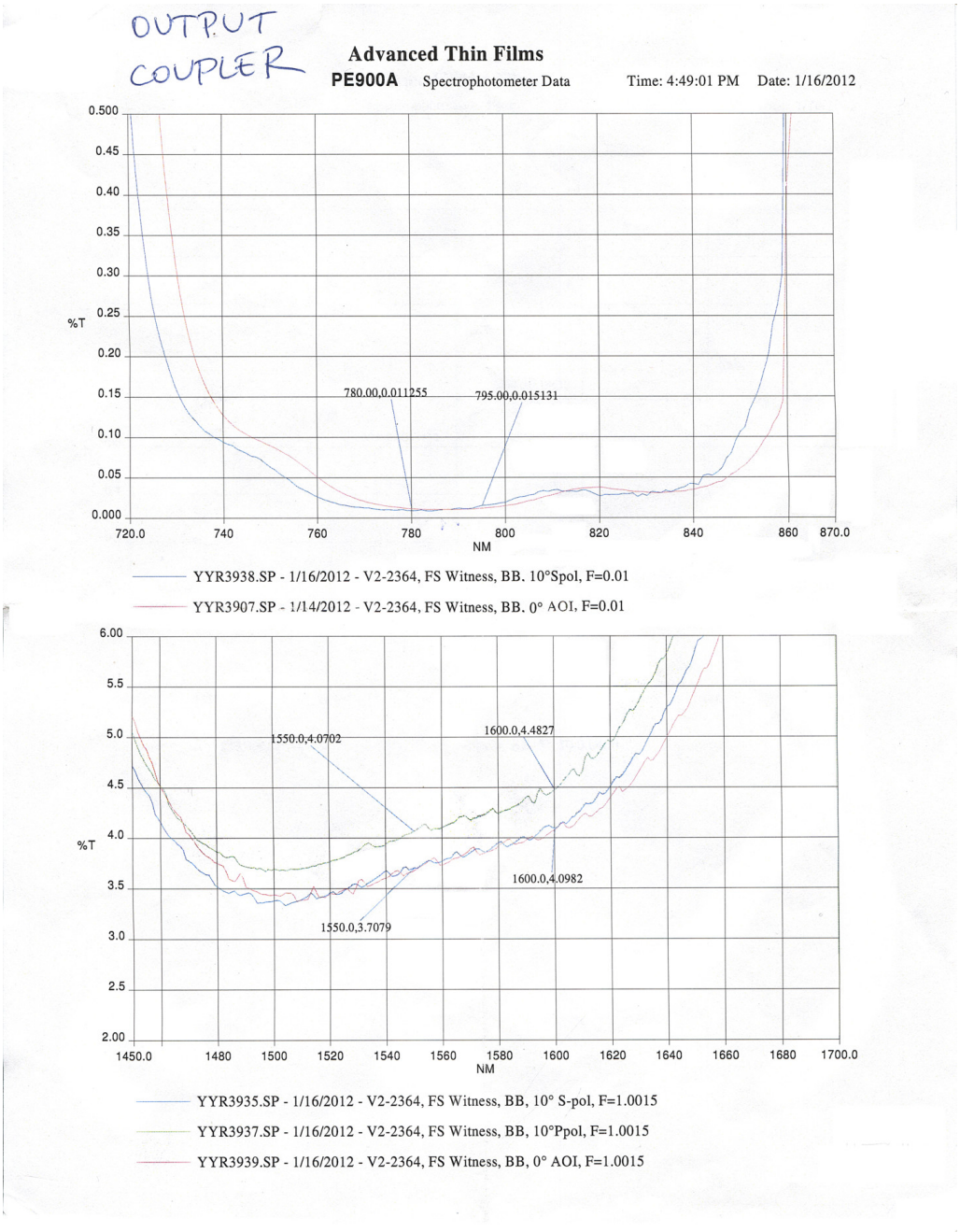

Figure A.2: Data referring to the transmission by the mirror of the output of the resonant beams with the cavity of the OPO.

Bibliography

[1] Antonio Sales Oliveira Coelho. *Emaranhamento multicolor para redes de informação quântica.* PhD thesis, Universidade de São Paulo, 2013.

[2] Lu-Ming Duan, G. Giedke, J. I. Cirac, and P. Zoller. Inseparability criterion for continuous variable systems. *Phys. Rev. Lett.*, 84:2722–2725, Mar 2000.

[3] Peter van Loock and Akira Furusawa. Detecting genuine multipartite continuous-variable entanglement. *Phys. Rev. A*, 67:052315, 2003.

[4] R.Simon. Peres-horodecki separability criterion for continuous variable systems. *Phys. Rev. Lett.*, (84):2726, 2000.

[5] M. D. Reid. Demonstration of the einstein-podolsky-rosen paradox using nondegenerate parametric amplification. *Phys. Rev. A*, 40:913–923, Jul 1989.

[6] Hoi-Kwong Lo, Sandu Popescu, and Tim Spiller. *Introduction to Quantum Computation and Information.* World Scientific Pub Co Inc, 2001.

[7] A. Furusawa, J.L Sorensen, S. L. Braunstein, C. A. Fuchs, H. J. Kimble, and E. S. Polzisk. Unconditional quantum teleportation. *Science*, 282:706, 1998.

[8] A. I. Lvovsky, B.C. Sanders, and W. Tittel. Optical quantum memory. *Nat. Phot.*, 3:706–714, 2009.

[9] A. Einstein, B. Podolsky, and N. Rosen. Can quantum-mechanical description of physical reality be considered complete? *Phys. Rev.*, 47:777, 1935.

[10] N. Bohr. Can quantum mechanical description of physical reality be considered complete? *Phys. Rev.*, 48:696, 1935.

[11] E. Schrödinger. Discussion of probability relations between separated systems. *Proc. Cambr. Phil. Soc.*, 31:555, 1935.

[12] J. S. Bell. On the einstein-podolsky-rosen paradox. *Physics*, 1:195, 1964.

[13] M. A. Nielsen and I. L. Chuang. *Quantum Computation and Quantum Information*. Cambridge Univ. Press, 2000.

[14] J. H. Kimble. The quantum internet. *Nature*, 453:1023–1030, 2008.

[15] P.K.Lam and T. C. Ralph. Quantum cryptography: Continuous improvement. *Nat. Phot.*, 7:350–352, 2013.

[16] Flávio Campopiano Dias de Moraes. Construção e caracterização de um laser contínuo de titânio-safira. Master's thesis, Universidade de São Paulo, 2013.

[17] www.rp-photonics.com/optical-fiber-communications.html.

[18] A. S. Coelho, F. A. S. Barbosa, J. E. S. Cesar, A. S. Villar, K. N. Cassemiro, M. Martinelli, and P. Nussenzveig. Three color entanglement. *Science*, 326:823–826, 2009.

[19] P. van Loock, Samuel L. Braunstein, and H. J. Kimble. Broadband teleportation. *PhysRevA*, 62:022309, jul 2000.

[20] Marlan O. Scully and M. Suhail Zubairy. *Quantum Optics*. Cambridge University Press, 1997.

[21] Christopher Gerry and Peter Knight. *Introductory Quantum Optics*. Cambridge University Press, 2004.

[22] Katiúscia Nadyne Cassemiro. *Correlações Quânticas Multicolores no Oscilador Paramétrico Ótico*. PhD thesis, Universidade de São Paulo, 2008.

[23] Roy J. Glauber. The quantum theory of optical coherence. *Phys. Rev.*, 130:2529–2539, Jun 1963.

[24] JeanPierre Gazeau. *Coherent States in Quantum Physics*. WileyVCH Verlag GmbH & Co. KGaA, 2010.

[25] R. E. Slusher, L. Hollberg, B. Yurke, J. C. Mertz, and J. F. Valley. Squeezed states in optical cavities: A spontaneous-emission-noise limit. *Phys. Rev. A*, 31:3512–3515, May 1985.

[26] G.J. Milburn D.F.Walls. *Quantum Optics*. Springer-Verlag, 1994.

[27] Christian Weedbrook, Stefano Pirandola, Raúl García-Patrón, Nicolas J. Cerf, Timothy C. Ralph, Jeffrey H. Shapiro, and Seth Lloyd. Gaussian quantum information. *Rev. Mod. Phys.*, 84:621–669, May 2012.

[28] Wolfgang P. Schleich. *Quantum Optics in Phase Space*. WILEY-VCH, 2001.

[29] E. Wigner. On the quantum correction for thermodynamic equilibrium. *Phys. Rev.*, 40:749–759, Jun 1932.

[30] ULF Leonhardt. *Essential Quantum Optics*. Cambrigde University press, 2010.

[31] F. A. S. Barbosa, A. S. Coelho, K. N. Cassemiro, P. Nussenzveig, C. Fabre, A. S. Villar, and M. Martinelli. Quantum state reconstruction of spectral field modes: Homodyne and resonator detection schemes. *Phys. Rev. A*, 88:052113, November 2013.

[32] Felippe Alexandre Silva Barbosa. *Robustez do emaranhamento em variáveis contínuas e fotodetecção de feixes intensos no domínio espectral*. PhD thesis, USP, 2013.

[33] Leonard Mandel and Emil Wolf. *Optical Coherence and Quantum Optics*. Cambridge University Press, 1995.

[34] L. A. Porreca M. G. Tombesi P.Leuchs G. Galatola, P. Lugiato. System control by variation of the squeezing phase. *Optics Communications*, 85:95–103, 08 1991.

[35] Alessandro Villar. Estudo de emaranhamento no oscilador paramétrico Ótico não-degenerado acima do limiar. Master's thesis, Unversidade de São Paulo, 2004.

[36] Asher Peres. Separability criterion for density matrices. *Phys. Rev. Lett.*, 77:1413–1415, Aug 1996.

[37] Pawel Horodecki. Separability criterion and inseparable mixed states with positive partial transposition. *Physics Letters A*, 232(5):333 – 339, 1997.

[38] Gerardo Adesso and Fabrizio Illuminati. Entanglement in continuous-variable systems: recent advances and current perspectives. *Journal of Physics A: Mathematical and Theoretical*, 40(28):7821, 2007.

[39] Gerardo Adesso. *Entanglement of Gaussian States*. PhD thesis, Università degli Studi di Salerno, 2006.

[40] John Williamson. On the algebraic problem concerning the normal forms of linear dynamical systems. *American Journal of Mathematics*, 1936.

[41] J. Peltola M. Vainio, M. Siltanen and L. Halonen. Grating-cavity cw optical parametric oscillators for high-resolution mid-infrared spectroscopy. *Appl. OPtics*, 2011.

[42] M. Slipchenko and J. Cheng. Multimodal nonlinear optical microscopy. *OSA Technical Digest*, 2010.

[43] M. Metsälä O. Vaittinen, F. Schmidt and L. Halonen. Exhaled breath biomonitoring using laser spectroscopy. *Curr. Anal. Chem*, 2013.

[44] Howard Carmichael. *Optics System Approach to Quantum Optics*. Springer-Verlag, 1991.

[45] Antônio Sales Coelho Luis Ortiz-Gutiérrez Marcelo Martinelli Paulo Nussenzveig Alessandro S. Villar Luis F. Muñoz-Martínez, Felippe Alexandre Silva Barbosa. Exploring six modes of an optical parametric oscillator. *eprint arXiv:1710.02905*, 2017.

[46] J. E. S. Cesar, A.S. Coelho, K.N. Cassemiro, A.S. Villar, M. Lassen, P. Nussenzveig, and M. Martinelli. Extra phase noise from thermal fluctuations in nonlinear optical crystals. *Physical Review A*, 79:063816, 2009.

[47] Antonio Sales Oliveira Coelho. Emaranhamento tripartite no oscilador paramétrico Ótico. Master's thesis, Universidade de Sao Paulo, 2009.

[48] C. Fabre e E. Giacobino S. Reynaud. Quantum fluctuations in a two-mode parametric oscillator. *J. Opt. Soc. Am. B*, 1987.

[49] Alessandro de Sousa Villar. *Emaranhamento Multicolor entre Feixes Intensos de Luz*. PhD thesis, USP, 2007.

[50] A. S. Villar, L. S. Cruz, K. N. Cassemiro, M. Martinelli, and P. Nussenzveig. Generation of bright two-color continuous variable entanglement. *Phys. Rev. Lett.*, 95:243603, 2005.

[51] Run Yan Teh Qihuang Gong Qiongyi He Jiri Janousek-Hans-Albert Bachor Margaret D. Reid & Ping Koy Lam Seiji Armstrong, Meng Wang. Multipartite einstein–podolsky–rosen steering and genuine tripartite entanglement with optical networks. *Nature Physics*, 11:167–172, 2015.

[52] Samuel L. Braunstein and Peter van Loock. Quantum information with continuous variables. *Rev. Mod. Phys.*, 77:513–577, Jun 2005.

[53] F. Furrer, T. Franz, M. Berta, A. Leverrier, V. B. Scholz, M. Tomamichel, and R. F. Werner. Continuous variable quantum key distribution: Finite-key analysis of composable security against coherent attacks. *Phys. Rev. Lett.*, 109:100502, Sep 2012.

[54] M. D. Reid, P. D. Drummond, W. P. Bowen, E. G. Cavalcanti, P. K. Lam, H. A. Bachor, U. L. Andersen, and G. Leuchs. Colloquium: The einstein-podolsky-rosen paradox: From concepts to applications. *Rev. Mod. Phys.*, 81:1727–1751, Dec 2009.

[55] M. D. Reid, P. D. Drummond, W. P. Bowen, E. G. Cavalcanti, P. K. Lam, H. A. Bachor, U. L. Andersen, and G. Leuchs. Colloquium: The einstein-podolsky-rosen paradox: From concepts to applications. *Rev. Mod. Phys.*, 81:1727–1751, Dec 2009.

[56] Charles H. Bennett, Gilles Brassard, Claude Crepeau, Richard Jozsa, Asher Peres, and William K. Wootters. Teleporting an unknown quantum state via dual classical and einstein-podolsky-rosen channels. *PhysRevLett*, 1993.

[57] Cyril Branciard, Eric G. Cavalcanti, Stephen P. Walborn, Valerio Scarani, and Howard M. Wiseman. One-sided device-independent quantum key distribution: Security, feasibility, and the connection with steering. *Phys. Rev. A*, 85:010301, Jan 2012.

[58] Akira Furusawa and Peter van Loock. *Quantum Teleportation and Entanglement.* Wiley-CH, 2011.

[59] Klaus Mattle Manfred Eibl Harald Weinfurter Anton Zeilinger Dik Bouwmeester, Jian-Wei Pan. Experimental quantum teleportation. *Nature*, 1997.

[60] Lev Vaidman. Teleportation of quantum states. *Physical Review A*, 1994.

[61] Samuel L. Braunstein and H. J. Kimble. Teleportation of continuous quantum variables. *Phys. Rev. Lett.*, 1998.

[62] Selected Topics in Quantum Elestronics. Unity gain and nonunity gain quantum teleportation. *IEEE Journal of Electronics*, 2003.

[63] H. J. Kimble Samuel L. Braunstein, Christopher A. Fuchs. Criteria for continuous variable quantum teleportation. *Journal of Modern Optics*, 2000.

[64] Frédéric Grosshans and Philippe Grangier. Quantum cloning and teleportation criteria for continuous quantum variables. *Phys. Rev. A*, 2001.

[65] Jing Zhang and Kunchi Peng. Quantum teleportation and dense coding by means of bright amplitude-squeezed light and direct measurement of a bell state. *Phys. Rev. A*, 62:064302, Nov 2000.

[66] P. F. Moulton. Spectroscopic and laser characteristics of ti:al2o3. *J. Opt. Soc. Am. B*, 3(1):125–133, Jan 1986.

[67] A. Sanchez, R. E. Fahey, A. J. Strauss, and R. L. Aggarwal. Room-temperature continuous-wave operation of a ti:al2o3 laser. *Opt. Lett.*, 11(6):363–364, Jun 1986.

[68] Michael Bass, Casimer DeCusatis, Jay Enoch, Vasudevan Lakshminarayanan, Guifang Li, Carolyn MacDonald, Virendra Mahajan, and Eric Van Stryland. *Handbook of Optics, Third Edition Volume IV: Optical Properties of Materials, Nonlinear Optics, Quantum Optics (set).* McGraw Hill Professional, 2009.

[69] G. D. Boyd and D. A. Kleinman. Parametric interaction of focused gaussian light beams. *J. Appl. Phys.*, 39:3597, 1968.

[70] H. Kogelnik and T. Li. Laser beams and resonators. *Applied Optics*, 5:10, 1966.

[71] http://pmaweb.caltech.edu/ ph77/labs/optics/pdh.pdf.

[72] Yongmin Li, Xiaomin Guo, Zengliang Bai, and Chunchun Liu. Generation of two-color continuous variable quantum entanglement at 0.8 and 1.5micrometers. *Applied Physics Letters*, 97(3):031107, 2010.

[73] Nicolai Bernd Grosse. Harmonic entanglement and photon ant-buching, 2009.